Theses and Dissertations--Chemical and Materials Engineering

Chemical and Materials Engineering

2019

FUNCTIONALIZATION OF IRON OXIDE NANOPARTICLES AND THE IMPACT ON SURFACE REACTIVE OXYGEN SPECIES GENERATION FOR POTENTIAL BIOMEDICAL AND ENVIRONMENTAL APPLICATIONS

Trang Mai
University of Kentucky, trangmt23@gmail.com
Digital Object Identifier: https://doi.org/10.13023/etd.2019.296

Right click to open a feedback form in a new tab to let us know how this document benefits you.

STUDENT AGREEMENT:

I represent that my thesis or dissertation and abstract are my original work. Proper attribution has been given to all outside sources. I understand that I am solely responsible for obtaining any needed copyright permissions. I have obtained needed written permission statement(s) from the owner(s) of each third-party copyrighted matter to be included in my work, allowing electronic distribution (if such use is not permitted by the fair use doctrine) which will be submitted to UKnowledge as Additional File.

I hereby grant to The University of Kentucky and its agents the irrevocable, non-exclusive, and royalty-free license to archive and make accessible my work in whole or in part in all forms of media, now or hereafter known. I agree that the document mentioned above may be made available immediately for worldwide access unless an embargo applies.

I retain all other ownership rights to the copyright of my work. I also retain the right to use in future works (such as articles or books) all or part of my work. I understand that I am free to register the copyright to my work.

REVIEW, APPROVAL AND ACCEPTANCE

The document mentioned above has been reviewed and accepted by the student's advisor, on behalf of the advisory committee, and by the Director of Graduate Studies (DGS), on behalf of the program; we verify that this is the final, approved version of the student's thesis including all changes required by the advisory committee. The undersigned agree to abide by the statements above.

<div align="right">

Trang Mai, Student

Dr. J. Zach Hilt, Major Professor

Dr. Stephen Rankin, Director of Graduate Studies

</div>

FUNCTIONALIZATION OF IRON OXIDE NANOPARTICLES AND THE IMPACT ON

SURFACE REACTIVE OXYGEN SPECIES GENERATION FOR POTENTIAL

BIOMEDICAL AND ENVIRONMENTAL APPLICATIONS

DISSERTATION

A dissertation submitted in partial fulfillment of the
requirements for the degree of Doctor of Philosophy in the
College of Engineering
at the University of Kentucky

By
Trang Thi Thu Mai

Lexington, Kentucky

Director: Dr. J. Zach Hilt, Professor of Chemical & Materials Engineering

Lexington, Kentucky

2019

ABSTRACT OF DISSERATION

FUNCTIONALIZATION OF IRON OXIDE NANOPARTICLES AND THE IMPACT ON
SURFACE REACTIVE OXYGEN SPECIES GENERATION FOR POTENTIAL
BIOMEDICAL AND ENVIRONMENTAL APPLICATIONS

Iron oxide nanoparticles (IONPs) have been widely studied for a variety of applications, from biomedical applications (e.g., cell separation, drug delivery, contrast agent for magnetic resonance imaging and magnetically mediated energy delivery for cancer treatment) to environmental remediations (e.g., heavy metal removal and organic pollutants degradation). It has been demonstrated that IONPs can induce the production of reactive oxygen species (ROS) via Fenton/Haber-Weiss reactions which has been shown to be one of the key underlying mechanisms of nanoparticles toxicity. This inherent toxicity of nanoparticles has been shown to enhance the efficacy of traditional cancer therapies such as chemotherapy and radiation. In addition, the generation of ROS induced by IONPs has been also studied as advanced oxidation processes (AOP) for wastewater treatment. Recent research has also shown that exposure to an alternating magnetic field can significantly enhance the generation of ROS induced by IONPs. Moreover, the coatings of IONPs play an important role on the surface reactivity of nanoparticles since it can prevent the generation of ROS via Fenton chemistries at the surface of the nanoparticles.

In this work, co-precipitated IONPs were functionalized with small molecules including citric acid, sodium phosphate, amino silane and dopamine. The impact of coating on surface reactivity of the as-synthesized particles was studied using methylene blue dye degradation assay under AMF exposure. With the coatings of these small molecules, the IONPs induced ROS generation was significantly decreased because of the dense surface coverage. To study the effect of polymeric coatings, a degradable poly (beta amino ester) (PBAE) polymer coating was synthesized with dopamine as an anchor to bind to nanoparticles. The surface reactivity of the particles was expected to be recovered once the polymer coating was degraded. Furthermore, the impact of non-degradable PEG-based polymer coating on surface reactivity via ROS generation was also investigated using methylene blue decolorization assay with the presence of AMF. The retention of surface reactivity of PEG-based polymer coated IONPs shows promise for cancer treatment.

The application of IONPs as heterogeneous catalyst for organic contaminant degradation was investigated. Bisphenol A (BPA) was used as a model compound, and Fenton reactions were induced by IONPs with the presence of hydrogen peroxide and hydroxylamine as well as alternating magnetic field exposure. The kinetics of BPA degradation under water bath and AMF exposure at 37°C was also studied, and the results showed potential applications of IONPs for organic pollutants remediation.

KEYWORDS: Magnetic nanoparticles, reactive oxygen species, Fenton catalyst, magnetically mediated energy delivery, advanced oxidation processes, organic pollutants degradation

Trang Mai

Jun 18, 2019

FUNCTIONALIZATION OF IRON OXIDE NANOPARTICLES AND THE IMPACT ON
SURFACE REACTIVE OXYGEN SPECIES GENERATION FOR POTENTIAL
BIOMEDICAL AND ENVIRONMENTAL APPLICATIONS

By

Trang Thi Thu Mai

<div style="text-align:right">

Dr. J. Zach Hilt
Director of dissertation

Dr. Stephen Rankin
Director of Graduate Studies

Date

</div>

Table of contents

List of tables

List of figures

Chapter 1: Introduction

This dissertation investigated the effect of functionalization of iron oxide nanoparticles on surface reactive oxygen species generation upon alternating magnetic field (AMF) exposure. Iron oxide nanoparticles were used as the core materials and have been used in a variety of applications. Being magnetic, iron oxide nanoparticles can convert the energy absorbed from an alternating magnetic field (AMF) into heat through Neel relaxation (i.e., rotation of the magnetic moment to align with the field) and Brownian relaxation (i.e., the physical rotation of the particles in response to the magnetic field). This heat conversion has been extensively studied as magnetically mediated hyperthermia for cancer treatment. However, it has been demonstrated that intracellular effects (e.g., localized heating) without increasing bulk temperature seems to be more effective in the treatment of cancer. This conversion of magnetic field energy to heat, rotational work, etc. without significant increasing bulk temperature has been described as magnetically mediated energy delivery (MagMED). In addition to surface heating and rotational work, another potential effect of MagMED is the production of reactive oxygen species (ROS) such as hydroxyl radicals, superoxide radicals and hydrogen peroxide (OH$^\bullet$, HO$_2^\bullet$, H$_2$O$_2$) induced by iron oxide nanoparticles through via Fenton reactions and Haber-Weiss cycle. Free radicals produced through Fenton-like chemistry with the presence of endogenous hydrogen peroxide can cause cellular oxidative stress and lead to cell death. This is considered as the one of the key underlying mechanisms of nanoparticle toxicity. Several researches have shown that enhanced ROS generation can be utilized as a cancer therapy or to enhance activity of anticancer drugs which suggests a potential approach for combined treatment. Chapter 2 summarizes recent studies on magnetic nanoparticles and their ROS generation as well as potential applications in therapeutics.

To improve stability and biocompatibility, prevent agglomeration and provide functional groups, iron oxide nanoparticles are usually coated and coated by small molecules or polymers. However, the coatings can also inhibit the surface ROS generation induced by IONP occurring at the nanoparticles surface. To study the effect of small molecule coatings on surface ROS generation, chapter 3 presents the functionalization of iron oxide nanoparticles with several small molecules including citric acid, sodium phosphate, amino silane and dopamine and the generation of ROS under the presence of AMF. Biodegradable polymer coatings have shown very interesting results in biomedical applications. In chapter 4, PEG-based poly (beta amino ester) (PBAE) polymers were prepared and used as coating layer for iron oxide nanoparticles. Once this coating was degraded, the nanoparticles were expected to be re-exposed to the surrounding environment, and the surface reactivity of the particles was expected to be similar to uncoated iron oxide nanoparticles. The ability to produce ROS under AMF exposure of the degradable PBAE coated IONP was assessed before and after the hydrolysis of the polymers. Moreover, to investigate the impact of non-degradable polymer coating on surface reactivity of the nanoparticles, PEG-Dopamine polymers with various molecular weights were functionalized onto iron oxide nanoparticles surface in chapter 5, and the ROS formation via methylene blue decolorization assay was studied. In this chapter, the influence of coating process temperature as well as the initial polymer concentration on surface ROS formation was also studied.

In addition, Fenton processes have been widely used as advanced oxidation processes (AOPs) for wastewater treatments. This is based on the high potential oxidation of hydroxyl radical which can react with most organic substrate unselectively. Nevertheless, the environmental application of Fenton systems is still limited due to strict pH range and accumulation of sludges. To overcome these drawbacks, heterogeneous

catalysts such as iron oxides have been studied and shown to expand pH working range and prevent the formation of sludges. Besides, hydroxylamine has been demonstrated that it can accelerate the transformation of Fe (III) to Fe (II) and enhance the Fe (III)/Fe (II) redox cycle, thus increasing Fenton reaction rate and reducing sludge formation. The impact of hydroxylamine addition on the surface ROS generation induced by uncoated and several coated nanoparticles as well as the kinetics of methylene blue decolorization are presented in chapter 6. Lastly, in chapter 7, the application of uncoated iron oxide nanoparticles as a heterogeneous catalyst for the degradation of bisphenol A via Fenton process was studied with the presence of hydroxylamine upon AMF exposure.

1.1. Specific objectives

The overall objective of this research was to study the impact of functionalization of iron oxide nanoparticles on surface reactive oxygen species generation under the exposure of alternating magnetic field. This involved four projects, and the specific objectives of these projects are outlined below.

1. Functionalization of iron oxide nanoparticles with small molecules and study surface ROS generation under the exposure of AMF
   a. Synthesize uncoated iron oxide nanoparticles
   b. Functionalize uncoated particles with the small molecules (citric acid, sodium phosphate, amino silane and dopamine)
   c. Characterize of these synthesized particles
   d. Study surface reactive oxygen species generation via methylene blue dye decolorization.
2. Synthesis and functionalization of iron oxide nanoparticles with degradable poly (beta amino ester) for potential cancer treatment

a. Synthesize of uncoated iron oxide nanoparticles

b. Prepare and characterize poly (beta amino ester) (PBAE) polymers

c. Functionalize uncoated particles with PBAE polymers and properties characterization

d. Investigate surface reactivity of the degradable coated particle via methylene blue decolorization

3. Synthesis of PEG-based polymer coated iron oxide nanoparticles and study the impact of coating on surface reactive oxygen species generation upon AMF exposure

a. Synthesize and characterize uncoated nanoparticles

b. Prepare PEG-Dopamine coated iron oxide nanoparticles and characterize nanoparticle properties

c. Determine the effect of coating on surface ROS generation

4. Organic contaminant degradation via Fenton reaction induced by magnetite nanoparticle in the presence of alternating magnetic field

a. Prepare and characterize uncoated nanoparticles

b. Investigate the degradation of bisphenol A induced by uncoated nanoparticles under AMF exposure

c. Determine kinetic behavior of the degradation upon AMF exposure

Chapter 2: Magnetic nanoparticles: Reactive oxygen species generation and potential therapeutic applications

Abstract. Magnetic nanoparticles have been demonstrated to produce reactive oxygen species (ROS), which play a major role in various cellular pathways, via Fenton and Haber-Weiss reaction. ROS act as a double-edged sword inside the body. At normal conditions, the generation of ROS is in balance with their elimination by scavenger systems, and they can promote cell proliferation as well as differentiation. However, at an increased level, they can cause damages to protein, lead to cellular apoptosis, and contribute to many *diseases* including cancer. Many recent studies proposed a variety of strategies to either suppress toxicity of ROS generation or exploit the elevated ROS stress for cancer therapy.

Keyword. magnetic nanoparticles, oxidative stress, antioxidant, reactive oxygen species, biomedicine

2.1. Introduction

Magnetic nanoparticles (MNPs) possess many unique and novel characteristics compared to bulk materials [1], and these include comparable size to many biological molecules, high surface-to-volume ratio, and superparamagnetic properties. First, the increase of surface-to-volume ratio as the size of the particles decrease to nanoscale leads to many advantages in physical, chemical, electrochemical properties [2]. Second, the comparable size with biological molecules (protein, gene, cells, etc.) allows them to interact with or bind to biological entity and prolong their circulation time with appropriated coatings [3]. Third, superparamagnetic nanoparticles enable them to be manipulated by external magnetic field exposure without remanence once the field is removed [4]. These properties result in MNPs being promising for a variety of applications in diagnosis and

cancer therapy. The most common biomedical applications of the MNPs includes cell separation [5] and labeling [6]; targeted drug delivery [7], hyperthermia treatment [8, 9] and magnetic resonance imaging (MRI) [10-12].

MNPs are often coated with polymers or small molecules to enhance stability in aqueous and physiological media since uncoated MNPs have the tendency to aggregate together through their interaction with each other or with other biological molecules [13]. In addition to increasing colloidal stability, coatings also prevent MNPs from early elimination, prolongs circulation time in blood vessels as well as make them compatible for further functionalization [13-15].

Recently, MNPs have been proposed to generate reactive oxygen species (ROS) which has attracted much attention on ROS toxicity and its potential therapeutic applications (table 2.1). ROS are chemically reactive molecules, which have been proved to be either protective or harmful for living organism. ROS can promote cell proliferation and differentiation at a moderate level but damage DNA, protein and lipids at an excessive amount [16]. Recent studies showed that generation of ROS through Fenton and Haber-Weiss chemistries (Fig. 2.1) is one of the key underlying mechanisms for cytotoxicity of the MNPs [17]. Free radicals produced through Fenton-like chemistry with the presence of endogenous hydrogen peroxide can cause cellular oxidative stress and lead to cell death. It has been recently shown that ROS generation can be enhanced with the application of alternating magnetic field (AMF) without a measurable temperature rise [18].
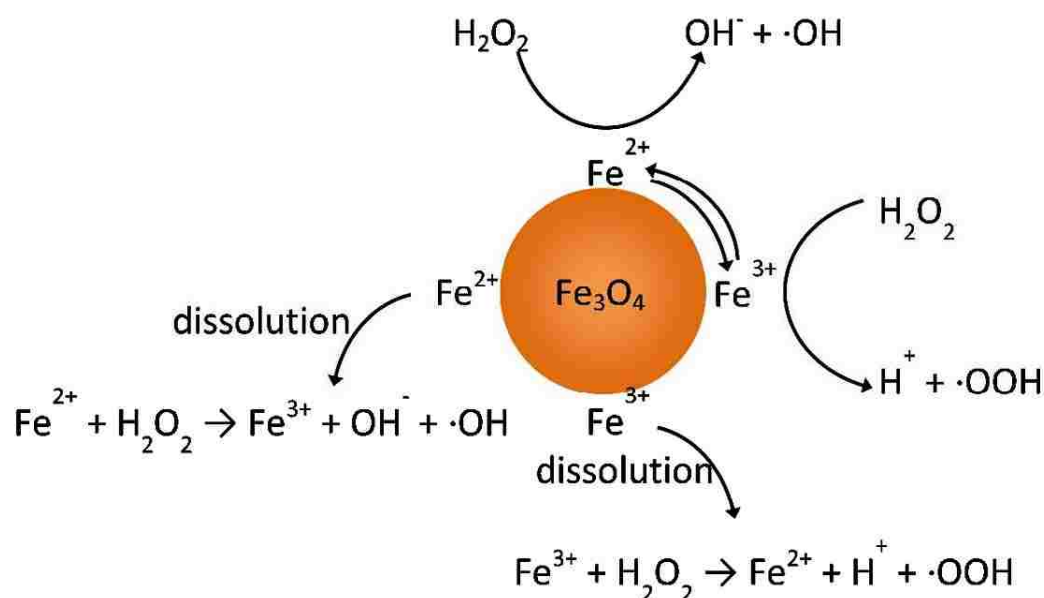
Figure 2.1: Fenton and Haber-Weiss reactions via iron oxide nanoparticles [18] (Reproduce with permission from RSC Advances)

Intracellular ROS generation is considered as a double-edged sword in therapeutic applications. As mentioned above, an elevated level of ROS can cause severe damage to the DNA, protein and cells. Especially, ROS production is proven to significantly enhance in the presence of nanoparticles, which in turns lead to increased toxicity and cellular death. Many studies have been carried out with the aim to either suppress the intracellular ROS formation or to increase ROS generation for cancer treatment (table 1). Researches have showed that ROS generation can be used to enhance activity of anticancer drugs which suggests a potential approach for combined treatment [19]. It has been exhibited that enhanced ROS production through AMF treatment led to an efficient internalization and significant apoptosis [17].

The main objective of this review is to summary recent studies on MNPs and their ROS generation as well as potential applications in therapeutics. Exploiting the increased ROS levels and altered oxidase-reduction reactions induced by MNPs for therapy will be capitalized. In addition, the potential of using antioxidants to suppress MNPs toxicity when needed via ROS reduction are also addressed. While most of the examples highlighted in this review focus on cancer applications, the modulation of ROS generation is applicable in many other disease states too [20, 21].

Table 2.1. Summary of ROS-related research with magnetic nanoparticles

Nanomaterial System			In vitro study				Ref
Nano-materials	Functionalization	Co-treatment	Cell line	Concentration of particles	Time of exposure	Response	
Fe_3O_4	Uncoated		Rat lung epithelial	0.5-20 µg/ml	78h	Inhibited cell proliferation and induced ROS	[22]
	Uncoated	L-ascorbic acid (AA)	HepG2 and A549	0-100 µg/ml	24h	Selectively induced apoptosis in cancer cell via ROS generation Prevent ROS generation with AA exposure	[23]
	PEG-silane coated		3T3, RAW267.4, MCF7	1; 10; 100 µg/ml	24h	Strong linear relationship between ROS generation and cytotoxicity	[24]
	Sodium oleate; Sodium oleate-PEG; Sodium		A549; HEL1249	0.1-2 mmol/l	30min-24h	Significant induction of DNA breakage in A549 cells but not HEL12469	[25]

						Induced variable low levels of intracellular ROS, but no remarkable increase in oxidative damage to DNA in either cell line	
oleate-PEG-PLGA coated							
PEG-*b*-PDPA micelle	β-lapachone	A549	0.14 mmol/l	48h		ROS promoting	[19]
Citric acid/glucose coated	AMF	CT26	5mg/ml	1h		Increased apoptosis when exposed to AMF	[17]
Citric coated	Poly(trolox) ester (PTx)	HUVECs	30 µg/ml	24h		Reduced free radical generation and recovered cell viability	[26]
Trans-activating transcriptional activator (TAT)	Radiation	A549	100-500 µg/ml	24h		Induced ROS generation and synergistic decrease in cell viability when combined with radiation	[27]

	peptide functionalized						
	TAT-functionalized	AMF	A549, H358	500 µg/ml	24h	Increased apoptosis when combined with AMF	[28]
Fe_2O_3	Uncoated		HepG2	25-100 µg/ml	12-24h	Induced oxidative stress by NPs with concentration and time dependence	[29]
$NiFe_2O_4$	Uncoated	AA	A549	0-100 µg/ml	24h	Induced oxidative stress via ROS generation and glutathione (GSH) depletion Mitigated ROS generation and GSH with AA co-treatment	[30]
	Uncoated	N-acetyl-cysteine (NAC)	HepG2; MCF7	5-25 µg/ml	24h	Co-treatment with NAC prevented cytotoxicity induced by $NiFe_2O_4$	[31]
$ZnFe_2O_4$	Uncoated	NAC	A549, A431, HepG2	10-40 µg/ml	24h	Significantly induced ROS generation and decreased cell	[32]

						viability of A549, HepG2, A431 ROS generation and cell death of all three cell lines were abrogated by co-treatment with NAC	
ZnO	Uncoated		RAW 264.7, BEAS-2B	0-50 µg/ml	1-16h	Induced toxicity in both cells, led to ROS generation and cell death	[33]
	Uncoated		HepG2, A549, BEAS-2B	5-15 µg/ml	24h	Induced ROS generation and apoptosis in cancer cells via p53 pathway	[34]
	Uncoated		S91	5-100 µg/ml	24h	Induced intracellular ROS production which correlated to apoptosis	[35]

	Aminopolysiloxane capped		RGC-5	0.63-10 µg/ml	24-72h	Increased ROS production led to cell damages and induced apoptosis/necrosis	[36]
NiO	Uncoated	Curcumin	Hep2; MCF7	1-100 µg/ml	24h	Induced oxidative stress and ROS production Significantly attenuated cytotoxicity and oxidative stress	[37]
CeO$_2$	Uncoated		RAW 264.7, BEAS-2B	25 µg/ml	1-16h	Suppressed ROS production and enhanced cell resistance to an exogenous oxidative stress source	[33]
	Oleic acid coated		Fibroblasts	50ppm	24h	Reduced intracellular ROS generation in fibroblasts 9-time higher than commercial trolox	[38]

Ni	Uncoated		HepG2	1-100 µg/ml	24h	Induced ROS generation and cytotoxicity and increase apoptosis	[39]

2.2. Suppressing cellular ROS formation

Oxidative stress is believed to be one of the key factors in the formation of a variety of diseases, including cancer, aging, cardiovascular and neurodegenerative diseases [40, 41]. It is induced by excessive ROS formation which can damage DNA, protein and lipid leading to cellular disfunction and death [26]. Therefore, concern has arisen regarding the severe side effect of ROS to the cells. Studies have shown that antioxidant and other cell redox modulating enzyme systems (AA, catalase, superoxide dismutase, GSH peroxidases and peroxiredoxins) can attenuate ROS generation [33, 40, 42-44]. Natural antioxidants which have been used to suppress cellular ROS formation include quercetin [45], curcumin [37], green tea polyphenol [46] and anthocyanins [47]. In addition to these natural antioxidants, poly (trolox ester) polymer and cerium oxide nanoparticles also exhibit antioxidant properties, which in turn reduce cellular ROS generation [26, 38, 41, 48].

In general, the toxicity of nanoparticles and magnetic nanoparticles particularly is still a debated issue, although there have been a variety of studies on nanoparticles and their toxicity in vitro and in vivo [49-51]. MNPs have been shown to enhance the formation of ROS intracellular, which results in cell damage and death [52, 53]. Several therapeutic strategies have been proposed to alleviate oxidative stress induced by MNPs. In this section, we focus on the recent studies on suppressing MNPs toxicity by reducing cellular ROS generation [20].

One potential approach to suppress MNPs toxicity is using an antioxidant to inhibit ROS generation, and in the following, we highlight a few recent studies using antioxidants to attenuate cellular ROS generation. In one example, Cochran et al. developed a targeted system based on an antioxidant PTx [26]. Once the polymeric nanoparticles were

enzymatically hydrolyzed, active trolox was locally released which in turn provided protection against the cytotoxicity induced by iron oxide nanoparticles (IONPs). While there was no significant protection against cytotoxicity of IONPs in the case of non-targeted polymer nanoparticles, the targeted ones showed 43.5 and 47.7% suppression of injury at 1 and 0.5 mg/ml, respectively (Fig. 2.2a). The results also showed a recovery in viability of 92% at 1 mg/ml and 65% at 0.5 mg/ml (Fig. 2.2b).
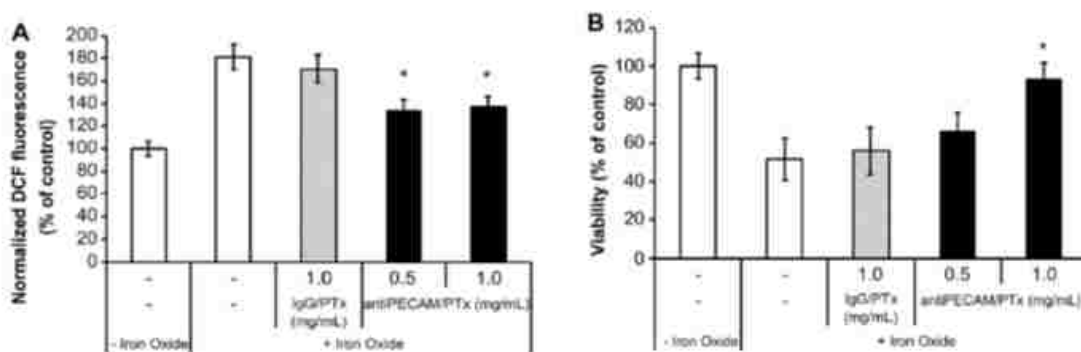
Figure 2.2. Suppression of iron oxide injury on human umbilical vein endothelial cells (HUVECs) at a concentration of 30 mg/ml after 1h incubation of poly(trolox) particles. (A) Dichlorofluorescein Fluorescence and (B) cellular viability 24 h after injury (* $p < 0.05$). [26] (Reprint with permission of Elsiver)

In another example of suppressing cytotoxicity of IONPs against two cell lines (human liver carcinoma HepG2 and human lung adenocarcinoma A549), Ahamed et al. used AA as an antioxidant for oxidative stress reduction [23]. It was found that IONPs induced the depletion of GSH and promoted the production of ROS in both types of cancer cells through p53 pathway while they did not affect these in normal cells. Moreover, it was also demonstrated that co-treatment with AA alleviated the cellular ROS generation in both two cancer cell lines (Fig. 2.3).
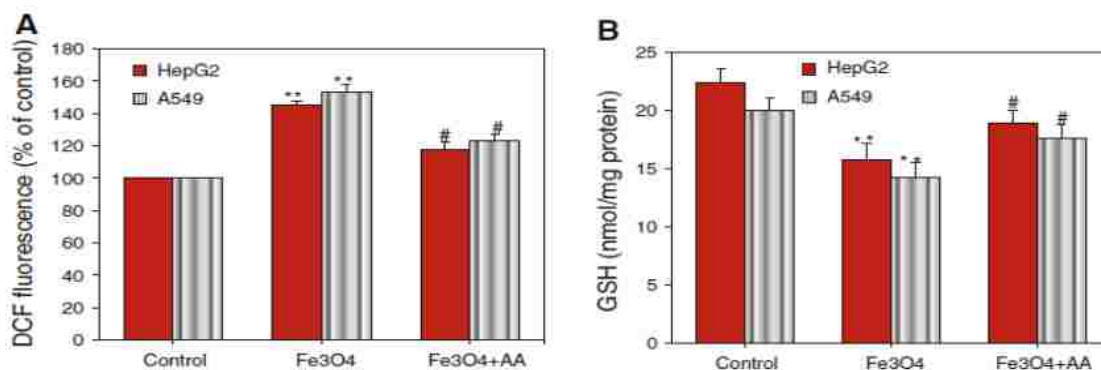
Figure 2.3. Fe$_3$O$_4$ NPs-induced oxidative stress in HepG2 and A549 cancer cells. (A) ROS level and (B) GSH level. (** Statistically significant difference compared to the control group (p < 0.01), # significant inhibitory effect of AA (p < 0.05)) [23] (Reprint with permission from Springer Nature)

With a similar idea of using AA as an antioxidant, the follow-up work studied on the activity of AA in mitigating cytotoxicity of nickel ferrite nanoparticle [30]. The results indicated a significant induction the intracellular production of ROS (1.52-fold) at concentration of 100 µg/ml for 24 hours when A549 cells were incubated with nickel ferrite nanoparticles. In addition, it also showed significant reduction in ROS generation and increase in GSH levels upon AA co-exposure (Fig. 2.4).
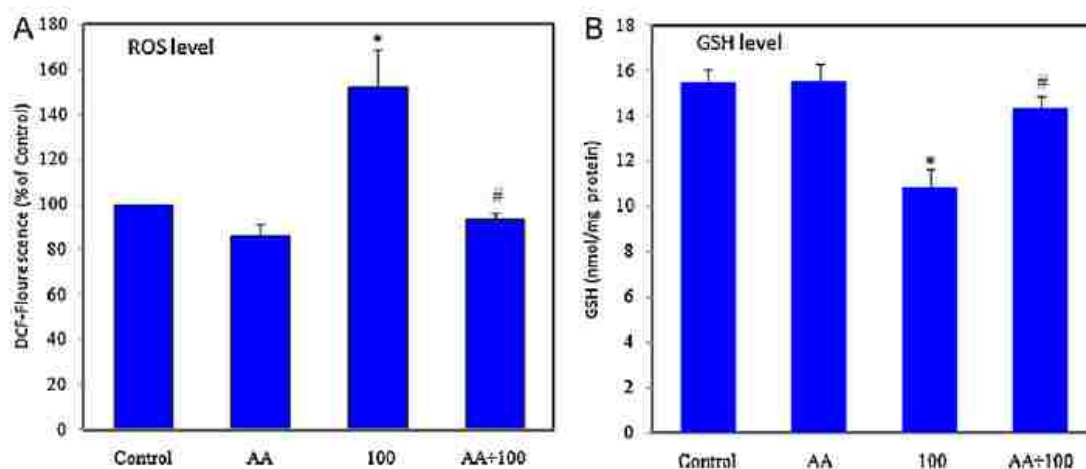
Figure 2.4. Nickel ferrite nanoparticle-induced oxidative stress in A549 lung cancer cells at a concentration of 100_g/ml for 24 h. (A) ROS level and (B) GSH level. (** Statistically significant difference compared to the control group ($p < 0.05$), # significant inhibitory effect of AA ($p < 0.05$)) [30] (Reproduce with permission of Elsevier)

Another example of preventing ROS generation was studied by Ahamed et al. where they used NAC as a ROS scavenger [31]. Nickel ferrite nanoparticles were shown to induce cytotoxicity to HepG2 and MCF7 cells in 5-25 µg/ml concentration range with a dose-dependent manner. Also, the oxidative stress induction was exhibited via the increase of intracellular ROS generation levels when exposed to nickel nanoparticles at concentration of 25 µg/ml (Fig. 2.5a). Furthermore, with the treatment of antioxidant NAC, the production of intracellular ROS was efficiently prevented leading to remarkable reduction in cytotoxicity of nickel nanoparticles. Similarly, Alhaqlaq et al. studied the cytotoxicity through ROS generation induced by zinc ferrite nanoparticles [32]. They showed that zinc ferrite nanoparticles induced ROS generation in a dose-dependent manner in A549, HepG2 and A431 cell lines. Furthermore, with the presence of NAC, ROS generation and cellular toxicity of zinc ferrite nanoparticles was almost abrogated in all three cell lines.
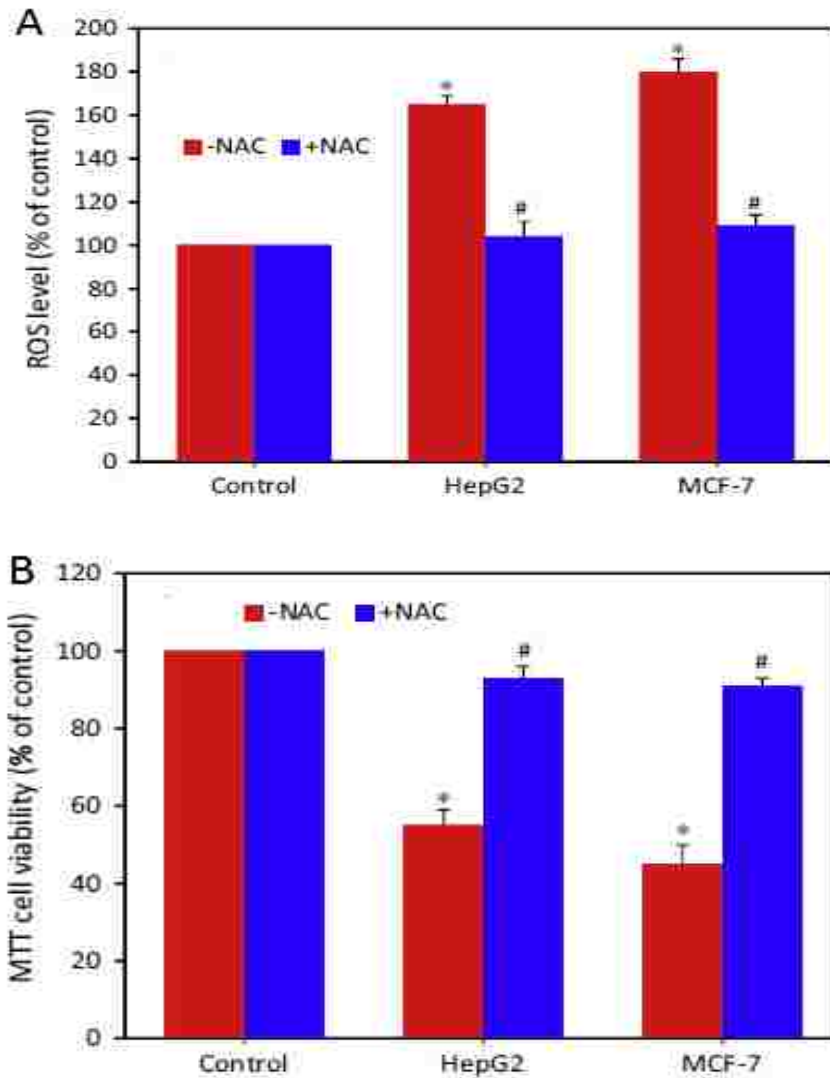
Figure 2.5. Cytotoxicity induction in liver cancer cells HepG2 and MCF-7 breast cancer cells through oxidative stress at 25 µg/ml of nickel ferrite NPs in the presence of 10 mM NAC for 24 h. (a) ROS level and (b) MTT cell viability. (* Statistically significant difference compared to the controls ($p < 0.05$), # significant inhibitory effect of NAC ($p < 0.05$)) [31] (Reprint with permission of Elsevier)

In other work, Shen et al. demonstrated the use of horseradish peroxidase to eliminate intracellular reactive oxygen species generation [54]. In this design, the horseradish peroxidase was immobilized onto magnetic mesoporous silica nanoparticles

(MMSNs) via the reaction between amino groups of horseradish peroxidase and carboxyl groups on the MMSNs surface. The results showed that cell viability increased with increasing concentration of MMSNs (0 - 400 µg/ml), which could be attributed to the ROS elimination effect.

2.3. Promoting ROS production in therapy

Recently, strategies exploiting increased ROS levels have been studied for therapeutic purposes. As previously mentioned, elevated levels of ROS can damage protein, DNA and lipids, which can lead to apoptosis/necrosis and cellular death. In the presence of endogenous hydrogen peroxide, the surfaces of IONPs can induce ROS production through Fenton-like reaction. In this section, we highlight recent efforts in using IONPs to induce ROS generation for cancer therapy enhancement.

Researchers have applied the ROS generation induced by IONPs to trigger apoptosis for cancer therapy. For example, Ahamed et al. demonstrated a selectively induced apoptosis in cancer cells (HepG2 and A549) via p53 pathway by IONPs with no toxicity to normal cells [23]. Similar finding was revealed by Hsieh et al. in which there is a strong linear correlation between increased ROS levels and cytotoxicity of the IONP on cancer cells but not normal cells [24]. Another study by Yu et al. showed that significant ROS formation was induced by 30 nm bare IONP while minimal ROS generation was induced by 5 nm particle. This study also revealed that either PEG or Dextran coating also reduced the cytotoxicity of the IONP [55].

In another example, Klein et al. showed the role of IONP on enhancing X-rays efficiency on ROS generation and releasing iron ions to the ROS generation via Fenton and Haber-Weiss reaction [56]. Recently, Hauser et al. also showed that TAT peptide functionalized IONP increased ROS generation significantly in combination with

radiotherapy at 5 Gy [27]. Additionally, Wydra et al. studied the effect of AMF on IONPs cytotoxicity through ROS generation [17]. In this study, various IONPs systems have been used for ROS enhancement study under the application of AMF at nanoparticle concentrations where there was no measurable temperature rise. There appears to be an increase in ROS generation in cells exposed to all of the IONPs systems upon AMF exposure compared to the control (Fig. 2.6a). Apoptosis study on CT26 cell line shows significant increase in percent apoptosis of cells exposed to all the IONPs systems with AMF exposure compared to no AMF exposure (Fig. 2.6b). Similar result was reported by Hauser et al. in which dextran coated IONP with TAT peptide functionalization showed an increase in cellular ROS generation upon AMF exposure without a measurable temperature rise [28].
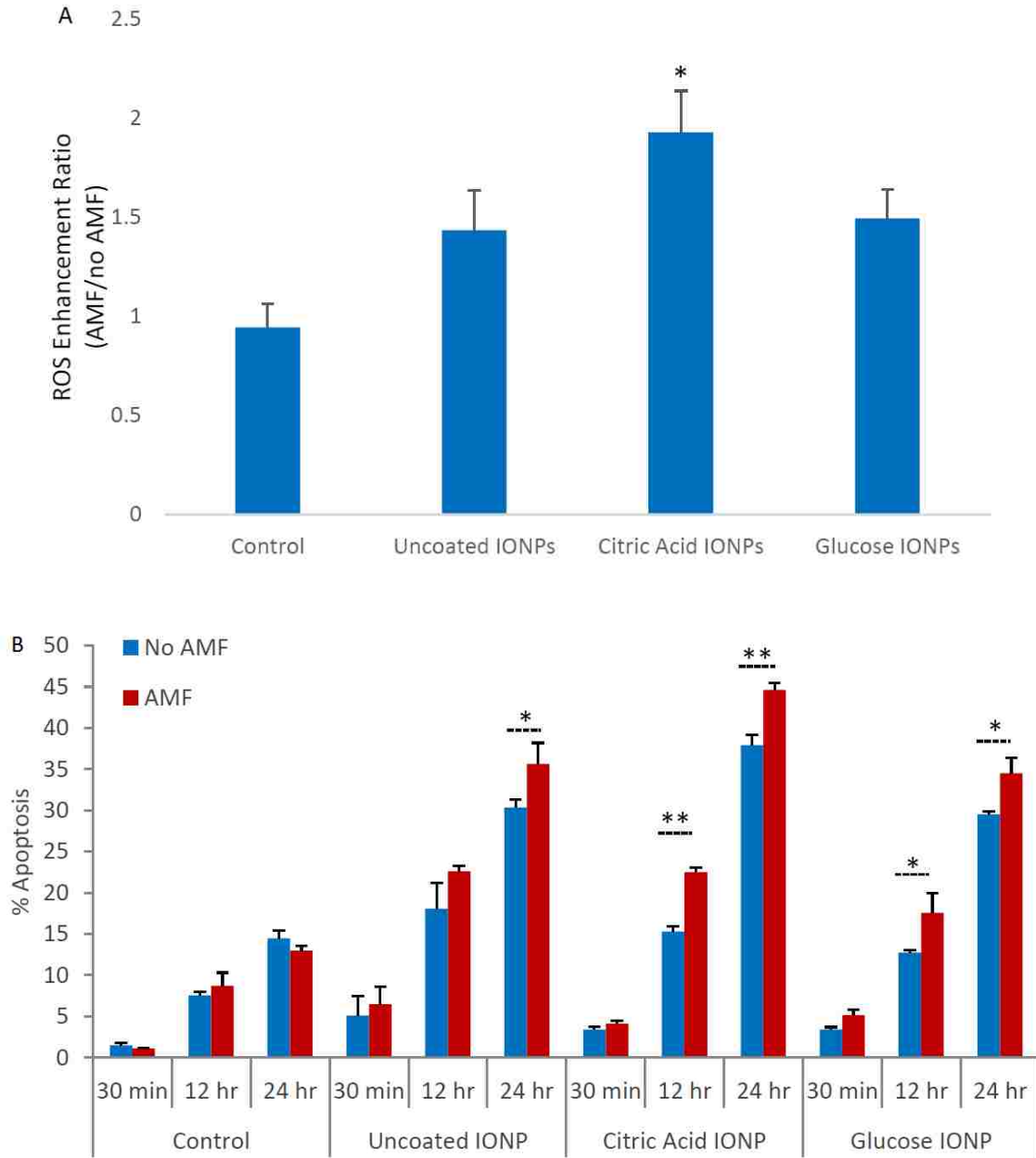
Figure 2.6. (A) ROS enhancement ratio of field exposure and no field exposure and (B) apoptosis percentage of CT26 colon cancer cells with and without AMF after 30 min, 12h and 24h eposure of treatment. (* $p < 0.05$, ** $p < 0.01$) [17] (Reprint with permission of Elsevier)

In addition to the various strategies to enhance ROS generation induced by IONP, several groups have exploited ROS generation induced by IONP for therapeutic enhancement of chemotherapy agents. Recently, Sahu et al. showed the synergistic effect of chemotherapy and ROS in killing cancer cells. In this study, PEGylated FePt-Fe_3O_4 composite nano-assemblies were combined with doxorubicin, a widely used anticancer drug, in the treatment of HeLa cancerous cells, which resulted in almost complete cell death while sparing normal cells [57]. In another example, Huang et al. developed a pH responsive superparamagnetic iron oxide nanoparticles (SPION) micelle system to amplify ROS stress and demonstrated the improved anticancer efficacy of β-lapachone, a novel anticancer drug [19]. Inside cancer cells, iron ions were selectively released from the micelles and reacted with hydrogen peroxide produced from β-lapachone. Hence, ROS levels were 10-fold increased through Fenton reaction in drug exposed cancer cells which led to significantly increased cellular death and greatly enhanced therapeutic efficacy (Fig. 2.7).
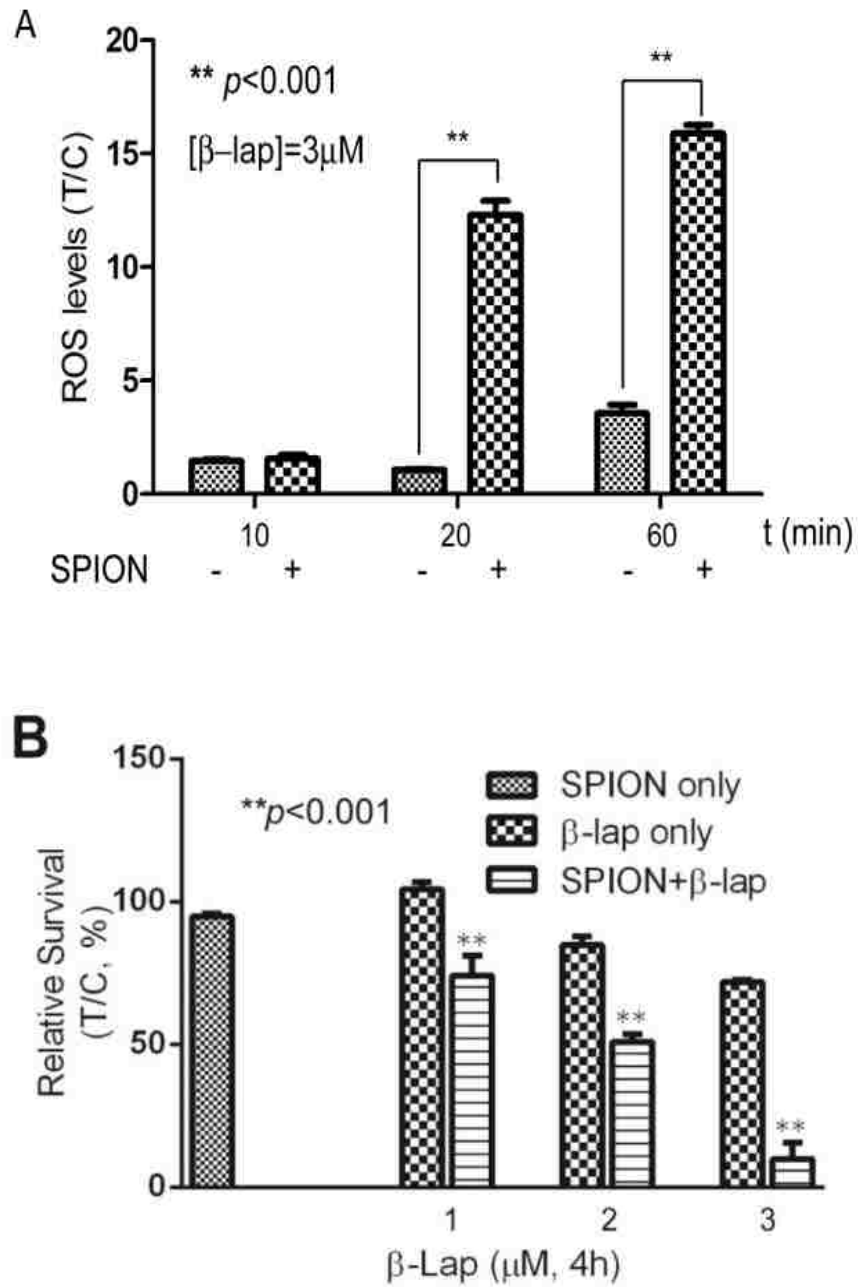
Figure 2.7. Quantifications of ROS levels (A) and Cell survival study (B) in A549 lung cancer cells with or without SPION-micelles pretreatment and by β-lap exposure (- associated to cells without SPION exposure, + associated to cells with SPION exposure) [19] (no required permission for reproduction)

2.4. Conclusions and future perspectives

The unique properties of nanomaterials have led to a remarkable increase in their application, and magnetic nanoparticles are one of the most widely applied nanomaterials, especially in biomedical fields. However, their toxicity has been a potential concern. Recently, many studies have addressed the toxicity of nanoparticles related to intracellular reactive oxygen species. In this review, we summarized the recent research on either suppressing or utilizing the toxicity of magnetic nanoparticles via reactive oxygen species generation.

Reactive oxygen species play an important role in many cellular pathways. However, they can also be troublesome if their concentrations are elevated inside the body. Also, induction of reactive oxygen species has been proposed as a key cytotoxicity mechanism of many nanoparticles such as zinc, nickel and iron oxide nanoparticles. With the idea of using antioxidants as an approach to inhibit intracellular ROS induction, several studies have been carried out to suppress ROS formation. Many kinds of antioxidants or substances that possess antioxidant activity have been used including AA, curcumin, quercetin, green tea polyphenol, NAC and PTx. They have gained some promising results in eliminating intracellular ROS generation and reducing cytotoxicity of magnetic nanoparticles

On the other side, utilizing the toxicity of nanoparticles as a strategy to improve current cancer therapies has gained much attention. Recent efforts have focused on exploiting the elevated reactive oxygen species formation for cancer treatment by increasing cellular apoptosis/necrosis via p53 pathway. Moreover, upon the application of an alternating magnetic field without a measurable temperature rise, the ROS generation can be triggered and result in a cellular effect. In addition to being used as a single

treatment, ROS formation can be used to enhance bioactivity of other treatments such as radiation and chemotherapy. Several recent studies have shown synergistic effects when combined ROS generation with either radiation or an anticancer agent. These results show great potential for therapeutic applications.

Although magnetic nanoparticles have been one of the most widely studied and applied materials in biomedical applications, there are still some aspects that have only been scratched at the surface. Reactive oxygen species generation induced by magnetic nanoparticles is one of these subjects. With appropriate design, we can either suppress the toxicity of magnetic nanoparticles or turn on the toxicity for therapeutic purposes. By controlling the toxicity of magnetic nanoparticles, there is great potential for medical treatments in the future, especially with targeting systems and/or the co-exposure of other treatments such as alternating magnetic field, radiation and chemotherapy.

2.5. References

1.   Wu, W., Q. He, and C. Jiang, *Magnetic Iron Oxide Nanoparticles: Synthesis and Surface Functionalization Strategies.* Nanoscale Research Letter, 2008. **3**: p. 397-415.

2.   Issa, B., et al., *Magnetic Nanoparticles: Surface effects and Properties Related to Biomedicine Applications.* International Journal of Molecular Sciences, 2013. **14**: p. 21266-21305.

3.   Pankhurst, Q.A., et al., *Applications of magnetic nanoparticles in biomedicine.* Journal of Physics D: Applied Physics, 2003. **36**: p. R167-R181.

4.   Laurent, S. and M. Mahmoudi, *Superparamagnetic iron oxide nanoparticles: promises for diagnosis and treatment of cancer.* International Journal of Molecular Epidermiology and Genetics, 2011. **2**(4): p. 367-390.

5.   Wang, D., et al., *Superparamagnetic Fe2O3 Beads−CdSe/ZnS Quantum Dots Core−Shell Nanocomposite Particles for Cell Separation.* Nano Letters, 2004. **4**(3): p. 409-413.

6.   Lewin, M., et al., *Tat peptide-derivatized magnetic nanoparticles allow in vivo tracking and recovery of progenitor cells.* Nature Biotechnology, 2000. **18**(4): p. 410-414.

7.   Namdeo, M., et al., *Magnetic nanoparticles for drug delivery applications.* J Nanosci Nanotechnol, 2008. **8**(7): p. 3247-3271.

8.   Pankhurst, Q.A., et al., *Progress in applications of magnetic nanoparticles in biomedicine.* Journal of Physics D: Applied Physics, 2009. **42**(22): p. 224001.

9.   Kruse, A.M., et al., *Synthesis and characterization of CREKA-conjugated iron oxide nanoparticles for hyperthermia applications.* Acta Biomaterialia, 2014. **10**: p. 2622-2629.

10.   Weissleder, R., et al., *MR imaging of splenic metastases: ferrite-enhanced detection in rats.* AJR Am J Roentgenol, 1987. **149**(4): p. 723-6.

11.   Weissleder, R., et al., *Ultrasmall superparamagnetic iron oxide: characterization of a new class of contrast agents for MR imaging.* Radiology, 1990. **175**(2): p. 489-93.

12. McCarthy, J.R. and R. Weissleder, *Multifunctional magnetic nanoparticles for targeted imaging and therapy.* Advanced Drug Delivery Reviews, 2008. **60**(11): p. 1241-51.

13. Amstad, E., M. Textor, and E. Reimhult, *Stabilization and functionalization of iron oxide nanoparticles for biomedical applications.* Nanoscale, 2011. **3**(7): p. 2819-2843.

14. Gupta, A.K. and M. Gupta, *Synthesis and surface engineering of iron oxide nanoparticles for biomedical applications.* Biomaterials, 2005. **26**(18): p. 3995-4021.

15. Frimpong, R.A. and J.Z. Hilt, *Magnetic nanoparticles in biomedicine: synthesis, functionalization and applications.* Nanomedicine (Lond), 2010. **5**(9): p. 1401-14.

16. Trachootham, D., J. Alexandre, and P. Huang, *Targeting cancer cells by ROS-mediated mechanisms: a radical therapeutic approach.* Nature review: drug discovery, 2009. **8**: p. 579-591.

17. Wydra, R.J., et al., *The role of ROS generation from magnetic nanoparticles in an alternating magnetic field on cytotoxicity.* Acta Biomaterialia, 2015. **25**: p. 284-292.

18. Wydra, R.J., et al., *Accelerated generation of free radicals by iron oxide nanoparticles in the presence of an alternating magnetic field.* Royal Society of Chemistry Advances, 2015. **5**(25): p. 18888-18893.

19. Huang, G., et al., *Superparamagnetic Iron Oxide Nanoparticles: Amplifying ROS Stress to Improve Anticancer Drug Efficacy.* Theranostics, 2013. **3**(2): p. 116-126.

20.   Poljsak, B., *Strategies for Reducing or Preventing the Generation of Oxidative Stress.* Oxidative Medicine and Cellular Longevity, 2011. **2011**.

21.   He, F. and L. Zuo, *Redox Roles of Reactive Oxygen Species in Cardiovascular Diseases.* International Journal of Molecular Sciences, 2015. **16**(11): p. 27770-27780.

22.   Ramesh, V., et al., *Magnetite induces oxidative stress and apoptosis in lung epithelial cells.* Molecular and Cellular Biochemistry, 2012. **363**: p. 225-234.

23.   Ahamed, M., et al., *Selective killing of cancer cells by iron oxide nanoparticles mediated through reactive oxygen species via p53 pathway.* Journal of Nanoparticles Research, 2013. **15**: p. 1225-1235.

24.   Hsieh, H.-C., et al., *ROS-induced toxicity: exposure of 3T3, RAW264.7, and MCF7 cells to superparamagnetic iron oxide nanoparticles results in cell death by mitochondriadependent apoptosis.* Journal of Nanoparticles Research, 2015. **17**: p. 70-83.

25.   Mesárosová, M., et al., *The role of reactive oxygen species in the genotoxicity of surface-modified magnetite nanoparticle.* Toxicology Letters, 2014. **226**: p. 303-313.

26.   Cochran, D.B., et al., *Suppressing iron oxide nano particle toxicity by vascular targeted antioxidant polymer nanoparticles* Biomaterials, 2013. **34**: p. 9615-9622.

27.   Hauser, A.M., et al., *Targeted iron oxide nanoparticles for the enhancement of radiation therapy.* Biomaterials, 2016. **105**: p. 127-135.

28.   Hauser, A.M., K.W. Anderson, and J.Z. Hilt, *Peptide conjugated magnetic nanoparticles for magnetically mediated energy delivery to lung cancer cells.* Nanomedicine (Lond), 2016.

29.   Sadeghi, L., F. Tanwir, and V.Y. Babadi, *In vitro toxicity of iron oxide nanoparticle: Oxidative damages on HepG2 cells.* Experimental and Toxicologic Pathology, 2015. **67**: p. 197-203.

30.   Ahamed, M., et al., *Oxidative stress mediated apoptosis induced by nickel ferrite nanoparticles in cultured A549 cells.* Toxicology, 2011. **283**: p. 101-108.

31.   Ahamed, M., et al., *Comparative cytotoxic response of nickel ferrite nanoparticles in human liver HepG2 and breast MFC-7 cancer cells.* Chemosphere 2015. **135**: p. 278-288.

32.   Alhadlaq, H.A., M.J. Akhtar, and M. Ahame, *Zinc ferrite nanoparticle-induced cytotoxicity and oxidative stress in diffrent human cells.* Cell and Bioscience, 2015. **5**(1): p. 1-11.

33.   Xia, T., et al., *Comparison of the Mechanism of Toxicity of Zinc Oxide and Cerium Oxide Nanoparticles Based on Dissolution and Oxidative Stress Properties.* ACS Nano, 2008. **2**(10): p. 2121-2135.

34.   Akhtar, M.J., et al., *Zinc oxide nanoparticles selectively induce apoptosis in human cancer cells through reactive oxygen species.* International Journal of Nanomedicine, 2012. **7**: p. 845-857.

35.   Wahab, R., et al., *ZnO Nanopar ticles Induce Oxidative Stress in Cloudman S91 Melanoma Cancer Cells.* Journal of Biomedical Nanotechnology, 2013. **9**(3): p. 441-449.

36.   Guo, D., et al., *Reactive oxygen species-induced cytotoxic effects of zinc oxide nanoparticles in rat retinal ganglion cells.* Toxicology in Vitro, 2013. **27**: p. 731-738.

37.   Siddiqui, M.A., et al., *Nickel oxide nanoparticles induce cytotoxicity, oxidative stress and apoptosis in cultured human cells that is abrogated by the dietary antioxidant curcumin.* Food and chemical toxicology, 2012. **50**: p. 641-647.

38.   Lee, S.S., et al., *Antioxidant properties of cerium oxide nanocrystal as a function of nanocrystal diameter and surface coating* ACS Nano, 2013. **7**(11): p. 9693-9703.

39.   Ahmad, J., et al., *Concentration dependant induction of ROS, cell cycle arrest and apoptosis in human liver cells after nickel nanoparticles exposure* Experimental Toxicology 2013. **30**(2): p. 137-148.

40.   Poljsak, B., D. Šuput, and I. Milisav, *Achieving the Balance between ROS and Antioxidants: When to Use the Synthetic Antioxidants.* Oxidative Medicine and Cellular Longevity, 2013. **2013**: p. 1-11.

41.   Wattamwar, P.P., et al., *Antioxidant activity of degradable polymer poly(trolox ester) to suppress oxidative stress injury in the cells* Advanced Functional Materials, 2010. **20**: p. 147-154.

42.   Karihtala, P. and Y. Soini, *Reactive oxygen species and antioxidant mechanisms in human tissues and their relation to malignancies.* APMIS, 2007. **115**: p. 81-103.

43.   Richard, P.U., et al., *New concepts to fight oxidative stress: nanosized three dimensional supramolecular antioxidant assemblies.* Expert Opinion on Drug Delivery, 2015. **12**(19-27).

44.   Novo, E. and M. Parola, *Redox mechanisms in hepatic chronic wound healing and fibrogenesis.* Fibrogenesis & Tissue Repair, 2008. **1**(5): p. 1-58.

45.   Chen, T.-J., et al., *Quercetin inhibition of ROS-dependent and -independent apoptosis in rat glioma C6 cell.* Toxicology, 2006. **223**: p. 113-126.

46.   Guo, S., E. Bezard, and B. Zhao, *Protective effect of green tea polyphenols on the SH-SY5Y cells against 6-OHDA induced apoptosis through ROS – NO pathway.* Free Radical Biology & Medicine, 2005. **39**: p. 682-695.

47.   Tsuda, T., F. Horiob, and T. Osaw, *The role of anthocyanins as an antioxidant under oxidative stress in rat.* BioFactors, 2000. **13**: p. 133-139.

48.   Wenzel, U., et al., *Ascorbic acid suppresses drug-induced apoptosis in human colon cancer cells by scavenging mitochondrial superoxide anions.* Carcinogenesis, 2004. **25**(5): p. 703-712.

49.   Yang, W.J., et al., *Difference betwen toxicities of iron oxide magnetic nanoparticles with various surface functional groups against human normal fibroblast and fibrosarcoma cells.* Materials Chemistry and Physics, 2013. **6**: p. 4689-4706.

50.   Nel, A., et al., *Toxic Potential of Materials at the Nanolevel.* Science, 2006. **311**: p. 622-628.

51.   Aljarrah, K., et al., *Magnetic nanoparticles sensitize MCF-7 breast cancer cells to doxorubicin-induced apoptosis.* World Journal of Surgical Oncology, 2012. **10**: p. 62-62.

52.   Manke, A., L. Wang, and Y. Rojanasakul, *Mechanisms of Nanoparticle-Induced Oxidative Stress and Toxicity.* Biomedical Research International, 2013: p. 1-15.

53.   Fu, P.P., et al., *Mechanisms of nanotoxicity: Generation of reactive oxygen species.* Journal of Food and Drug Analysis 2014. **22**: p. 64-75.

54.   Shen, Y., et al., *Horseradish peroxidase-immobilized magnetic mesoporous silica nanoparticles as a potential candidate to eliminate intracellular reactive oxygen species.* Nanoscale, 2015. **7**: p. 2941-2950.

55.   Yu, M., et al., *Dextran and Polymer Polyethylene Glycol (PEG) Coating Reduce Both 5 and 30 nm Iron Oxide Nanoparticle Cytotoxicity in 2D and 3D Cell Culture.* International Journal of Molecular Sciences, 2012. **13**: p. 5554-5570.

56.   Klein, S., et al., *Superparamagnetic iron oxide nanoparticles as radiosensitizer via enhanced reactive oxygen species formation.* Biochemical and Biophysical Research Communications, 2012. **425**: p. 393-397.

57.   Sahu, N.K., J. Gupta, and D. Bahadur, *PEGylated FePt–Fe3O4 composite nanoassemblies (CNAs): in vitro hyperthermia, drug delivery and generation of reactive oxygen species (ROS).* Dalton Transactions, 2015. **44**: p. 9103-9113.

Chapter 3: Functionalization of iron oxide nanoparticles with small molecules and the impact on reactive oxygen species generation for potential cancer therapy

Abstract. Iron oxide nanoparticles (IONPs) and their cytotoxicity via reactive oxygen species (ROS) generation have attracted much attention in the last several years. Recent studies show that alternating magnetic field (AMF) exposure can enhance the production of ROS by IONPs, and these ROS have potential use in therapeutic applications. The aim of this research was to develop iron oxide nanoparticles-based platforms with small molecule coatings and to study impact of the coating on the surface reactivity of the particles. Iron oxide nanoparticles were synthesized by a co-precipitation process and coated with citric acid, sodium phosphate, amino-silane, or dopamine. Physicochemical properties of the particles including hydrodynamic size, amount of coating, and AMF heating ability were investigated. Surface reactivity via ROS generation by the particles was evaluated using a methylene blue decolorization assay with hydrogen peroxide and various AMF exposures. It was demonstrated that in general small molecule coatings decreased surface reactivity of IONPs by inhibiting ROS generation compared to uncoated IONPs. These results indicated that small molecules inhibit the ability to use enhancement of ROS generation, and this is important to consider in the design of these systems for cancer therapy and other therapeutic applications.

3.1. Introduction

Iron oxide nanoparticles (IONP) have been widely used for a variety of biomedical applications including magnetic resonance imaging (MRI) [1-3], drug delivery [4], cell separation and labeling [5, 6] and magnetically mediated hyperthermia (MMH) [7, 8]. In MMH, the particles absorb energy from alternating magnetic field (AMF) and convert it into

heat through Neel and Brownian relaxation [9]. Moreover, it has been shown recently that AMF exposure can induce cellular toxicities of the nanoparticles without a significant temperature rise [10-12]. Creixell et al. has shown that the internalized magnetic nanoparticles can significantly reduce cell viability without a sensible bulk temperature rise [10] while Villanueva et al. demonstrated that HeLa cell death can be triggered by silica-coated manganese oxide nanoparticles with temperature increase of lower than $0.5\,^{\circ}C$ [11]. This phenomenon has been coined as magnetically mediated energy delivery (MagMED) which describes the conversion of magnetic field energy to other forms such as heat or rotation work without significant bulk temperature rise [13].

In addition to thermal and mechanical effects of MagMED, chemical effects of the rotation of the nanoparticles under AMF exposure may induce toxicity. One of the potential chemical effects would be the production of reactive oxygen species (ROS) induced by IONP. IONP can induce the formation of hydroxyl radical, one of the highly reactive ROS, in biological systems via Fenton (equation 1) and Haber-Weiss reaction (equation 2).

$$Fe^{3+} + O_2^{\cdot-} \rightarrow Fe^{2+} + O_2$$
$$Fe^{2+} + H_2O_2 \rightarrow Fe^{3+} + OH^- + OH^{\cdot} \tag{1}$$

$$\tag{2}$$
$$O_2^{\cdot-} + H_2O_2 \rightarrow O_2 + OH^- + OH^{\cdot}$$
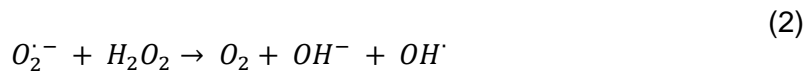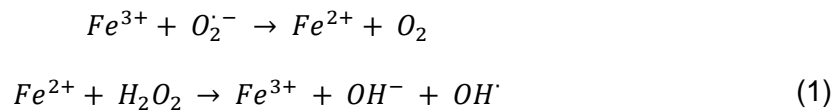
Inside the cells, ions can be released into the cytosol and catalyze Haber-Weiss reaction or the reactions can happen at the surface of the nanoparticles [14]. Free radical generation can cause oxidative stress to the cells which is considered as one of the key underlying mechanism of cytotoxicity [15, 16]. Recent study by Wydra et al. showed that ROS generation induced by IONP can be enhanced in the presence of AMF with no measurable temperature rise [17].

In order to increase stability and biocompatibility in physiological media, IONP are usually coated with either small molecules or polymers to prevent them from agglomerating or interacting with each other and biomolecules [18]. These coatings include inorganic materials (gold [19], silica [20, 21]), small molecules (carboxylates, phosphates, sulfates, etc.) [22, 23] or polymeric stabilizers (dextran, PEG, chitosan, etc.) [7, 23, 24]. Coatings also help to prolong circulation time in blood vessels and to avoid early elimination out from the body [18, 25, 26]. However, on the other side, coatings may affect surface reactivity of nanoparticles since they cover some surface area of the particles [27].

In this work, IONPs were synthesized by a coprecipitation method and coated with four different small molecules including citric acid, sodium phosphate, amino silane and dopamine. These molecules are known to have strong binding to iron oxide nanoparticles. The crystallinity properties of the particles before and after surface modification was studied using X-ray diffraction (XRD) while the coating was confirmed through Fourier transform infrared spectra (FTIR) and thermogravimetric analysis (TGA). Particles properties including hydrodynamic size and specific adsorption rate were also examined. The ability to generate ROS of the uncoated and coated particles was studied using a methylene blue decolorization assay under AMF exposure for 30 minutes.

3.2. Materials and methods

3.2.1. Materials

Iron (III) chloride hexahydrate ($FeCl_3 \cdot 6H_2O$), iron (II) chloride tetrahydrate ($FeCl_2 \cdot 6H_2O$), dopamine hydrochloride, hydrogen peroxide and methylene blue were obtained from Sigma Aldrich (St. Louis MO). Citric acid monohydrate and sodium phosphate dibasic anhydrous was from Fisher Scientific. Ammonium hydroxide was purchased from EMD chemicals (Gibbstown, NJ). 3-aminopropyl trimethoxysilane was from Gelest Inc. (Morrisville, PA). All materials were used without any modification.

3.2.2. Iron oxide nanoparticles (IONP) synthesis

A one-pot co-precipitation method was used to synthesize the uncoated iron oxide nanoparticles (UC-IONP) [28]. Typically, 40 ml aqueous solution of $FeCl_3 \cdot 6H_2O$ and $FeCl_2 \cdot 6H_2O$ in 2:1 molar ratio (2.2g and 0.8g, respectively) was prepared in a sealed three-neck flask. The mixture was heated to 85^oC while vigorous stirring under inert environment (nitrogen flow). Once the temperature reached 80^oC, 5 ml of NH_4OH was added into the mixture and the reaction was performed for one hour at 85^oC. The particles were then magnetically decanting and washed three time with deionized (DI) water. The nanoparticles were then re-suspended in DI water and dialyzed against DI water for 24 hours with water changing every 2-3 hours.

3.2.3. Small molecule functionalized iron oxide nanoparticle synthesis

Citric acid coated (CA-IONP), and sodium phosphate coated (SP-IONP) iron oxide nanoparticles were prepared using a modified one-pot approach described in previous section in which 4 ml of 2M citric acid or sodium phosphate was injected after the addition of ammonium hydroxide into the system [28]. The reaction was also carried out for one hour at 85^oC. The samples were dialyzed for 48 hours against DI water and water was changed frequently after 2-3 hours.

For amino silane coated iron oxide nanoparticles (AS-IONP), UC-IONP (100mg) were dispersed into 15ml of DI water and stirred with 3-aminopropyl trimethoxysilane (dissolved in 5ml of ethanol) for 24 hours at room temperature. The molar ratio of Fe_3O_4 particles to amino silane was 1: 2. The functionalized particles were then washed with ethanol and DI water three times to remove unreacted amino silane. The particles were finally dispersed in DI water by probe sonication for 10 minutes and dialyzed against DI water for 24 hours (changing water every 2-3 hours).

The UC-IONP were surface modified with dopamine (DA-IONP) using procedure reported by Gao in which 100mg of uncoated particles were added to 40ml of DI containing 100mg of dopamine hydrochloride [29]. The reaction mixture was sonicated for 30 minutes and stirred at room temperature for 24 hours. The product was then washed three time with DI water and dialyzed against DI water for 24 hours while changing water after 2-3 hours.

3.2.4. Particle characterization

X-ray powder diffraction (XRD) was used to confirm the magnetite crystal structure of the synthesized iron oxide nanoparticles. The XRD measurement was performed on a Siemens D500 X-ray spectrometer with a CuKα radiation source at 40kV and 30mA from 5° to 65° with the rate of 1° per minute.

Dynamic light scattering (DLS) was performed to analyze size distribution of nanoparticles while zeta potential was done to measure the potential at the surface of the particles. Nanoparticles were prepared at concentration of 0.1 mg/ml in DI water and PBS for DLS and DI water for zeta poential and ultrasonicated for 10 min. DLS and zeta potential measurements were performed triplicate using Malvern Zetasizer, Nano ZS90 instrument.

Fourier transformed infrared spectroscopy (FTIR) was used to characterized surface functionalization of the particles. Dried samples were loaded on a diamond attenuated total reflectance (ATR) crystal and the spectrum was recorded from 700 cm-1 to 4000 cm-1 using ATR FTIR with Varian Inc. 7000e spectrometer*.*

Thermogravimetric analysis (TGA) was used to determine the amount of polymer coating in nanoparticles (TA instrument Q50 TGA/DSC system). Dried particles (5-10mg) were heated at a rate of 5°/min to 120°C at which it was held isothermally for 20 min to remove any residual water. The samples were then heated continuously at 5°/min until

reaching 500°C and held there for another 20 min. The mass loss was normalized to the mass after isothermal heating at 120°C.

Ultraviolet visible (UV-Vis) spectroscopy was used to study stability of nanoparticles in DI water. The synthesized nanoparticles were dispersed into DI water at concentration of 0.1 mg/ml and the kinetic measurement was performed for 12 hours at wavelength of 540nm. The data was normalized to the initial absorbance of the particles.

Alternating magnetic field (AMF) heating was done to measure heating profiles of the nanoparticles using a Taylor Winfield magnetic induction source. Temperature was measured using a fiber optic temperature sensor (Luxtron FOT Lab kit). Nanoparticles were suspended in DI water to a concentration of 3 mg/ml iron oxide. One ml of the solution was placed in a centrifuge tube and placed in the center of AMF induction coil. The solution was heated under the magnetic field of 58 kA/m and 292 kHz for 15 min. The specific adsorption rate (SAR) values were calculated using the following equation (1)

$$SAR = \frac{C_{p,Fe}m_{Fe} + C_{p,H_2O}m_{H_2O}}{m_{Fe}} \frac{\Delta T}{\Delta t} \tag{1}$$

where C_p is the specific heat capacity (0.65 and 4.18 J/g*K for iron oxide and water, respectively), m_{Fe}, m_{H_2O} is the mass of iron and water respectively. $\Delta T/\Delta t$ is the initial slope of the heating profile which is calculated from 20 and 30 second time point.

3.2.5. Evaluation of ROS generation

The generation of ROS was measured using methylene blue decolorization assay [9]. The methylene blue degradation experiments were performed at either 37°C controlled water bath or exposed to an AMF. One ml of sample was prepared by diluting stock concentrations of methylene blue to 5 µg/ml and iron oxide nanoparticles to 75 µg/ml with

DI water. The samples were placed in the water bath for 10 min to equilibrate to the set temperature. The degradation was initiated by spiking the samples with 25 µl of H_2O_2. After given time intervals the samples were centrifuged at 6000rpm for 2 minutes, magnetically decanted for 30 seconds, and the supernatants were measured using UV-visible spectroscopy (maximum absorbance at 665 nm) with a Varian Cary. To account for nanoparticle scattering from the nanoparticles that remain in suspension, samples containing only nanoparticles were measured and subtracted out from the sample absorbance. Samples exposed to the AMF were prepared as described above. They were placed in water baths which corresponded to the expected steady state temperature by AMF exposure (37°C). Then, the samples were exposed to a field of approximately 58.0 kA/m in strength at 292 kHz frequency while temperature was measured with a Luxtron FOT Lab Kit. Statistical analysis of the ROS generation was completed using a two-way ANOVA test with replication.

3.3.   Results and discussion

3.3.1.   Nanoparticles synthesis and functionalization

Uncoated iron oxide nanoparticles were synthesized through coprecipitation method using 30% ammonium hydroxide as reducing agent with 2:1 ratio of iron salts. The coating of small molecule systems onto uncoated iron oxide nanoparticles was illustrated in figure 3.1. Citric acid interacted with IONP via interaction of carboxylate groups while phosphate groups conjugated the particles with sodium phosphate. Amino-silane is bound to the surface of IONP through silane functional groups while IONP was coated with dopamine through the catechol group or the formation of polydopamine on to particle surface. XRD was used to study crystalline properties of the as-synthesized uncoated and coated nanoparticles. The observed peaks at 30°, 35.3°, 43.2°, 53.6°, 57.2° and 62.5° can be assigned to (220), (311), (400), (422), (511) and (440) planes of magnetite

nanoparticles in cubic phases [29]. Though these peaks also match closely with XRD pattern of γ-Fe$_2$O$_3$, the black color indicated the presence of Fe$_3$O$_4$ in the uncoated particles as well as nanoparticles after coated with small molecules
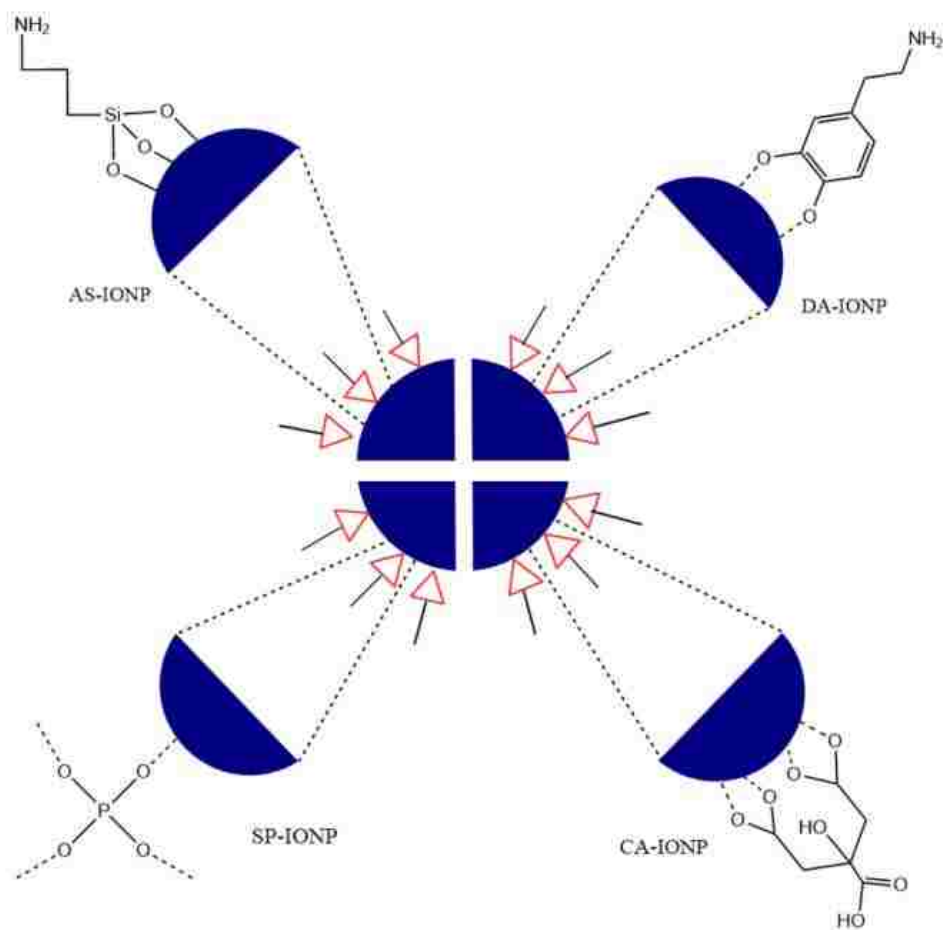
Figure 3.1. Illustration of small molecules coated iron oxide nanoparticles
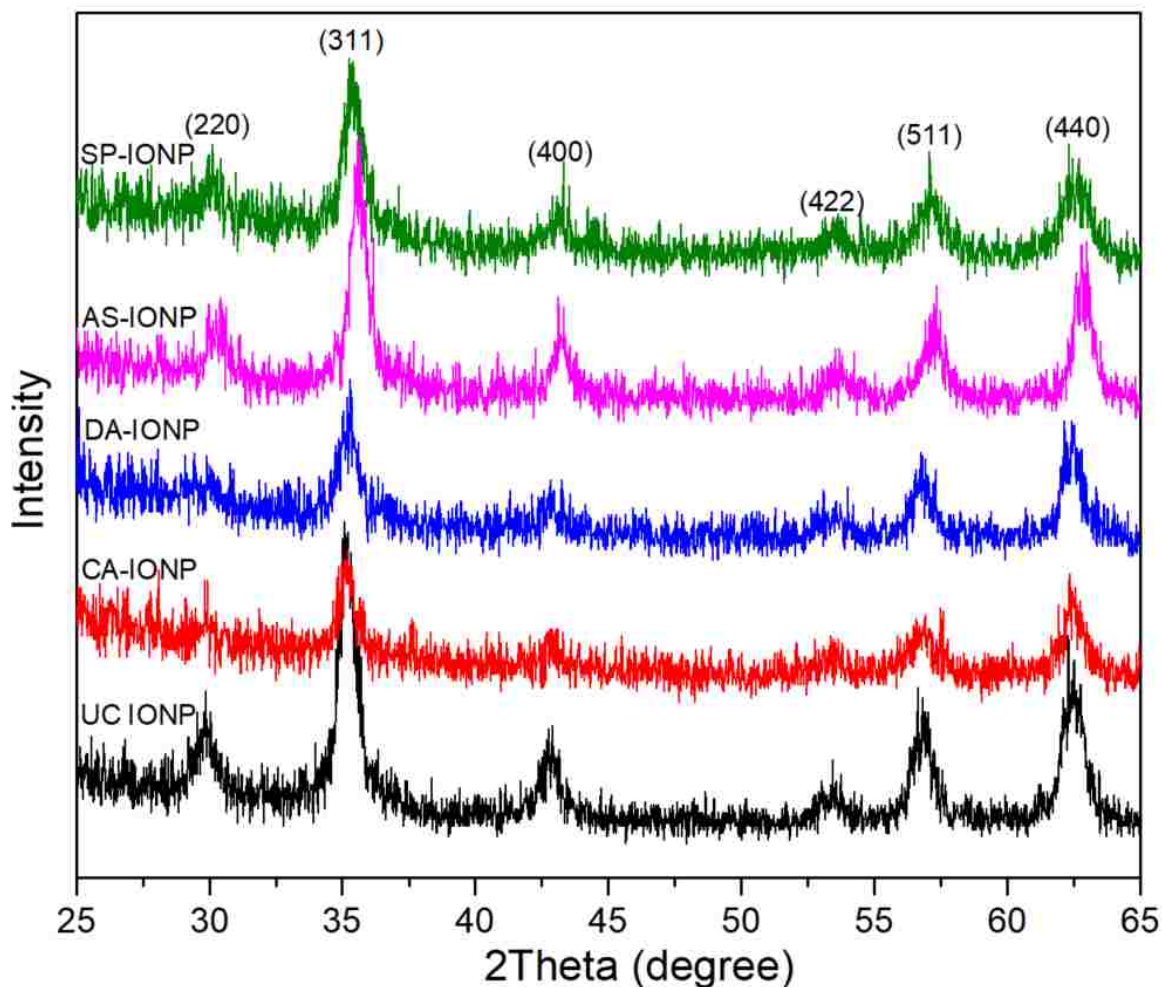
Figure 3.2. XRD patterns of the uncoated and coated nanoparticles

The coating of small molecules onto the particle was confirmed using FTIR which is shown in figure 3.2. For CA-IONP spectrum, the 1600 cm^{-1} peak can be assigned to the C=O symmetric stretching from the carboxyl group of citric acid while peak at 1360 cm^{-1} corresponded to asymmetric stretching of C–O group from the COOH group. This peaks are similar with the one reported by Racuciu et al. [30]. For SP-IONP, the appearance of broad peak between 900–1150 cm^{-1} corresponded to P–O–Fe stretching band confirmed the interaction of phosphate with particles [31]. In the spectrum of AS-IONP, the broad and low-density bands at 1400-1600 cm^{-1} are assigned to amino groups (both associated and free), which are possibly overlapped by vibration of hydroxyl group [32]. The peak at

42

1454 cm^{-1} is attributed to vibration of NH$_3^+$ in the bond of SiO- and NH$_3^+$ [32] while the one at 1103 cm^{-1} corresponds to siloxane anchoring group (Si–O–Si) [33]. The bands observed at 1400-1600 cm^{-1} in spectrum of DA-IONP are attributed to the symmetric and asymmetric stretching vibration of aromatic C–C bands [29]. The observation of all characteristic peaks of small molecules in FTIR spectra confirmed the successful coating of those small molecules onto the particle surface.
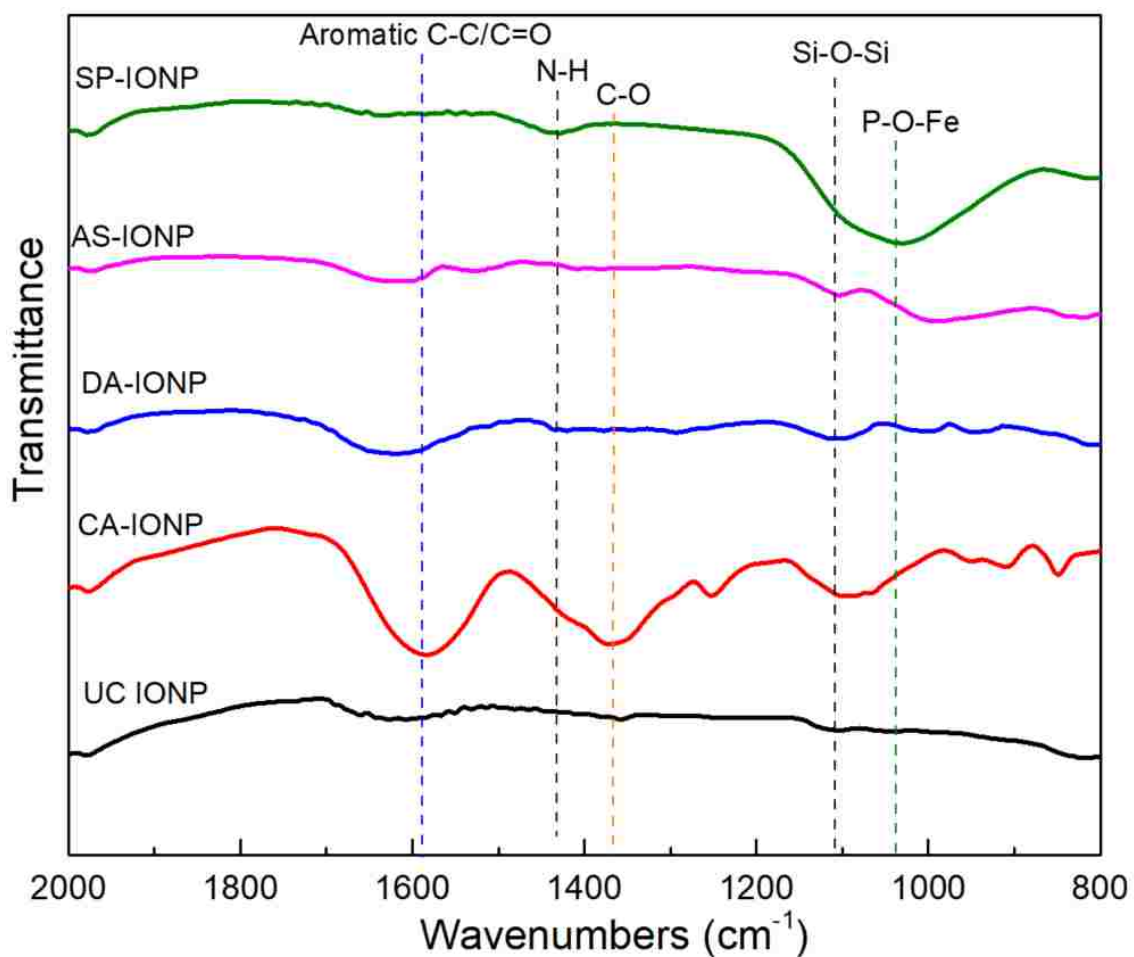
Figure 3.3. FTIR spectra of uncoated iron oxide nanoparticles and small molecule coated particles.

3.3.2. Nanoparticle properties

Size and zeta potential measurements of uncoated and small molecule coated IONP are summarized in table 3.1 (with n = 6 for each sample). The main peak of UC-IONP was about 100nm in DI water. After coating with small molecules, it increased to 140-160nm for most of the cases except for the citric acid coated. This could be explained by the adsorption of citric acid onto particles surface could inhibit the nuclei growth resulting in smaller particle size. It should be noted that the small molecule coating onto nanoparticles in some cases are not very stable and can be desorbed. UC-IONP has a relatively neutral surface charge while there are two main trends in coated particles. CA-IONP and SP-IONP are highly negatively charged (-35 mV for both systems) due to the carboxylate and phosphate at the surface of the particle. This is quite close with value reported by literature [31, 34, 35] On the other hand, AS-IONP and DA-IONP with amino groups located at the particles surface have a relatively positive charge, 27 and 11 mV respectively, which is lower than some previously reported values [33, 36].

Table 3.1. Summary of nanoparticle properties

Samples	Main peak (nm)	PDI	Zeta potential (mV)	SAR (W/g)
UC-IONP	106.4 ± 2.1	0.292 ± 0.01	8.8 ± 1.3	379.4 ± 8.4
CA-IONP	87.0 ± 1.4	0.225 ± 0.01	-35.2 ± 1.1	305.7 ± 15.8
SP-IONP	160.4 ± 5.8	0.236 ± 0.02	-35.1 ± 2.0	240.8 ± 49.6
AS-IONP	156.7 ± 1.6	0.146 ± 0.02	27.0 ± 2.1	264.9 ± 18.3
DA-IONP	141.1 ± 1.0	0.178 ± 0.01	11.4 ± 0.6	334.1 ± 45.2

TGA was used to further confirm the presence of the coatings and to determine the amount of coatings on the IONP. As shown in figure 3.4, the UC-IONP showed about 2% mass loss, which is likely due to some organic contaminants on the surface. For the

coated particles, there were similar amounts of mass loss between those coatings, which ranged from 4.3 to 6.5%. From these values, the surface coverage of small molecules onto iron oxide nanoparticles surface was calculated to be from 15-18 molecules/nm^2. The heating properties of the nanoparticles systems under AMF exposure (58kAm^{-1} and 292kHz) was studied at concentration of 3 mg/ml and the specific adsorption rate (SAR) was calculated using equation 1. The calculated SAR values were summarized in table 3.1. The SAR value of UC-IONP was determined to be about 380 W/g which is the highest value for these systems. After coating, SAR values decreased to around 300 W/g for CA- and DA- coated IONP. The SAR of AS-IONP was about 260 W/g while that of SP-IONP was 240 W/g, the lowest one).
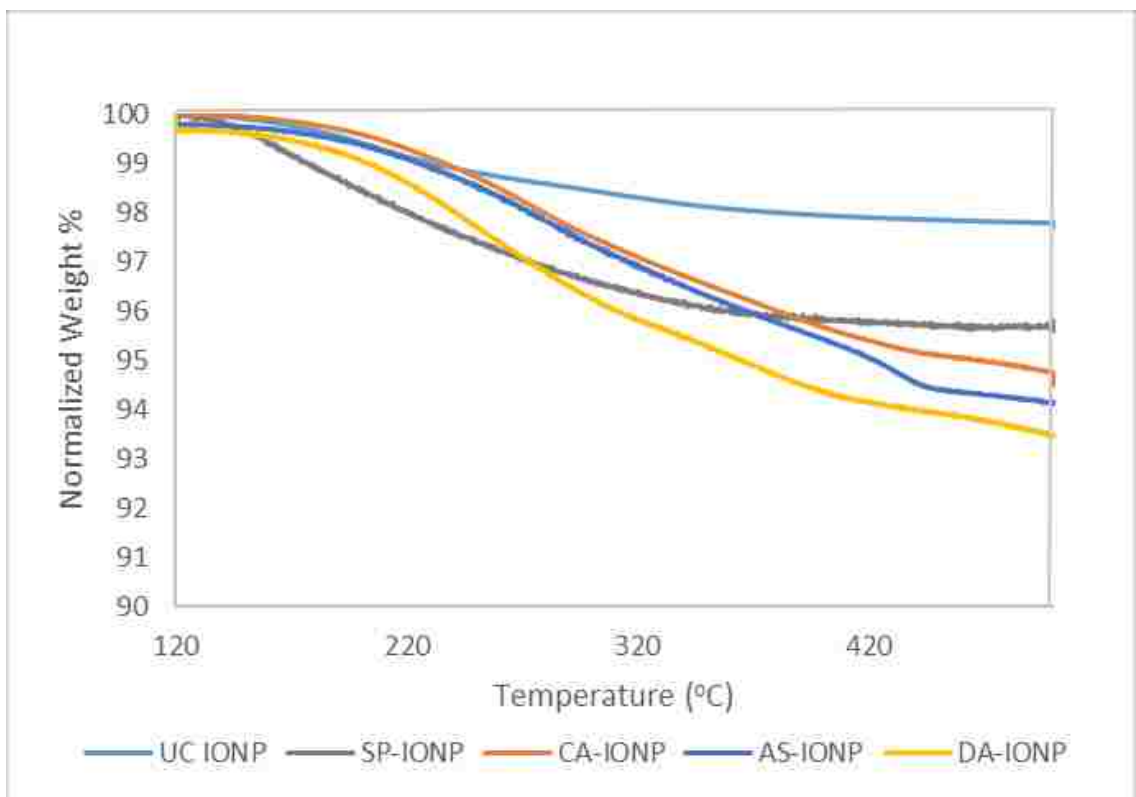
Figure 3.4. Normalized mass loss profile of uncoated and coated nanoparticle systems

3.3.3. Surface ROS generation

IONP can generate ROS via Fenton and Haber-Weiss reactions. To determine the amount of ROS generation, a methylene blue decolorization assay was used. Theoretically, highly reactive hydroxyl and superoxide radicals generated from reaction of iron ions with hydrogen peroxide will attack and degrade methylene blue into colorless products. The amount of ROS generation can be determined via measuring the absorbance of methylene blue. Figure 3.5 displayed the reactivity of all synthesized system with and without AMF exposure. As can be seen in figure 5, the methylene blue control was not affected by the application of AMF for 30 min. The UC-IONP, CA-IONP and DA-IONP showed significantly decrease in absorbance of methylene blue after 30 min AMF exposure with $p = 0.01$ while SP-IONP and AS-IONP displayed significant reduction with $p = 0.05$. Without AMF exposure, uncoated and all coated nanoparticles except AS-IONP have significant decrease in absorbance ($p = 0.01$). However, the application of AMF for 30 min did significantly reduce the absorbance of methylene blue which in turn demonstrated that AMF application could accelerate the formation of ROS. Similar result has been obtained by Wydra et al. [17]. It is also revealed that uncoated nanoparticles are the most reactive system degrading about 40% over 30 minutes of AMF exposure. After coating, there was a significant inhibition in surface reactivity of the nanoparticles with increasing absorbance compared to the uncoated nanoparticles. The presence of small molecules at the surface of the particles blocked the surface area participating in Fenton/Haber-Weiss reaction which in turn reduce surface reactivity of the particles via ROS generation. There was also a larger variation in surface reactivity of SP-IONP than other coated systems and future work will be continued to explain this unique behavior.
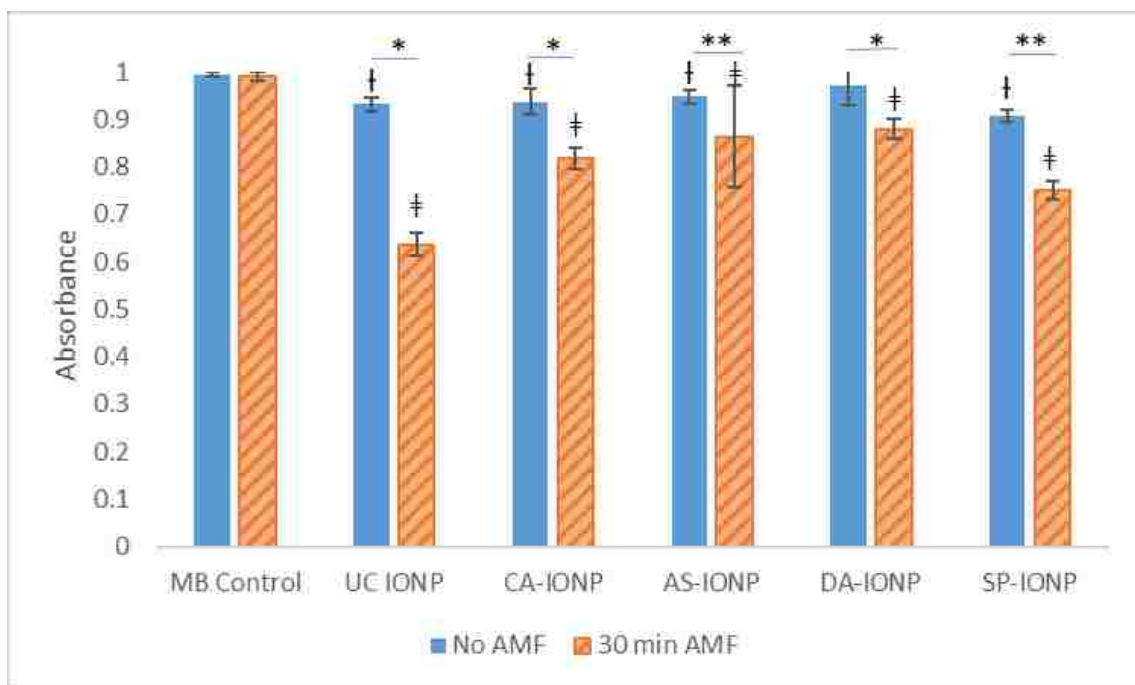
Figure 3.5. Normalized absorbance of methylene blue after exposed to nanoparticles with and without AMF exposure. Error bars represent standard error (n = 18 for SP-IONP and n = 6 for all other systems) and * and ** indicates a significant difference between no AMF and 30 min AMF exposure compared to the control with p = 0.01, and p = 0.05 respectively, ꟼ indicates a significant difference from the control with no AMF exposure (p = 0.01) and ‡ indicates a significant difference from the control with 30 min AMF exposure (p = 0.01), via a two-way ANOVA with an interaction term.

In addition to the interaction with the iron ions at the surface of the nanoparticles, hydroxyl radicals can also interact with the coating such as citric acid and dopamine. It has been shown that the interaction of hydroxyl radicals with citric acid can occur at one of these positions: the carboxyl group or the hydroxyl group bound to the tertiary carbon, the methylenic group or the carboxyl group bound to the methylenic group. The main intermediates are 3-oxoglutaric acid, acetoacetic, lactic, malic, etc. In this case, the two carboxyl groups bound to CH_2 group formed an interaction with the nanoparticles, so the

interaction at this position is less likely to occur. Figure 3.6 showed one possible reaction between citric acid and hydroxyl radicals at the hydroxyl group of the central carbon.
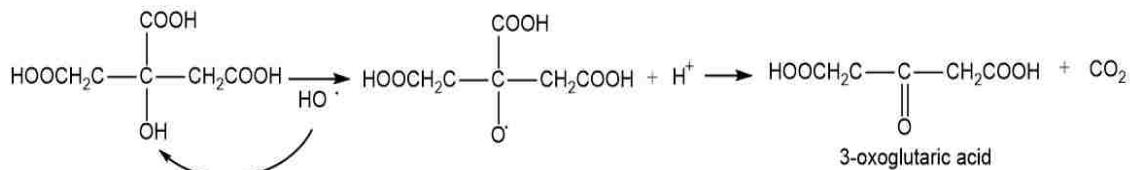
Figure 3.6. Reaction of hydroxyl radicals with citric acid at hydroxyl group of tertiary carbon.

The oxidation mechanism of dopamine by hydroxyl radicals has been studied by Richter and Waddell in which o-semiquinone and o-semiquinone anion radicals were formed [38]. The reaction included three steps: (1) addition of hydroxyl radicals to the benzene ring, (2) elimination of H_2O to form semiquinone radicals and (3) equilibration of semiquinone and semiquinone anion radicals as illustrated in figure 3.7.
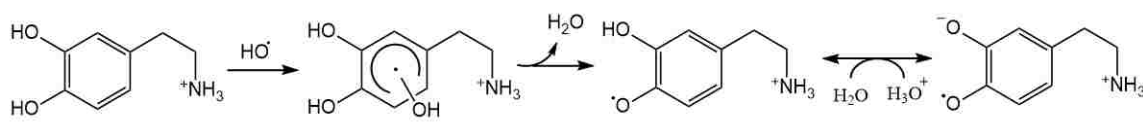
Figure 3.7. Reaction of dopamine with hydroxyl radicals to produce *o*-semiquinone and *o*-semiquinone anion radicals

3.4.   Conclusion

In this study, IONPs were successfully functionalized with citric acid, sodium phosphate, amino silane and dopamine via interaction of carboxylates, phosphate, silane and catechol groups with IONP, respectively. Physical and chemical properties of the particles with surface modification were also studied and compared to uncoated systems. The effect of these small molecule coating on the surface ROS generation induced by

IONP through Fenton chemistry was analyzed using a methylene blue decolorization assay under various AMF exposure times. The results showed that by coating the particles with small molecules, the amount of ROS generated under AMF exposure without remarkable temperature rise were significantly inhibited. Phosphate coated particles showed a much bigger variation in ROS generation compared to other systems..

3.5. References

1. J.R. McCarthy, R. Weissleder, Multifunctional magnetic nanoparticles for targeted imaging and therapy, Advanced drug delivery reviews, 60 (2008) 1241-1251.

2. R. Weissleder, P.F. Hahn, D.D. Stark, E. Rummeny, S. Saini, J. Wittenberg, J.T. Ferrucci, MR imaging of splenic metastases: ferrite-enhanced detection in rats, AJR. American journal of roentgenology, 149 (1987) 723-726.

3. R. Weissleder, G. Elizondo, J. Wittenberg, C.A. Rabito, H.H. Bengele, L. Josephson, Ultrasmall superparamagnetic iron oxide: characterization of a new class of contrast agents for MR imaging, Radiology, 175 (1990) 489-493.

4. M. Namdeo, S. Saxena, R. Tankhiwale, M. Bajpai, Y.M. Mohan, S.K. Bajpai, Magnetic nanoparticles for drug delivery applications, Journal of nanoscience and nanotechnology, 8 (2008) 3247-3271.

5. D. Wang, J. He, N. Rosenzweig, Z. Rosenzweig, Superparamagnetic Fe2O3 Beads−CdSe/ZnS Quantum Dots Core−Shell Nanocomposite Particles for Cell Separation, Nano Letters, 4 (2004) 409-413.

6   M. Lewin, N. Carlesso, C.H. Tung, X.W. Tang, D. Cory, D.T. Scadden, R. Weissleder, Tat peptide-derivatized magnetic nanoparticles allow in vivo tracking and recovery of progenitor cells, Nature Biotechnology, 18 (2000) 410-414.

7.   A.M. Kruse, S.A. Meenach, K.W. Anderson, J.Z. Hilt, Synthesis and characterization of CREKA-conjugated iron oxide nanoparticles for hyperthermia applications, Acta Biomaterialia, 10 (2014) 2622-2629.

8.   Q.A. Pankhurst, N.T.K. Thanh, S.K. Jones, J. Dobson, Progress in applications of magnetic nanoparticles in biomedicine, Journal of Physics D: Applied Physics, 42 (2009) 224001.

9.   R.J. Wydra, P.G. Rychahou, B.M. Evers, K.W. Anderson, T.D. Dziubla, J.Z. Hilt, The role of ROS generation from magnetic nanoparticles in an alternating magnetic field on cytotoxicity, Acta Biomaterialia, 25 (2015) 284-292.

10.   M. Creixell, A.C. Bohorquez, M. Torres-Lugo, C. Rinaldi, EGFR-Targeted Magnetic Nanoparticle Heaters Kill Cancer Cells Without A Sensible Temperature Rise, ACS Nano, 5 (2011) 7124–7129.

11.   A. Villanueva, P. de la Presa, J.M. Alonso, T. Rueda, A. Martínez, P. Crespo, M.P. Morales, M.A. Gonzalez-Fernandez, J. Valdés, G. Rivero, Hyperthermia HeLa Cell Treatment with Silica-Coated Manganese Oxide Nanoparticles, The Journal of Physical Chemistry C, 114 (2010) 1976-1981.

12   V. Grazú, A.M. Silber, M. Moros, L. Asín, T.E. Torres, C. Marquina, M.R. Ibarra, G.F. Goya, Application of magnetically induced hyperthermia in the model protozoan Crithidia fasciculata as a potential therapy against parasitic infections, International Journal of Nanomedicine, 7 (2012) 5351-5360.

13. B. Kozissnik, A.C. Bohorquez, J. Dobson, C. Rinaldi, Magnetic fluid hyperthermia: Advances, challenges, and opportunity, International Journal of Hyperthermia, 29 (2013) 706-714.

14. S. Klein, A. Sommer, L.V.R. Distel, W. Neuhuber, C. Kryschi, Superparamagnetic iron oxide nanoparticles as radiosensitizer via enhanced reactive oxygen species formation, Biochemical and Biophysical Research Communications, 425 (2012) 393-397.

15. D.B. Cochran, P.P. Wattamwar, Robert Wydra, J.Z. Hilt, K.W. Anderson, R.E. Eitel, T.D. Dziubla, Suppressing iron oxide nano particle toxicity by vascular targeted antioxidant polymer nanoparticles Biomaterials, 34 (2013) 9615-9622.

16. S. Naqvi, M. Samim, M. Abdin, F.J. Ahmed, A. Maitra, C. Prashant, A.K. Dinda, Concentration-dependent toxicity of iron oxide nanoparticles mediated by increased oxidative stress, Int J Nanomedicine, 5 (2010) 983-989.

17. R.J. Wydra, C.E. Oliver, K.W. Anderson, T.D. Dziubla, J.Z. Hilt, Accelerated generation of free radicals by iron oxide nanoparticles in the presence of an alternating magnetic field, Royal Society of Chemistry Advances, 5 (2015) 18888-18893.

18. E. Amstad, M. Textora, E. Reimhult, Stabilization and functionalization of iron oxide nanoparticles for biomedical applications, Nanoscale, 3 (2011) 2819-2843.

19. M. Chen, S. Yamamuro, D. Farrell, S.A. Majetich, Gold-coated iron nanoparticles for biomedical applications, Journal of Applied Physics, 93 (2003) 7551-7553.

20. C. Zhang, B. Wängler, B. Morgenstern, H. Zentgraf, M. Eisenhut, H. Untenecker, R. Krüger, R. Huss, C. Seliger, W. Semmler, F. Kiessling, Silica- and Alkoxysilane-Coated Ultrasmall Superparamagnetic Iron Oxide Particles: A Promising Tool To Label Cells for Magnetic Resonance Imaging, Langmuir, 23 (2007) 1427-1434.

21. P. Tartaj, T. González-Carreño, C.J. Serna, Synthesis of Nanomagnets Dispersed in Colloidal Silica Cages with Applications in Chemical Separation, Langmuir, 18 (2002) 4556-4558.

22. Y. Sahoo, H. Pizem, T. Fried, D. Golodnitsky, L. Burstein, C.N. Sukenik, G. Markovich, Alkyl Phosphonate/Phosphate Coating on Magnetite Nanoparticles: A Comparison with Fatty Acids, Langmuir, 17 (2001) 7907-7911.

23. S. Laurent, D. Forge, M. Port, A. Roch, C. Robic, L. Vander Elst, R.N. Muller, Magnetic Iron Oxide Nanoparticles: Synthesis, Stabilization, Vectorization, Physicochemical Characterizations, and Biological Applications, Chemical Reviews, 108 (2008) 2064-2110.

24. R.J. Wydra, A.M. Kruse, Y. Bae, K.W. Anderson, J.Z. Hilt, Synthesis and characterization of PEG-iron oxide core-shell composite nanoparticles for thermal therapy, Materials Science and Engineering C, 33 (2013) 4660-4667.

25. A.K. Guptaa, M. Gupta, Synthesis and surface engineering of iron oxide nanoparticles for biomedical applications, Biomaterials, 26 (2005) 3995-4021.

26. R.A. Frimpong, J.Z. Hilt, Magnetic nanoparticles in biomedicine: synthesis, functionalization and applications, Nanomedicine (London, England), 5 (2010) 1401-1414.

27.	M.A. Malvindi, V.d. Matteis, A. Galeone, V. Brunetti, G.C. Anyfantis, A. Athannassiou, R. Cingolani, P.P. Pompa, Toxicity assessment of silica coated iron oxide nanoparticles and biocompatibility improvement by surface engineering, Plos one, 9 (2014) e85835.

28.	R.A. Frimpong, J. Dou, M. Pechan, J.Z. Hilt, Enhancing remote controlled heating characteristics in hydrophilic magnetite nanoparticles via facile co-precipitation, Journal of Magnetism and Magnetic Materials 332 (2010) 326-331.

29.	F. Gao, H. Qu, Y. Duan, J. Wang, X. Song, T. Ji, L. Cao, G. Nieb, S. Sun, Dopamine coating as a general and facile route to biofunctionalization of superparamagnetic Fe3O4 nanoparticles for magnetic separation of proteins, RSC Advances, 4 (2014) 6657-6663.

30.	M. Racuciu, D.E. Creang, A. Airinei, Citric-acid–coated magnetite nanoparticles for biological applications, THE EUROPEAN PHYSICAL JOURNAL E, 21 (2006) 117-121.

31.	T. Muthukumaran, J. Philip, A single pot approach for synthesis of phosphate coated iron oxide nanoparticles, Journal of nanoscience and nanotechnology, 15 (2015) 2715-2725.

32.	Y. Zhang, N. Kohler, M. Zhang, Surface modification of superparamagnetic magnetite nanoparticles and their intracellular uptake, Biomaterials, 23 (2002) 1553-1561.

33.	R.A. Bini, R.F.C. Marques, F.J. Santos, J.A. Chaker, M. Jafelicci Jr, Synthesis and functionalization of magnetite nanoparticles with different amino-functional alkoxysilanes, Journal of Magnetism and Magnetic Materials, 324 (2012) 534-539.

34.	P. Kumar, S. Agnihotri, I. Roy, Synthesis of Dox drug conjugation and CA stabilized SPION for drug delivery, Biochemicstry & Physiology, 5 (2016) 1000194-1100199.

35.	M.E. de Sousa, M.B. Fernández van Raap, P.C. Rivas, P. Mendoza Zélis, P. Girardin, G.A. Pasquevich, J.L. Alessandrini, D. Muraca, F.H. Sánchez, Stability and Relaxation Mechanisms of Citric Acid Coated Magnetite Nanoparticles for Magnetic Hyperthermia, The Journal of Physical Chemistry C, 117 (2013) 5436-5445.

36.	S. Mumtaz, L.-S. Wang, M. Abdullah, S.Z. Hussain, Z. Iqbal, V.M. Rotello, I. Hussain, Facile method to synthesize dopamine-capped mixed ferrite nanoparticles and their peroxidase-like activity, Journal of Physics D: Applied Physics, 50 (2017) 11LT02-11LT10.

[37]	J.M. Meichtry, N. Quici, G. Mailhot, M.I. Litter, Heterogeneous photocatalytic degradation of citric acid over TiO2, Applied Catalysis B: Environmental, 102 (2011) 555-562.

[38]	H.W. Richter, W.H. Waddell, Mechanism of the oxidation of dopamine by the hydroxyl radical in aqueous solution, Journal of the American Chemical Society, 105 (1983) 5434-5440.

Chapter 4: Poly (beta amino ester) functionalized iron oxide nanoparticles and their effects on reactive oxygen species generation for potential cancer treatment

Abstract. Iron oxide nanoparticles can be utilized as catalyst for Fenton-like reactions, and Haber-Weiss cycle occur at surface of the particles with the presence of hydrogen peroxide. The ability to induce reactive oxygen species (ROS) generation of iron oxide nanoparticles can be significantly enhanced with the exposure of alternating magnetic field (AMF) while coatings can inhibit the surface ROS generation by covering particles surface. In the study, we synthesized degradable poly (beta amino ester) (PBAE) polymers containing dopamine which has a catechol group that provides high affinity anchoring sites to iron oxide nanoparticles surface. Once the PBAE is degraded, it was hypothesized that the iron oxide nanoparticle surfaces will be re-exposed to the surrounding environment and will have similar surface reactivity as the uncoated particles. The amount of surface ROS generation was determined using methylene blue decolorization assay over 30 minutes exposure to AMF. The surface ROS generation of the coated particles with small amounts of anchoring group (less than 10% of the total amine) is quite comparable to that the uncoated particles while it decreased with the increasing of dopamine content from 10% to 50%. However, surface reactivity similar to uncoated particles was not recovered after degradation, and this is likely due to an additional coating of hydrolysis products onto particles surface which inhibited the surface reaction and led to a reduction in ROS generation

4.1.   Introduction

Iron oxide nanoparticles (IONP) with their unique properties have been studied for various applications in magnetic resonance imaging, drug delivery, magnetically mediated hyperthermia [1-6]. Their potential uses in therapeutics and diagnosis arises from their

magnetic properties and biocompatibility [7-10]. Being magnetic, iron oxide nanoparticles can convert the energy absorbed from an alternating magnetic field (AMF) into heat through Neel relaxation (i.e., rotation of the magnetic moment to align with the field) and Brownian relaxation (i.e., the physical rotation of the particles in response to the magnetic field) [11]. This heat conversion has been extensively studied as magnetically mediated hyperthermia for cancer treatment [12, 13]. Instead of traditional hyperthermia in which the bulk temperature is increased to $42 – 45^{o}C$ appeared to have some adverse effects to the cells, intracellular hyperthermia was suggested in 1979 by Gordon et al. with more advantages for the treatment of cancer [14]. However, Rabin's theoretical calculations claimed that the heat conduction from the surface of nanoparticles to the surroundings is greater than the heat generated from the nanoparticles indicating the improbability of intracellular hyperthermia [15]. Work reported by Creixell et al. demonstrated that nanoparticles can induced cellular toxicity under alternating magnetic field exposure without measurable temperature rise [16]. The conversion of magnetic field energy to other forms such as heat or rotation work without significant increasing bulk temperature was then described as magnetically mediated energy delivery (MagMED) [17]. The follow-up work by Polo-Corrales et al. confirmed that nanoparticle surface heating was occurred immediately once exposed to the AMF while the surrounding temperature remained constant [18].

In addition to the effect of nanoparticles heating at the surface, rotation work has also been considered as a potential effect of MagMED. When exposed to the AMF, magnetic nanoparticles physically rotate and then re-align along the magnetic field producing some mechanical forces. These mechanical forces have been used to increase lysosomal membrane permeabilization and induce cellular death [19-21]. Work by Sanchez et al. demonstrated that apoptosis and cell death through a lysosomal death pathway by magnetic nanoparticles decorated with a ligand of G-protein coupled receptor

was triggered with the application of alternating magnetic field without measurable temperature rise [22]. With the development of a unique dynamic magnetic field generator to control rotational movement of the magnetic nanoparticles in solution, Zhang et al. found that the shear force generated by this rotational activation can damage lysosomal membrane resulting in increased apoptosis and cell death [23]. These works demonstrated the important role of Brownian rotation of magnetic nanoparticles in the MagMED effects.

In addition to surface heating and rotation works, another potential chemical effect of MagMED is the production of reactive oxygen species (ROS) such as hydroxyl radicals, superoxide radicals and hydrogen peroxide ($OH^{\cdot}$, $HO_2^{\cdot}$, H_2O_2) induced by iron oxide nanoparticles through via Fenton reactions and Haber-Weiss cycle [24, 25]. After iron oxide nanoparticles are taken up into cells, iron ions are released in cytosol, chelated with citrate and adenosine phosphate and participated in Haber-Weiss cycle. Another pathway is that iron oxide nanoparticles may act as catalysts for the Fenton reaction and Haber-Weiss cycle occur at the surface of the particles [10, 26, 27]. Recent works indicated that cytotoxicity of iron oxide nanoparticles depends on their composition (Fe_3O_4, Fe_2O_3 or γ-Fe_2O_3) and surface modification [28, 29]. It has been reported by Voinov et al. that surface Fe^{3+} ions of γ-Fe_2O_3 displayed at least 50 times more efficient than dissolved Fe^{3+} ions in producing hydroxyl radicals [29]. Moreover, Aranda et al. suggested that Fe_3O_4 with both Fe^{3+} and Fe^{2+} ions would lead to greater ROS generation and oxidative stress than Fe_2O_3 with mostly Fe^{3+} ions [30].

In order to improve stability and biocompatibility, prevent agglomeration and provide functional groups, iron oxide nanoparticles can be surface coated and functionalized by surfactants or polymers [31-33]. However, the coatings can also inhibit the surface ROS generation induced by IONP occurring at the nanoparticles surface. To overcome this issue, we synthesized PEG-based poly (beta amino esters) (PBAE) as a

biodegradable coating for iron oxide nanoparticles. PBAE are formed through a Michael addition reaction between diacrylates and primary or secondary amines which results in a linear macromers/polymers with both esters and tertiary amines in their backbone [34]. Their properties, such as degradation profile, are tunable by varying the ratio of diacrylates to amines or hydrophobic/hydrophilic compositions [35, 36]. Containing tertiary amines in the structure, the PBAE polymers are pH- responsive making them very potential for drug delivery [37-39]. Fang et al. have successfully fabricated magnetic nanoparticles based nanosytem with pH- sensitive PBAE copolymers containing chemotherapeutic agent doxorubicin which was released once the PBAE degradation occurred, which is triggered at lower pH [40].

The main objective of this study was to determine the influence of degradable poly (beta amino ester) polymers coating on the ability to induce the production of reactive hydroxyl radicals by iron oxide nanoparticles under the alternating magnetic field exposure through Fenton-like reactions. The PEG-based PBAE polymers with different ratios of diacrylate to amine and different amounts of anchoring groups were coated on the nanoparticles. Once this coating was degraded, the nanoparticles were expected to re-exposed to the surrounding environment, and the surface reactivity of the particles was expected to be similar to uncoated iron oxide nanoparticles. The surface ROS generation was studied using methylene blue dye decolorization by PBAE coated iron oxide nanoparticles with the presence of hydrogen peroxide under AMF exposure for 30 minutes with a minimum bulk temperature rise.

4.2. Materials and methods

4.2.1. Materials

Iron (III) chloride hexahydrate ($FeCl_3 \cdot 6H_2O$), iron (II) chloride tetrahydrate ($FeCl_2 \cdot 6H_2O$), hydrogen peroxide and methylene blue were obtained from Sigma Aldrich

(St. Louis MO). Diethylene glycol diacrylate (DEGDA) and polyethylene glycol (N=400) diacrylate (PEG400DA) were from Polysciences Inc (Warrington, PA). Isobutylamine and dopamine (DOPA) hydrochloride were also obtained from Sigma Alrich. Ammonium hydroxide (NH4OH) was from EMD Chemicals (Gibbstown, NJ). All materials were used without further modification.

4.2.2. Iron oxide nanoparticles (IONP) synthesis

A one-pot co-precipitation method was used to synthesize the uncoated iron oxide nanoparticles (UC-IONP) [41]. Typically, 40 ml aqueous solution of $FeCl_3 \cdot 6H_2O$ and $FeCl_2 \cdot 6H_2O$ in 2:1 molar ratio (2.2g and 0.8g, respectively) was prepared in a sealed three-neck flask. The mixture was heated to 85°C while vigorous stirring under inert environment. At 80°C, 5 ml of NH_4OH was added into the mixture and the reaction was performed for one hour at 85°C. The particles were then magnetically decanting and washed three time with deionized (DI) water. The nanoparticles were then re-suspended in DI water and dialyzed against DI water for 24 hours (water was changed every 3 hours).

4.2.3. PBAE polymerization and particle coating

PBAE polymers were synthesized following procedure described by Anderson et al. [34]. All reactants were mixed in a 20 ml glass vial and reacted at 70°C in a pre-heated oil bath for 48 hours. The two diacrylates used were DEGDA and PEG400DA. The amines consisted of iso-butylamine and dopamine. The ratio of DEGDA: PEG400DA was kept at 1: 2 molar ratio while the ratio of total diacrylates over total amines was varied from 0.8 to 1.2. The amount of dopamine incorporated was altered from zero to 50 mole percent of the total amine. After 48 hours, the synthesized polymers were kept in fridge prior to future use.

PBAE coated IONP nanoparticles were synthesized through a surface addition process. Dried uncoated iron oxide nanoparticles were probe sonicated into anhydrous DMSO at concentration of 5mg/ml until well dispersed. PBAE polymer was added to particles suspension with a mass ratio of 10:1. The mixture was then reacted for 24 hours at room temperature. Once finished, nanoparticles were precipitated in ether, magnetically decanted and washed three time with acetone. The particles were vacuum dried and stored in a desiccator prior to analysis.

The degradation process was performed by suspending polymer coated particles into DI water at concentration of 5mg/ml and the suspension was dialyzed against water for 72 hours. After dialysis, the samples were magnetically decanted and washed 3 times with DI water. The final particles were vacuum dried overnight and kept under desiccation.

4.2.4. Particle and polymer characterization

X-ray powder diffraction (XRD) was used to confirm the magnetite crystal structure of the synthesized iron oxide nanoparticles. The measurement was performed on a Siemens D500 X-ray spectrometer with a CuKα radiation source at 40kV and 30mA from 5° to 65° with the rate of 1° per minute.

Dynamic light scattering (DLS) was performed to analyze size distribution of nanoparticles while *zeta potential* was done to measure the potential at the surface of the particles. Nanoparticles were prepared in DI water at concentration of 0.2 mg/ml and probe sonicated for 10 min. DLS and zeta potential measurements were performed triplicate using Malvern Zetasizer, Nano ZS90 instrument.

Fourier transformed infrared spectroscopy (FTIR) was used to characterized surface functionalization of the particles. The spectrum was recorded from 700 cm^{-1} to

4000 cm^{-1} using attenuated total reflectance ATR- FTIR with Varian Inc. 7000e spectrometer.

Proton nuclear magnetic resonance (^{1}H-NMR) analysis was used to confirm the formation of PBAE polymer. Sample was prepared by dissolving PBAE polymers in DMSO at concentration of 10 mg/ml and the measurement was performed on Bruker Avance NEO spectrometer operating at 400 MHz and 298K with 16 scans (Department of Chemistry, University of Kentucky).

Thermogravimetric analysis (TGA) was used to determine the amount of polymer coating in nanoparticles. Approximate 5-10 mg of dried particles were heated at 5°/min to 120°C and held there isothermally for 20 min to remove any residual water. The samples were then heated continuously at 5°/min until reaching 500°C and kept there for another 20 min. The measurement was performed on Q50 TGA/DSC system. The mass loss was normalized to the mass after isothermal heating at 120°C.

4.2.5. Evaluation of surface ROS generation

Methylene blue decolorization assay was used to determine the surface ROS generation [42]. The experiments were performed at 5 μg/ml of methylene blue and 75 μg/ml of iron oxide nanoparticles in DI water. The samples were placed in the water bath at 37°C for 10 minutes to equilibrate to the set temperature. The degradation was initiated by spiking the samples with 25 μl of H_2O_2 and exposed to a field of approximately 58.0 kA/m in strength at 292 kHz frequency while temperature was measured with a Luxtron FOT Lab Kit. After 30 minutes exposure to the AMF, the samples were centrifuged for 2 minutes using a Phenix Quickspin Centrifuge, magnetically decanted for 30 seconds. The absorbance of supernatants was measured using UV-visible spectroscopy (maximum absorbance at 665 nm) with a Varian Cary. To account for nanoparticle scattering from

the remaining nanoparticles in suspension, absorbance of nanoparticles only at the same concentration was measured and subtracted out from the sample absorbance. The absorbance of sample after 0- and 30- minute exposure was normalized to that of methylene blue control.

4.3. Results and discussion

4.3.1. PBAE polymer synthesis:

PBAE are synthesized through Michael addition reaction of diacrylate groups from DEGDA and PEGDA and amine groups from IBA and DOPA. DEGDA and PEGDA play a role as backbone units while IBA and DOPA provide amines group to the reaction (figure 4.1). The final polymers contain tertiary amines and ester bonds along the PBAE backbone. DOPA has catechol group which will served as the binding unit to iron oxide particles. PBAE polymers were characterized by ^{1}H-NMR spectroscopy. As shown in figure 4.2, peaks at δ = 3.6 ppm was assigned to proton of methylene group in DEG/PEG chain, while peaks at δ = 2.5-2.8 ppm correspond to ethylene group on the PBAE backbone. The peak at δ = 6.5 ppm was associated with phenyl ring of DOPA [40]
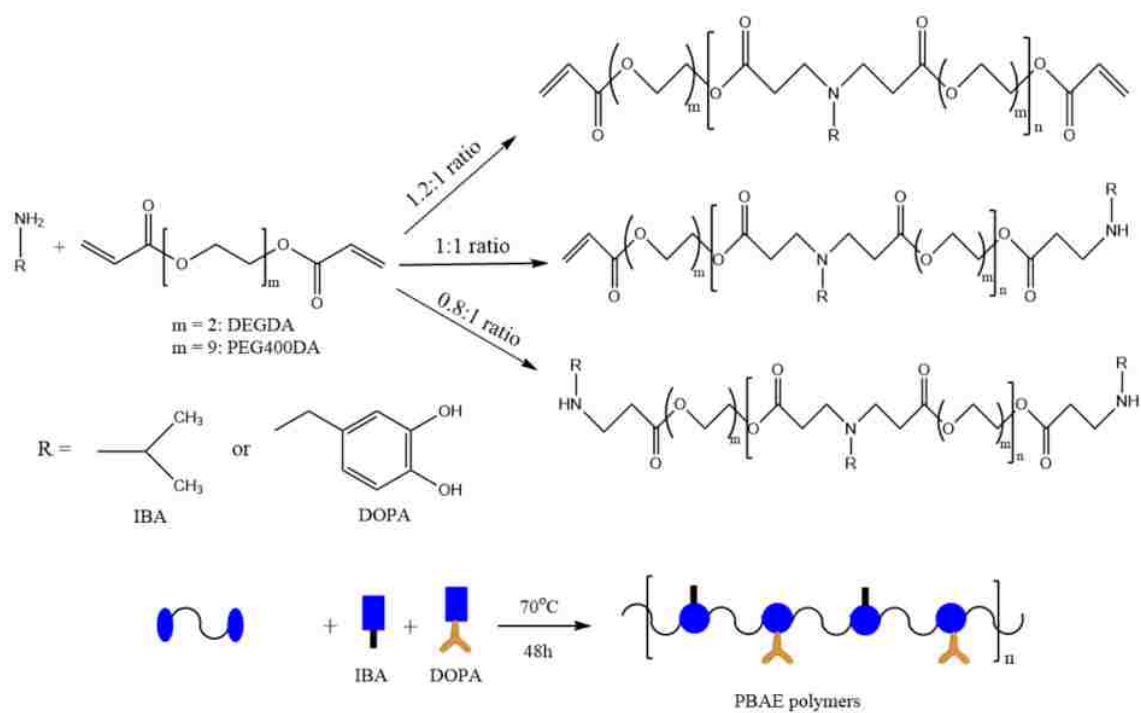
Figure 4.1. Schematic and illustration of poly (beta amino esters) synthesis
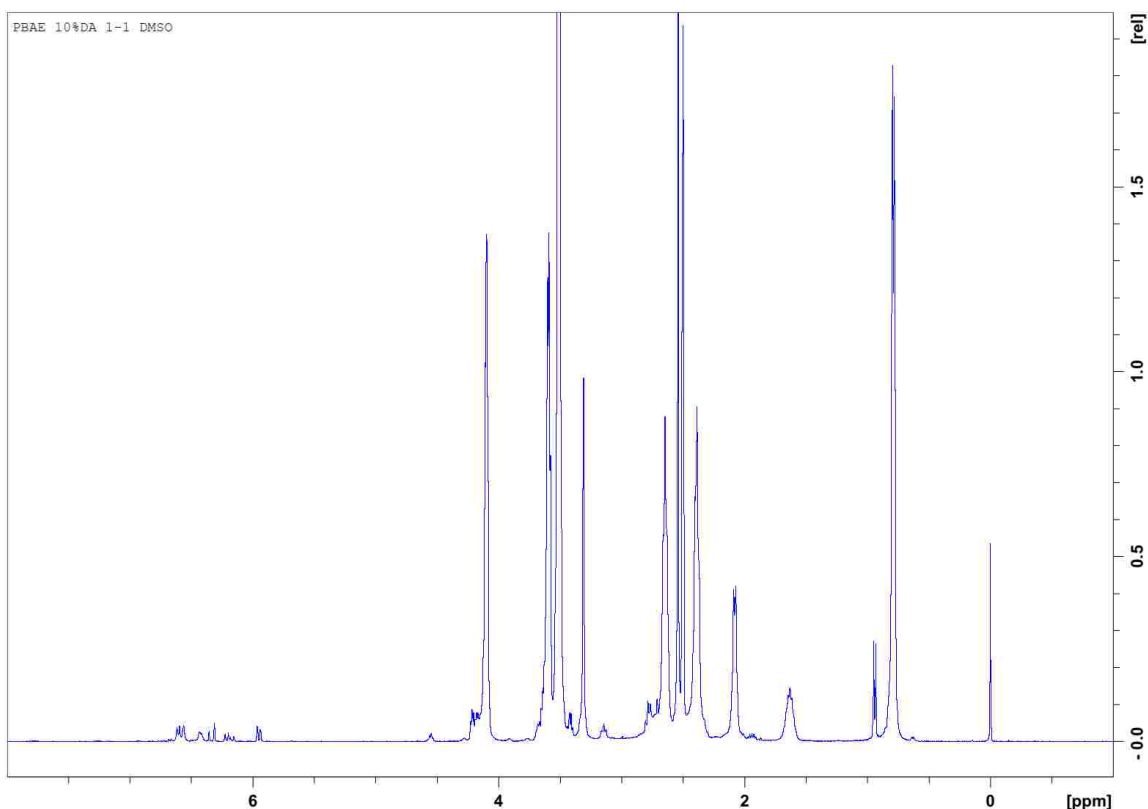
Figure 4.2. HNMR of PBAE-10% DOPA (1:1 ratio of diacrylate: amine) in deuterated DMSO

ATR-FTIR was also used to confirm the formation of PBAE polymers. Figure 4.3 showed FTIR of reactant mixture before and after reaction. In the spectrum of PBAE polymer after 48 hours of reaction, peak at 1637 cm^{-1} corresponded to C=C vibrations was decreased as C=C will react with NH$_2$ of IBA and DOPA to form ester bonds. However, this peak does not disappear completely as the final polymers have C=C bonds from DOPA or excess amount of DEGDA and PEGDA during polymer synthesis in case of 1.2:1 ratio [43]. Besides, peaks at 1728 cm^{-1} and 1100 cm^{-1} are associated with vibrations of C=O and C-O-C groups from the backbone of PBAE while peak at 1192 cm^{-1} contributed to vibration of C-O-H group from dopamine or C-N bond from the backbone of PBAE. As

shown in figure 3, there was no big difference in spectra of PBAE polymers with varying

ratio of diacrylate to amine groups as well as varying the amount of DOPA in polymers.
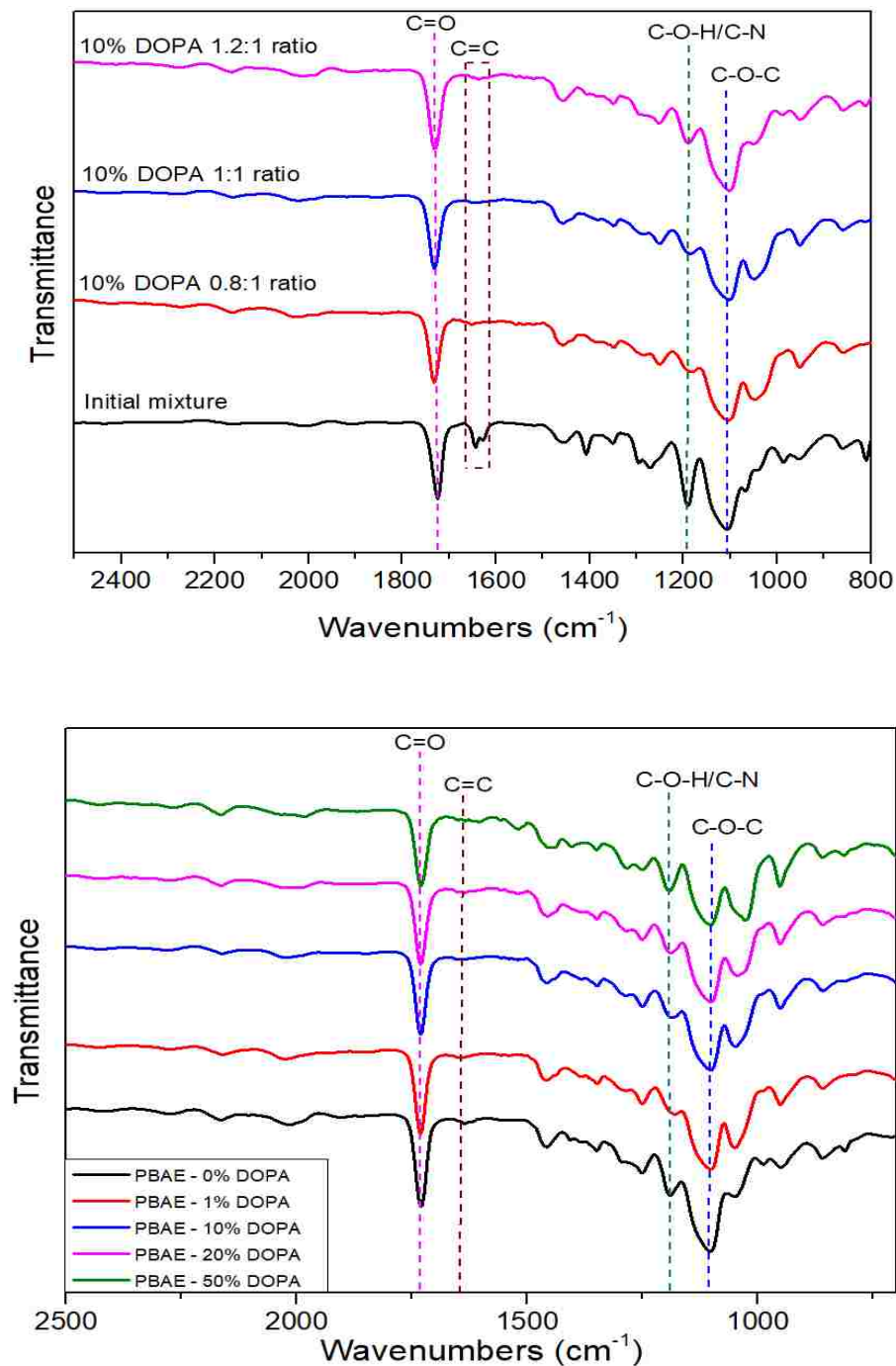
Figure 4.3**.** FTIR of PBAE polymer with varying diacrylate: amine ratio (top) and

varying dopamine amount (bottom)

4.3.2. Nanoparticles synthesis and functionalization
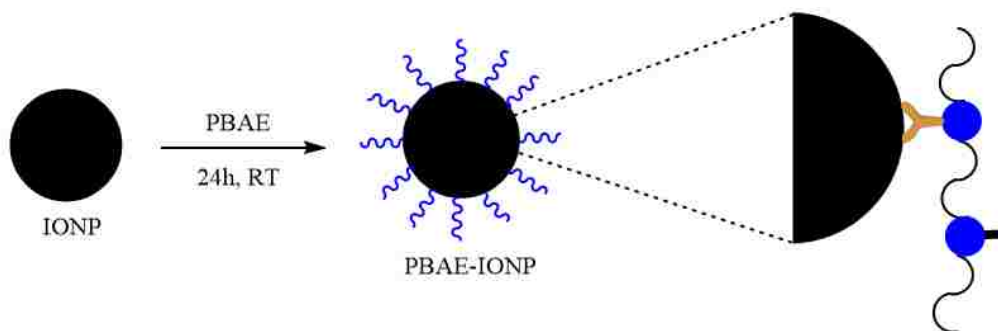
Figure 4.4. Illustration of coating of PBAE polymer on iron oxide nanoparticles

Iron oxide nanoparticles were coated through the addition of PBAE polymer into particles suspension is DMSO. Catechol groups from dopamine are the anchor to bind the PBAE polymers to particles surface as illustrated in figure 4.4. The ester bond of PBAE polymer are hydrolyzed in water to form smaller compounds such as diols, and β-amino acids [34]. To confirm the coating as well as the degradation of PBAE polymer onto particles surface, the nanoparticles were characterized using FTIR and results are shown in figure 4.5. After coating, characteristic vibrations of PBAE polymers were recorded in spectrum of the coated particles including C=O, C-O-C and C-O-H/C-N vibrations at 1730 cm^{-1}; 1190 cm^{-1} and 1110 cm^{-1}, respectively. The appearance of these peaks confirmed the successful coating of PBAE polymer onto particles surface. After hydrolysis, these key peaks are diminished, and the spectrum is very similar to that of uncoated particles.
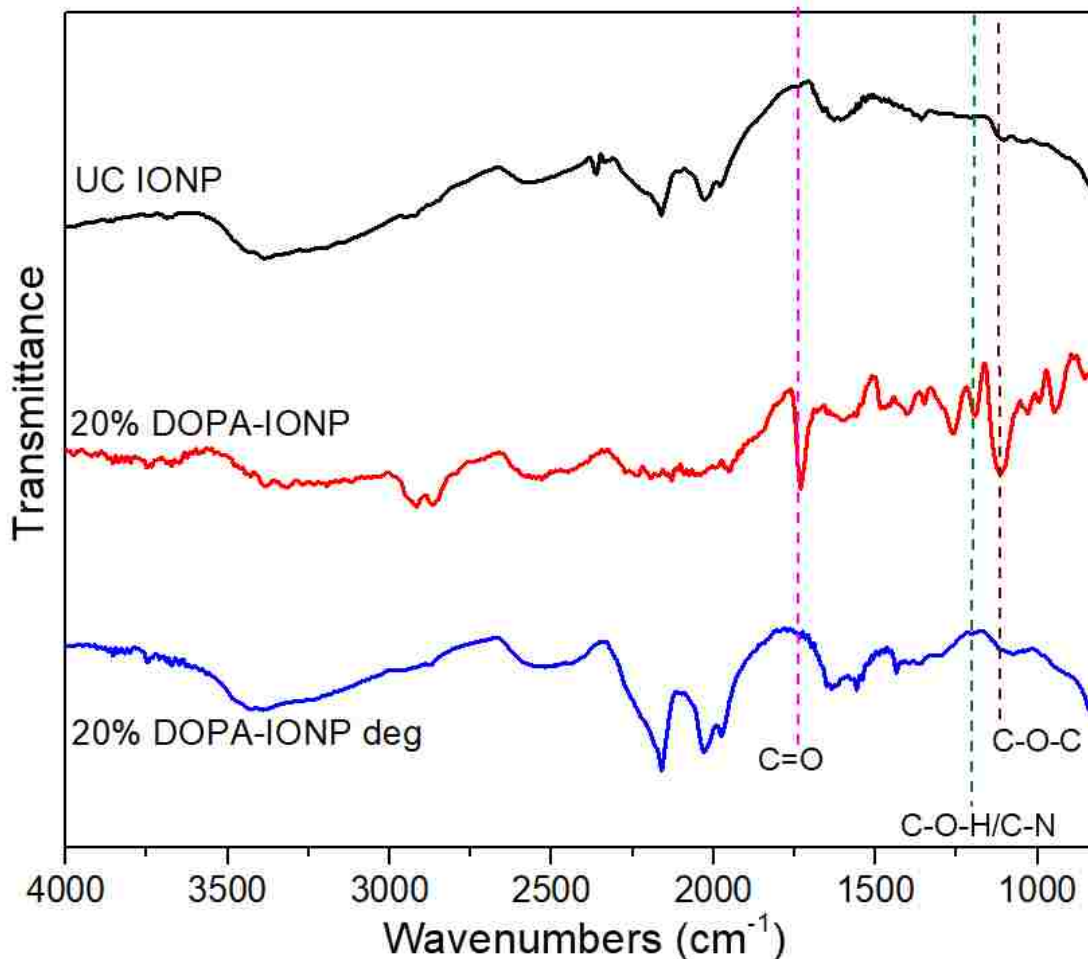
Figure 4.5. FTIR of UC IONP, PBAE-20% DA coated IONP before and after degradation

Crystalline properties of uncoated nanoparticles, PBAE polymers coated nanoparticles before and after hydrolysis were characterized via X-ray diffraction. XRD spectra of the uncoated particles, PBAE coated particles with 0 and 10% DA before and after degradation are shown in fig. 4.6. The peaks at 30°, 35.3°, 43.2°, 53.6°, 57.2° and 62.5° were assigned to (220), (311), (400), (422), (511) and (440) planes of magnetite nanoparticles in cubic phases [44]. These peaks also match with maghemite structure of Fe_2O_3. However, the appearance of these peaks along with the black color of the samples confirmed the crystallinity of the as-synthesized uncoated and PBAE coated particles both before and after polymer degradation.
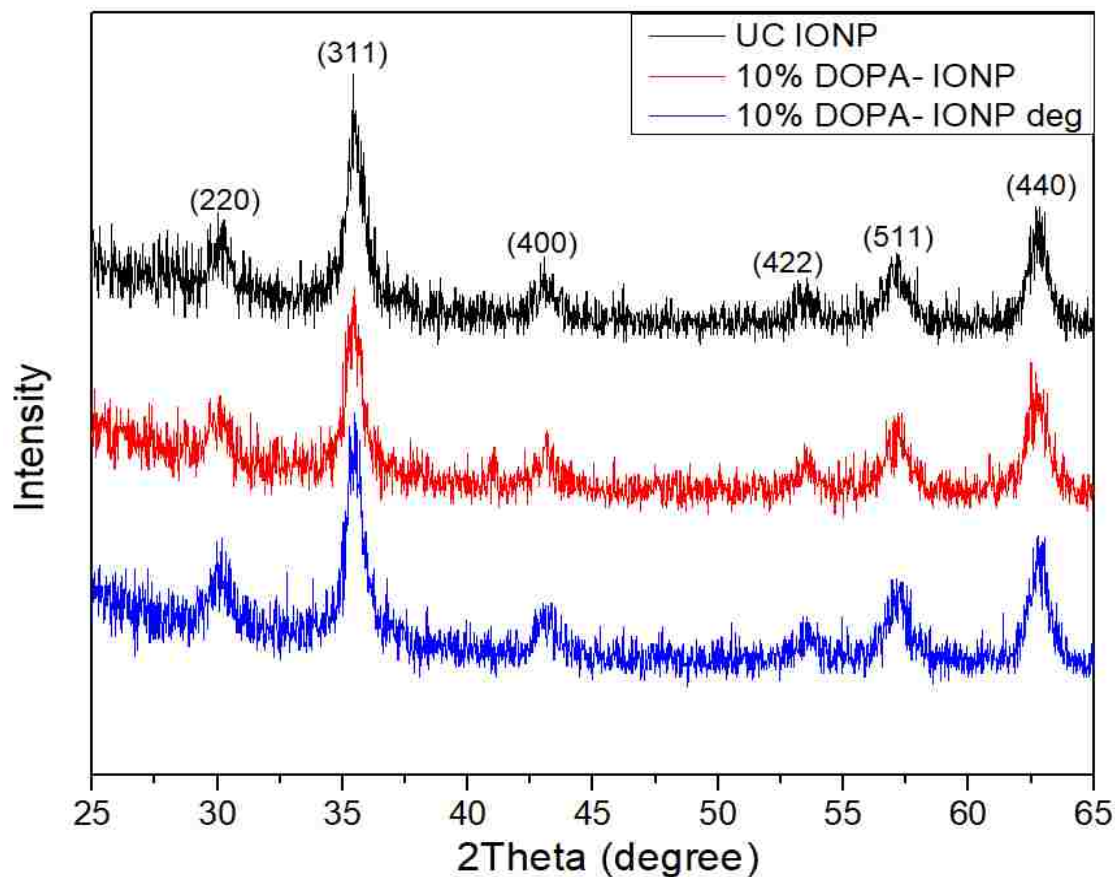
Figure 4.6. XRD pattern of uncoated particles, PBAE-10% DA coated particles before and after degradation

The hydrodynamic size and the amount of coating of the uncoated and coated nanoparticles with 1:1 ratio of diacrylate to amine was measure by DLS and reported in table 4.1. The uncoated particles are about 130nm in diameter and it increased to 155-180nm after coated with PBAE polymer. This further confirmed the successful coating of PBAE onto the particle. After hydrolysis, particles sizes reduced to 150-160nm which is slightly smaller than the coated particles but still larger than the uncoated nanoparticles. A possible reason for this would be the formation of an outer layer on the particles due to the diacid produced during the hydrolysis of PBAE. This is consistent with TGA data which is reported as mass loss in the last column of table 4.1. The mass loss of uncoated particles is 2.5% which can be attributed to chemically absorbed water. With PBAE

coating, the mass loss increased to 8% for PBAE with no DOPA and 9-11% for PBAE with 1-50% DOPA. After PBAE degradation, the mass loss decreased to 5-7%, confirming the removal of the coating polymer. However, they are still 2-4% more than that of the uncoated which could be attributed to the remain of the anchoring group or the presence of outer layer of PBAE hydrolysis products on the particles surface.

Table 4.1. Nanoparticles properties (1: 1 ratio of diacrylate: amine)

Samples	Z-average (d, nm)	PDI	Mass loss (%)
Uncoated IONP	128.5 ± 1.6	0.18 ± 0.03	2.5
0% DA-IONP	169.8 ± 4.2	0.18 ± 0.01	7.95
0% DA-IONP deg*	148.9 ± 2.3	0.25 ± 0.02	4.95
1% DA-IONP	179.7 ± 4.6	0.21 ± 0.01	11.1
1% DA-IONP deg	158.0 ± 9.5	0.27 ± 0.02	5.7
10% DA-IONP	157.0 ± 2.0	0.25 ± 0.01	9.8
10% DA-IONP deg	155.5 ± 2.4	0.25 ± 0.03	5.75
20% DA-IONP	159.1 ± 9.4	0.25 ± 0.03	9.8
20% DA-IONP deg	164.4 ± 3.1	0.25 ± 0.01	6.8
50% DA-IONP	153.2 ± 2.5	0.27 ± 0.02	9.25
50% DA-IONP deg	153.8 ± 3.6	0.26 ± 0.01	6.15

* deg means particles after polymer degradation for 3 days

4.3.3. Surface ROS generation

The surface reactivity of the as-synthesized nanoparticles was tested using methylene blue decolorization assay. The Fenton and Haber-Weiss reactions can occur at the surface of nanoparticles under the presence of hydrogen peroxide leading to the

formation of highly reactive hydroxyl and superoxide radicals. These radicals will attack the double bond of methylene blue and degrade it into colorless intermediates. The formation of these radicals is further enhanced with the exposure of alternating magnetic field. The absorbance of methylene blue can be measured after a certain time through UV-Vis. The decrease in methylene blue absorbance indicates the increase of ROS generation at the surface of the particles. Figure 4.7 displays the amount of methylene blue degraded by the uncoated and coated IONP with PBAE- 10% DOPA varying the ratio of diacrylate to amine from 0.8 to 1.2 over 30 min exposure to AMF. The nanoparticle concentration was kept at 75 µg/ml where there is about 1-2°C temperature increase due to nanoparticle heating. In all cases, exposure to AMF did enhance the reactivity of the particles via surface ROS generation. This is consistent with what was observed and reported by Wydra et al. [45]. Without coating, the uncoated particles are the most reactive particles which decolored about 35% of methylene blue over 30 min exposure to the AMF. The nanoparticles coated with PBAE- 10% DOPA with 1: 1 ratio of diacrylate to amine displayed a very similar degradation (35%) compared to the uncoated particles while the one with 0.8: 1 and 1.2: 1 diminished 20% and 18%, respectively. The PBAE with dopamine as anchoring group created a layer to prevent particles from agglomeration but still left some free area for reactivity at the surface of the particles. However, with the degradation of PBAE, the reactivity of the particles was decreased to 10%, 25% and 7% correspond to 0.8: 1; 1: 1 and 1.2: 1 diacrylate to amine ratio. The reduction in surface reactivity of the particles after PBAE degradation could be due to the extra coating layer of hydrolysis products on particles surface as mentioned in the TGA data analysis. With these results, the 1:1 ratio of diacrylate over amine seemed to be the most potential systems in retaining surface reactivity of the iron oxide nanoparticles and this ratio will be used in later experiments with varying amount of DOPA.

The surface reactivity of PBAE coated IONP with varying amount of DOPA from 0 to 50% was also studied and results are reported in figure 4.8. Similarly, PBAE coatings inhibited the formation of ROS and reduced methylene blue decolorization to 15-30% except for the case of 0% and 10% DOPA coated particles which degraded about the same with uncoated particles. Surface reactivity of the particles after PBAE degradation also decreased as in the case of varying diacrylate to amine ratio. However, no clear trend in surface reactivity of particles with increasing the amount of anchoring group was observed as we expected. When the amount of DOPA increased from 10% to 50% there is reduction in ROS generation, but there is no big difference in ROS generation with 0 to 10% of DOPA. Again, the generation of ROS was inhibited with the hydrolysis of PBAE due to the unexpected coating of degradation products on particles surface as explained previously. But interestingly, the surface reactivity of PBAE coated particles with none or small amount of DOPA (0 and 1%) did not change much after polymer degradation. To confirm this hypothesis, we degraded PBAE polymer in water for 3 days and mixed with the uncoated particles and followed by methylene blue decolorization assay to determine the ROS formation in this case. It showed a very similar degradation with the PBAE coated particle after degradation of the polymer (data not shown). This result along with the TGA data are strong indication of an additional coating of polymer hydrolysis products on the surface of iron oxide nanoparticle which turned to a reduction in ROS generation.
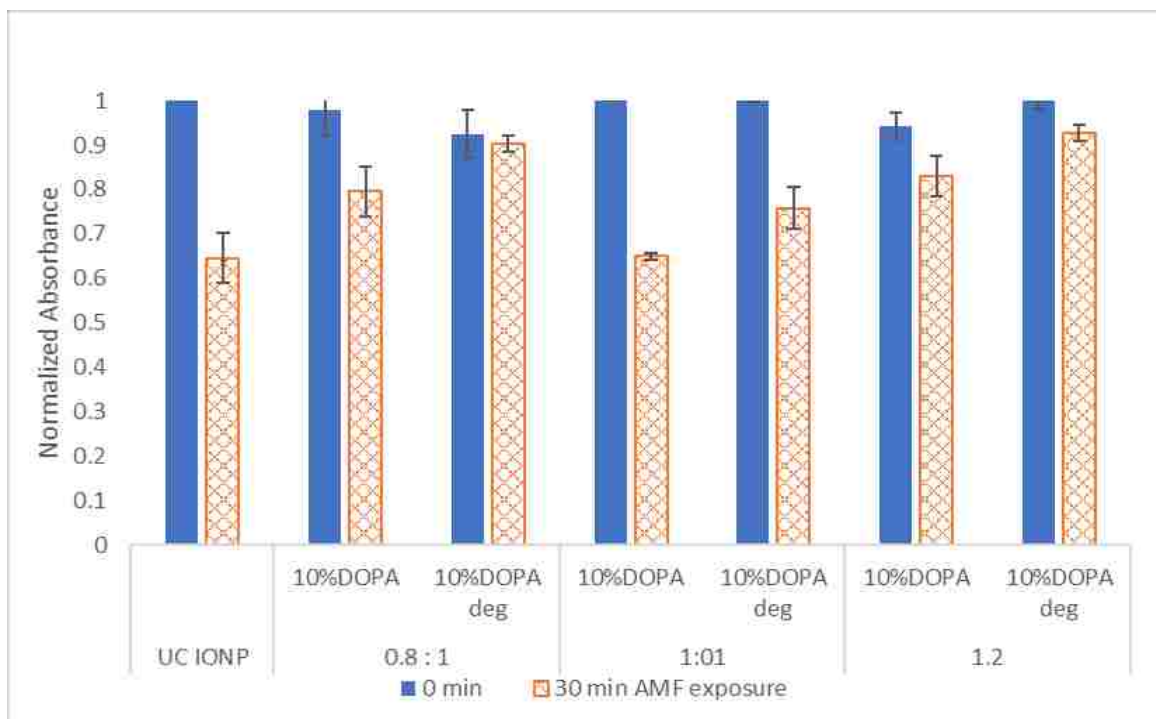
Figure 4.7. Surface ROS generation measured via methylene blue decolorization induced by PBAE- 10% DOPA coated IONP with various ratio of diacrylate over amine under AMF exposure for 30 minutes at 75 µg/ml of particles and 245mM of H_2O_2
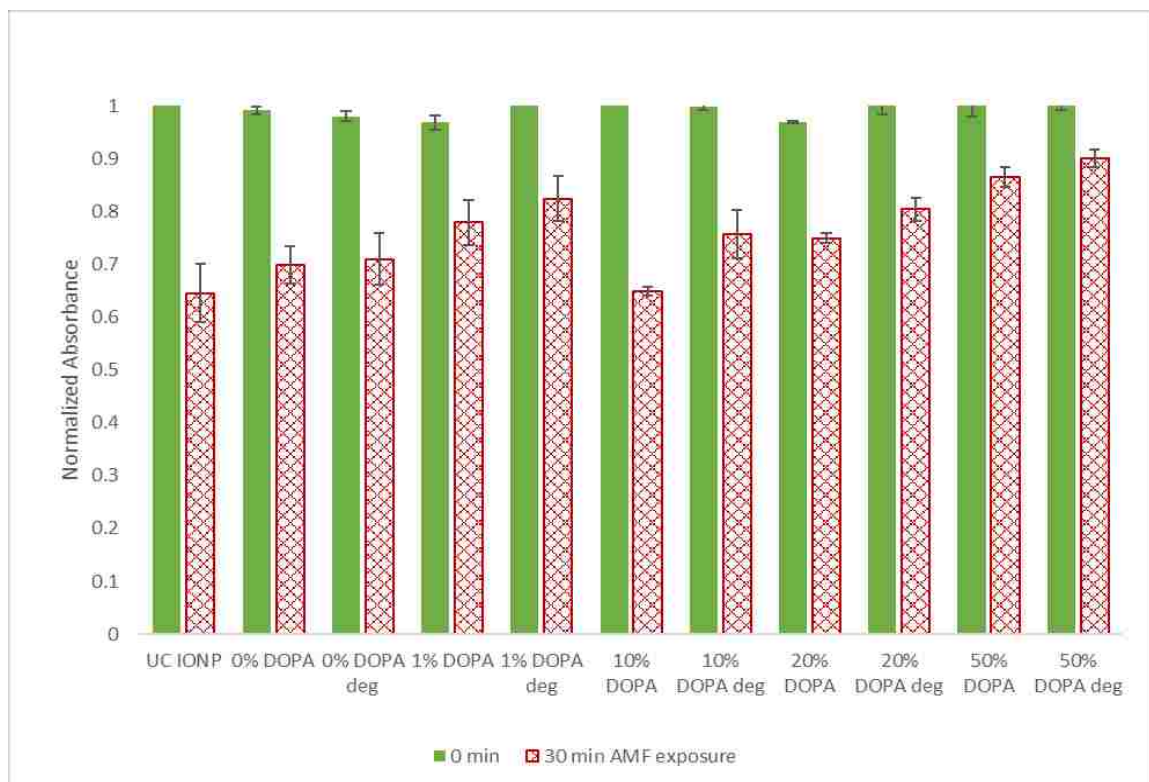
Figure 4.8. Normalized absorbance of methylene blue exposed to PBAE coated IONP with different amount of anchoring group under AMF presence for 30 minutes at 75 μg/ml of particles and 245mM of H_2O_2

4.4. Conclusion

In this work, the effect of degradable poly (beta amino ester) polymer coating on surface reactivity of iron oxide nanoparticles was studied using methylene blue dye decolorization assay. The addition as well as the degradation of various PBAE polymers from nanoparticles surface were successfully performed. The PBAE coated particles seemed to retain surface reactivity of the particles when a small amount of dopamine was used in polymer synthesis. At higher concentrations of dopamine (above 10% of the total amine), the ability to generate surface ROS decreased with increasing of dopamine concentration. However, the particles after the polymer coating was degraded did not display a similar performance with the uncoated as expected. This could be due to the

73

binding of polymer degradation products containing diacids to the particles surface thus inhibiting the Fenton-like reactions occurs at nanoparticle surface. If appropriate long-time degradable PBAE polymer can be developed and functionalized on iron oxide nanoparticles, this unique nanoparticle system can be potential for cancer treatment with enhanced ROS generation or in combination with other therapies such as radiation or chemotherapy.

4.5.　References

1.　Laurent, S., et al., *Magnetic fluid hyperthermia: Focus on superparamagnetic iron oxide nanoparticles.* Advances in Colloid and Interface Science, 2011. **166**(1): p. 8-23.

2.　Ito, A., et al., *Medical application of functionalized magnetic nanoparticles.* Journal of Bioscience and Bioengineering, 2005. **100**(1): p. 1-11.

3.　Dennis, C.L., et al., *Nearly complete regression of tumors via collective behavior of magnetic nanoparticles in hyperthermia.* Nanotechnology, 2009. **20**(39): p. 395103.

4.　Berry, C.C., *Progress in functionalization of magnetic nanoparticles for applications in biomedicine.* Journal of Physics D: Applied Physics, 2009. **42**(22): p. 224003.

5.　Sun, C., J.S.H. Lee, and M. Zhang, *Magnetic nanoparticles in MR imaging and drug delivery.* Advanced Drug Delivery Reviews, 2008. **60**(11): p. 1252-1265.

6. Yu, M.K., et al., *Drug-loaded superparamagnetic iron oxide nanoparticles for combined cancer imaging and therapy in vivo.* Angew Chem Int Ed Engl, 2008. **47**(29): p. 5362-5.

7. Tran, N. and T.J. Webster, *Magnetic nanoparticles: biomedical applications and challenges.* Journal of Materials Chemistry, 2010. **20**(40): p. 8760-8767.

8. Petri-Fink, A., et al., *Development of functionalized superparamagnetic iron oxide nanoparticles for interaction with human cancer cells.* Biomaterials, 2005. **26**(15): p. 2685-2694.

9. Lubbe, A.S., C. Alexiou, and C. Bergemann, *Clinical applications of magnetic drug targeting.* J Surg Res, 2001. **95**(2): p. 200-6.

10. Klein, S., et al., *Superparamagnetic iron oxide nanoparticles as radiosensitizer via enhanced reactive oxygen species formation.* Biochemical and Biophysical Research Communications, 2012. **425**: p. 393-397.

11. Rosensweig, R.E., *Heating magnetic fluid with alternating magnetic field.* Journal of Magnetism and Magnetic Materials, 2002. **252**: p. 370-374.

12. Jordan, A., et al., *Magnetic fluid hyperthermia (MFH): Cancer treatment with AC magnetic field induced excitation of biocompatible superparamagnetic nanoparticles.* Journal of Magnetism and Magnetic Materials, 1999. **201**(1): p. 413-419.

13. Moroz, P., S.K. Jones, and B.N. Gray, *Magnetically mediated hyperthermia: current status and future directions.* Int J Hyperthermia, 2002. **18**(4): p. 267-84.

14. Gordon, R.T., J.R. Hines, and D. Gordon, *Intracellular hyperthermia. A biophysical approach to cancer treatment via intracellular temperature and biophysical alterations.* Med Hypotheses, 1979. **5**(1): p. 83-102.

15. Rabin, Y., *Is intracellular hyperthermia superior to extracellular hyperthermia in the thermal sense?* Int J Hyperthermia, 2002. **18**(3): p. 194-202.

16. Creixell, M., et al., *EGFR-Targeted Magnetic Nanoparticle Heaters Kill Cancer Cells Without A Sensible Temperature Rise.* ACS Nano, 2011. **5**(9): p. 7124–7129.

17. Kozissnik, B., et al., *Magnetic fluid hyperthermia: Advances, challenges, and opportunity.* International Journal of Hyperthermia, 2013. **29**(8): p. 706-714.

18. Polo-Corrales, L. and C. Rinaldi, *Monitoring iron oxide nanoparticle surface temperature in an alternating magnetic field using thermoresponsive fluorescent polymers.* Journal of Applied Physics, 2012. **111**(7).

19. Connord, V., et al., *Real-Time Analysis of Magnetic Hyperthermia Experiments on Living Cells under a Confocal Microscope.* Small, 2015. **11**(20): p. 2437-45.

20. Erdal, H., et al., *Induction of lysosomal membrane permeabilization by compounds that activate p53-independent apoptosis.* Proc Natl Acad Sci U S A, 2005. **102**(1): p. 192-7.

21. Jaattela, M., *Multiple cell death pathways as regulators of tumour initiation and progression.* Oncogene, 2004. **23**(16): p. 2746-56.

22. Sanchez, C., et al., *Targeting a G-protein-coupled receptor overexpressed in endocrine tumors by magnetic nanoparticles to induce cell death.* ACS Nano, 2014. **8**(2): p. 1350-63.

23. Zhang, E., et al., *Dynamic Magnetic Fields Remote-Control Apoptosis via Nanoparticle Rotation.* ACS Nano, 2014. **8**(4): p. 3192-3201.

24. Nel, A., et al., *Toxic Potential of Materials at the Nanolevel.* Science, 2006. **311**: p. 622-628.

25. Lewinski, N., V. Colvin, and R. Drezek, *Cytotoxicity of nanoparticles.* Small, 2008. **4**(1): p. 26-49.

26. Emerit, J., C. Beaumont, and F. Trivin, *Iron metabolism, free radicals, and oxidative injury.* Biomed Pharmacother, 2001. **55**(6): p. 333-9.

27. Mahmoudi, M., et al., *A new approach for the in vitro identification of the cytotoxicity of superparamagnetic iron oxide nanoparticles.* Colloids Surf B Biointerfaces, 2010. **75**(1): p. 300-9.

28. Auffan, M., et al., *Relation between the Redox State of Iron-Based Nanoparticles and Their Cytotoxicity toward Escherichia coli.* Environmental Science & Technology, 2008. **42**(17): p. 6730-6735.

29. Voinov, M.A., et al., *Surface-Mediated Production of Hydroxyl Radicals as a Mechanism of Iron Oxide Nanoparticle Biotoxicity.* Journal of the American Chemical Society, 2011. **133**(1): p. 35-41.

30. Aranda, A., et al., *Dichloro-dihydro-fluorescein diacetate (DCFH-DA) assay: A quantitative method for oxidative stress assessment of nanoparticle-treated cells.* Toxicology in Vitro, 2013. **27**(2): p. 954-963.

31. Hauser, A.M., K.W. Anderson, and J.Z. Hilt, *Peptide conjugated magnetic nanoparticles for magnetically mediated energy delivery to lung cancer cells.* Nanomedicine (Lond), 2016.

32. Guptaa, A.K. and M. Gupta, *Synthesis and surface engineering of iron oxide nanoparticles for biomedical applications.* Biomaterials, 2005. **26**: p. 3995-4021.

33. Laurent, S., et al., *Magnetic Iron Oxide Nanoparticles: Synthesis, Stabilization, Vectorization, Physicochemical Characterizations, and Biological Applications.* Chemical Reviews, 2008. **108**(6): p. 2064-2110.

34. Anderson, D.G., et al., *A combinatorial library of photocrosslinkable and degradable materials.* Advanced Materials, 2006. **18**: p. 2614-2618.

35. Hawkins, A.M., et al., *Tuning biodegradable hydrogel properties via synthesis proce dure.* Polymer 2013. **54**: p. 5.

36. Brey, D.M., et al., *Controlling PBAE network properties through macromer branching.* Acta Biomaterialia, 2008. **4**: p. 207-217.

37. Song, W., et al., *Tunable pH-Sensitive Poly(b-amino ester)s Synthesized from Primary Amines and Diacrylates for Intracellular Drug Delivery.* Macromolecular Biosciences, 2012. **12**: p. 1375-1383.

38. Min, K.H., et al., *Tumoral acidic pH-responsive MPEG-poly(β -amino ester) polymeric micelles for cancer targeting therapy.* Journal of Controlled Release, 2010. **144**: p. 259-266.

39. Qiao, Z.-Y., et al., *One-pot synthesis of pH-sensitive poly(RGD-co-beta amino ester)s for targeted intracellular drug delivery.* Polymer Chemistry of Materials, 2014. **5**: p. 844-853.

40. Fang, C., et al., *Fabrication of magnetic nanoparticles with controllable drug loading and release through a simple assembly approach.* Journal of Controlled Release, 2012. **162**: p. 233-241.

41. Frimpong, R.A., et al., *Enhancing remote controlled heating characteristics in hydrophilic magnetite nanoparticles via facile co-precipitation.* Journal of Magnetism and Magnetic Materials 2010. **332**: p. 326-331.

42. Wydra, R.J., et al., *The role of ROS generation from magnetic nanoparticles in an alternating magnetic field on cytotoxicity.* Acta Biomaterialia, 2015. **25**: p. 284-292.

43. Meenach, S.A., et al., *Controlled synergistic delivery of paclitaxel and heat from poly (beta-amino ester)/iron oxide-based hydrogel nanocomposites.* Internation Journal of Pharmaceutics, 2012. **427**: p. 177-184.

44. Gao, F., et al., *Dopamine coating as a general and facile route to biofunctionalization of superparamagnetic Fe3O4 nanoparticles for magnetic separation of proteins.* RSC Advances, 2014. **4**: p. 6657-6663.

45. Wydra, R.J., et al., *Accelerated generation of free radicals by iron oxide nanoparticles in the presence of an alternating magnetic field.* Royal Society of Chemistry Advances, 2015. **5**(25): p. 18888-18893.

Chapter 5: Reactive oxygen species generation induced by PEG-based polymer coated iron oxide nanoparticles upon alternating magnetic field exposure

Abstract. Iron oxide nanoparticles exhibit the enhanced generation of free radicals through Fenton/Haber-Weiss reactions when exposed to alternating magnetic field (AMF). Surface coatings play an important role as they can inhibit the formation of reactive oxygen species (ROS) at surface of the nanoparticles. In this study, co-precipitated iron oxide nanoparticles were coated with PEG-DOPA polymers, and the ability to generate ROS of the coated particles under present of AMF was also investigated. PEG-DOPA polymers with molecular weight of 5k, 10k and 20k were used while the surface coating process temperature varied from 25° to 60°C to study the impact of surface coverage. The surface reactivity of the synthesized particles was examined using methylene blue decolorization assay. The surface generation of ROS was decreased with the increase of polymer molecular weight. However, the effect of surface coating process temperature was not significant. In contrast, increasing the polymer concentration during the coating process significantly decreased the ROS generated under AMF exposure due to increase of surface coverage.

5.1. Introduction

Iron oxide nanoparticles (IONPs) possess many unique and novel characteristics compared to their bulk form, including comparable size to many biological molecules, high surface-to-volume ratio, superparamagnetic properties, etc. [1]. These properties make IONPs promising for a variety of applications in diagnosis and cancer therapy including cell separation [2] and labeling [3]; targeted drug delivery [4], hyperthermia treatment [5, 6] and magnetic resonance imaging (MRI) [7-9]. However, the cytotoxicity of iron oxide nanoparticles remains a matter of some concern. Recent studies showed that cytotoxicity

of nanoparticles is induced via the generation of reactive oxygen species (ROS) via Fenton and Haber-Weiss reactions [10, 11]. Several studies have been carried out with the aim to suppress the intracellular ROS formation to reduce particles toxicity [12, 13]. In contrast, several studies recently showed that ROS generation induced by IONPs could be beneficial for cancer therapy, where the elevated level of ROS can result in damage to DNA, lipids, proteins, etc. leading to cellular apoptosis [14-16]. It has been recently shown that ROS generation induced by IONPs can be enhanced with the application of alternating magnetic field (AMF) [11].

IONPs are often coated with polymers or small molecules to enhance stability in aqueous and physiological media since uncoated IONPs have the tendency to aggregate together through their interaction with each other or with other biological molecules. In addition to increasing colloidal stability, coatings can also prolong circulation time in blood vessels as well as other functionalization [17-21]. However, the coating has been shown to inhibit surface reactivity of the particles via Fenton/Haber-Weiss reaction [15]. therefore, it is necessary to find a suitable coating that can protect the particles but not inhibit their surface reactivity for applications where this surface reactivity is to be utilized.

The functionalization of IONPs with poly (ethylene glycol) (PEG) is of great interest in biological applications since it can improve particle stability, prolong circulation time and provide a variety of functional groups. In addition, the thickness of polymer coating can influence particles properties including hydrodynamic size, stability, ability for biomolecules interaction [22, 23]. The solubility of the particles increases with the polymer molecular weight. At high molecular weight, hydrocarbon groups of PEG present in the interior and oxygen atoms exposed to interact with water thus influencing the coating thickness, hydrodynamic size, solubility and stability of the PEG functionalized particles [24]. It is also reported the increase in hydrodynamic size as the molecular weight of PEG-silane increased [23]. Moreover, the effect of PEG in preventing the access of reactive

molecules to nanoparticles surface has been also studied. It was showed that polymer molecular weight and graft density are important factors in blocking the absorption of phosphate groups on the particles surface [25]. Shorter chains are preferred over long polymers in increasing exposure of reactive biomolecules to the surface of the particles, promote cellular interactions [26]. However, longer chains have been proven to be more effective in increasing particle stability than shorter chains [23]. However, the effect of molecular weight of PEG on the ability to generate ROS has not yet been studied.

Carboxylic acid, silanes and phophonates are common binding groups that have been used for functionalization of iron oxide nanoparticles [22, 23, 27, 28]. However, recent studies have shown that catechols (3,4-dihydroxy-DL-phenylalanine, DOPA) and nitrocatechols as anchor groups provide significant advantages compared to other traditional binding groups due to their robust anchoring [29, 30]. It has been demonstrated that PEG polymers modified with DOPA are effective in stabilizing magnetite nanoparticles [31, 32]

The objective of this study is to functionalize iron oxide nanoparticles with PEG-DOPA polymers and to study the effect of the coating on surface reactive oxygen species generation induced by AMF exposure. Moreover, different molecular weights of PEG polymer, surface coating process temperatures as well as initial PEG concentrations were also studied.

a) Surface modification of IONP by PEG with different MWs

b) ROS induction by PEG coated IONP with low MW via Fenton chemistry

$$Fe^{3+} + H_2O_2 \longrightarrow Fe^{2+} + H^+ + {^\cdot}OOH$$

dissolution

$$Fe^{2+} + H_2O_2 \longrightarrow Fe^{3+} + OH^- + {^\cdot}OH$$

dissolution

Low MW Polymers

High MW Polymers
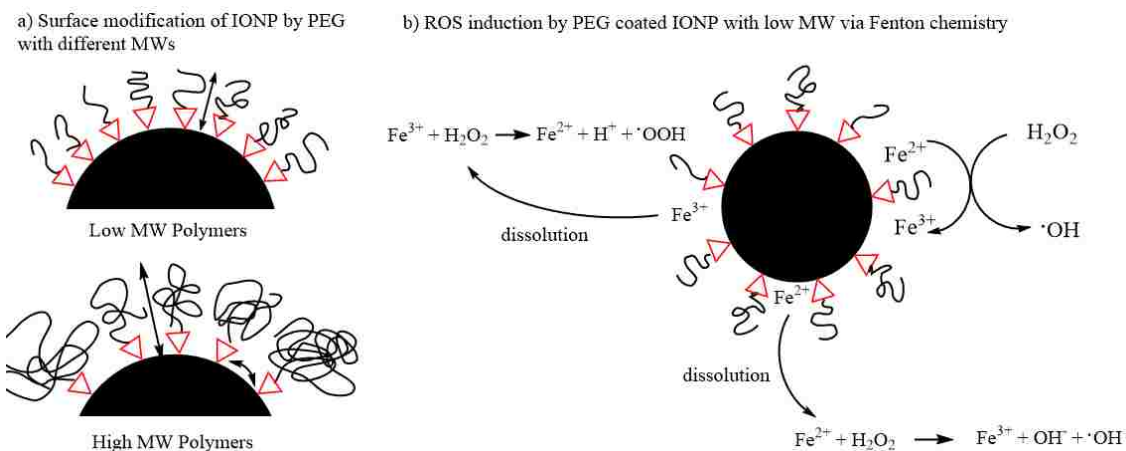
Figure 5.1. a) Surface modification of IONP by PEG with different MWs and b) ROS induction by PEG coated particles with low MW via Fenton reactions

5.2. Materials and methods

5.2.1. Materials

Iron (III) chloride hexahydrate (FeCl$_3$·6H$_2$O), iron (II) chloride tetrahydrate (FeCl$_2$·6H$_2$O), hydrogen peroxide and methylene blue were obtained from Sigma Aldrich (St. Louis MO). Ammonium hydroxide was purchased from EMD chemicals (Gibbstown, NJ). PEG-DOPA polymers were obtained from Mefford's group at Clemson University. All materials were used without any modification.

5.2.2. Iron oxide nanoparticles synthesis

Uncoated iron oxide nanoparticles (UC IONP) were synthesized via co-precipitation process as mentioned previously [32]. In brief, FeCl$_3$ and FeCl$_2$ was mixed at a molar ratio of 2: 1 and the experiment was performed at 85°C under nitrogen flow. Ammonium hydroxide (5ml) was added at 80°C and the reaction was continued for one hour. The reaction mixture was then magnetically decanting and washed three time with

deionized (DI) water. The final particles suspension in DI water was dialyzed against DI water for 24 hours and water was changed every 3 hours.

5.2.3. PEG-DOPA polymer coated IONPs preparation

To prepare PEG-DOPA coated IONPs, a certain amount of PEG-DOPA polymer was dissolved in DI water in a glass vial. The PEG-DOPA polymer solution was probe-sonicated while 100 mg of IONPs suspended in DI water was added to the polymer solution. PEG-DOPA polymers with molecular weight of 5000, 10000 and 20000 were used with concentration varying from 1 mM to 10 mM. After the addition of nanoparticles, the mixture was placed in the shaker to allow coating for 4 hours at $25^{\circ}C$ or $60^{\circ}C$. The resulting particles were centrifuged, and the precipitates were re-dispersed into water. The washing step was repeated three times to remove the unreacted polymer. The final particles were dried in vacuum oven overnight and kept in desiccator until use.

5.2.4. Polymer and particle characterization

PEG-DOPA polymers were characterized using proton nuclear magnetic resonance (^{1}H-NMR) and Fourier transform infrared spectroscopy (FTIR). ^{1}H-NMR was performed using Bruker 400MHz NMR instrument (Department of Chemistry, University of Kentucky). The samples were dissolved in deuterated chloroform and analyzed using 16 scans. FTIR spectroscopy was performed on using attenuated total reflectance (ATR) crystal with Varian Inc. 7000e spectrometer. The measurements were recorded from 700 cm^{-1} to 4000 cm^{-1}.

Dynamic light scattering (DLS) was used to measure hydrodynamic size of the particles. Nanoparticles suspension were prepared at concentration of 0.1 mg/ml in DI water via ultrasonication for 10 min. Measurements were performed triplicate using Malvern Zetasizer, Nano ZS90 instrument.

FTIR spectroscopy was used to characterize surface functionality of the particles. The measurement was performed using attenuated total reflectance (ATR) FTIR with

Varian Inc. 7000e spectrometer. A small amount of dried particles was added on the ATR crystal and the spectrum was recorded from 700 cm^{-1} to 4000 cm^{-1}.

Thermogravimetric analysis (TGA) was done to determine surface coverage of polymers on the surface of particles. Dried particles (5-10mg) were heated at a rate of 5°/min to 120°C at which it was held isothermally for 20 min to remove any residual water. The samples were then heated continuously at 5°/min until reaching 500°C and held there for another 20 min. The mass loss was normalized to the mass after isothermal heating at 120°C. The TGA mass loss was used to calculate surface coverage of the polymer onto particle surface. First, the surface area and volume of magnetite nanoparticles was calculated using uncoated particle diameter from DLS. The mass of iron oxide particles was calculated by multiplying particles volume and density. Second, TGA mass loss were used to determine polymer mass. The number of polymer chains was determined using polymer mass, molecular weight of polymer and Avogadro number. Finally, the surface coverage in chains per nanometer square was yielded by diving total number of polymers by the surface area.

AMF heating was done to measure heating profiles of the nanoparticles using a Taylor Winfield magnetic induction source. Temperature was measured using a fiber optic temperature sensor (Luxtron FOT Lab kit). Nanoparticles were suspended in DI water to a concentration of 3 mg/ml iron oxide. One ml of the solution was placed in a centrifuge tube and placed in the center of AMF induction coil. The solution was heated under the magnetic field of 58 kA/m and 292 kHz for 5 min. The specific adsorption rate (SAR) values were calculated using the following equation (1)

$$SAR = \frac{C_{p,Fe}m_{Fe} + C_{p,H_2O}m_{H_2O}}{m_{Fe}} \frac{\Delta T}{\Delta t} \tag{1}$$

where Cp is the specific heat capacity (0.65 and 4.18 J/g*K for iron oxide and water, respectively), m_{Fe}, m_{H2O} is the mass of iron and water respectively. $\Delta T/\Delta t$ is the initial slope of the heating profile which is calculated from 20 and 30 second time point.

5.2.5. Surface ROS generation via methylene blue decolorization

Methylene blue dye decolorization assay was used to determine the surface ROS generation induced by the as-synthesized particles. The experiments were performed at either controlled water bath or exposed to an AMF at 37°C. Methylene blue was used at 5 µg/ml while iron oxide nanoparticles concentration was 75 µg/ml. 1 ml of samples were placed in the water bath for 10 minutes to equilibrate to the set temperature. The degradation was initiated by spiking the samples with 25 µl of H_2O_2. After 30 minutes exposure, the samples were centrifuged for 3 minutes, magnetically decanted for 30 seconds, and the absorbance of supernatants was measured using UV-visible spectroscopy (maximum absorbance at 665 nm) with a Varian Cary. To account for nanoparticle scattering from the nanoparticles that remain in suspension, sample containing only nanoparticles at the same concentration was measured and subtracted out from the sample absorbance. Similarly, samples exposed to the AMF were prepared as described above. They were placed in water baths for 10 minutes to equilibrate to the expected steady state temperature by AMF exposure (37°C). Then, the samples were exposed to a field of approximately 58.0 kA/m in strength at 292 kHz frequency while temperature was measured with a Luxtron FOT Lab Kit. After 30 minutes exposed to the AMF, the sample was treated as those exposed to water bath. The absorbance of samples was normalized to the initial absorbance of methylene blue. Each experiment was repeated three times and the reported data is the average of three measurements.

5.3.   Results and discussions

5.3.1. PEG-DOPA polymer characterization

PEG-DOPA polymer (structure is illustrated in figure 5.2) was verified using proton NMR and the spectrum of PEG-DOPA with molecular weight of 20000 is shown in figure 5.3. The characteristic peaks include 2.65 ppm corresponded to succinic anhydride ($O=C=CH_2$-$CH_2=C=O$), 3.4 ppm and 3.65 attributed to methoxy end group (O-CH_3) and repeated unit (O-CH_2-CH_2-O) of PEG. The presence of dopamine was confirmed by peaks at 2.9 and 2.95 ppm (CH_2-CH_2, dopamine) and 8.0 ppm (CH ring, dopamine) [30]. Spectra of PEG-DOPA 5000 and 10000 are very similar to that of PEG-DOPA 20000.
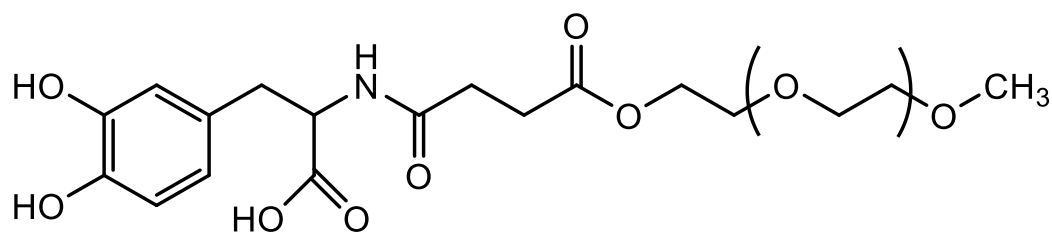
Figure 5.2. PEG-DOPA structure
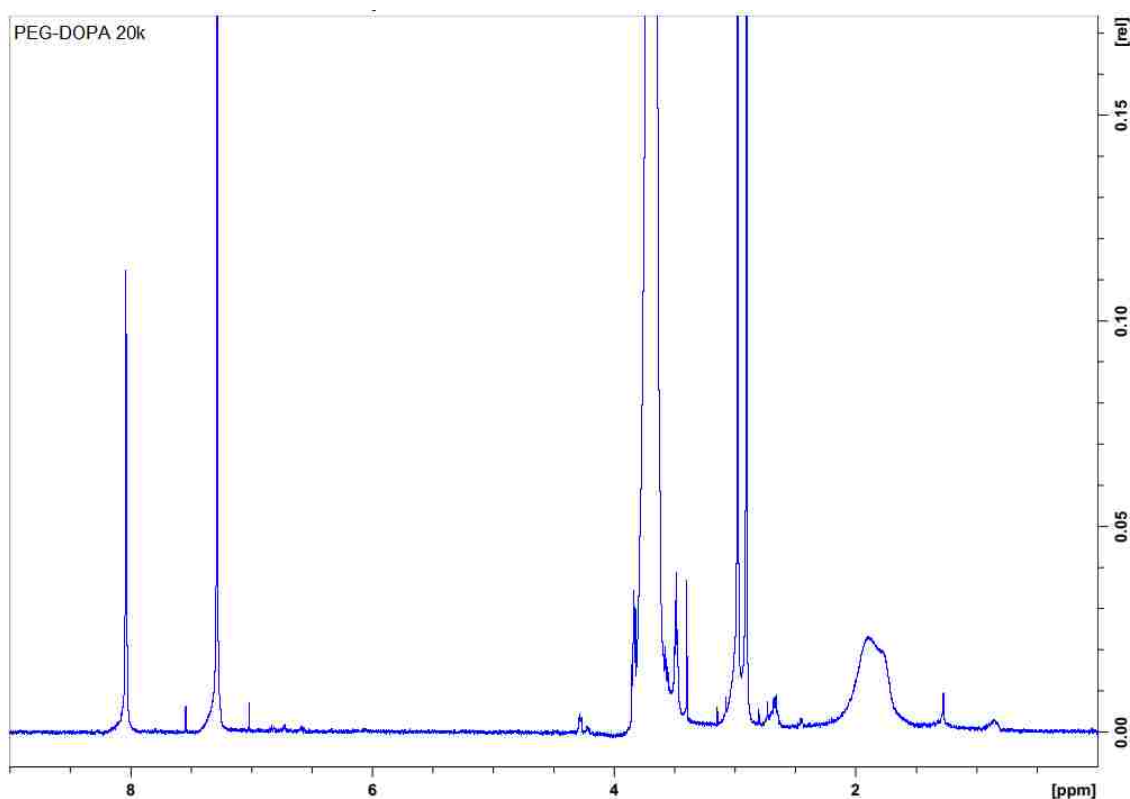
Figure 5.3. NMR spectra of PEG-DOPA 20000. The polymer was dissolved in deuterated chloroform with TMS

FTIR spectroscopy was performed to confirm the successful synthesis of PEG-DOPA. Figure 5.4 presented FTIR spectra of PEG-DOPA with molecular weight of 5000; 10000 and 20000. Peaks of alkyl (-CH$_2$) stretching band was observed at 2880 cm^{-1} while peaks at 1670 cm^{-1} and 1105 cm^{-1} are associated with vibrations of C = O and C-O-C groups. Characteristic peaks of dopamine were recorded at 1143 cm^{-1} and 1485 cm^{-1} corresponded to vibrations of C-O-H and aromatic C = C, respectively. There was no difference in FTIR spectra of PEG-DOPA with varying molecular weights.
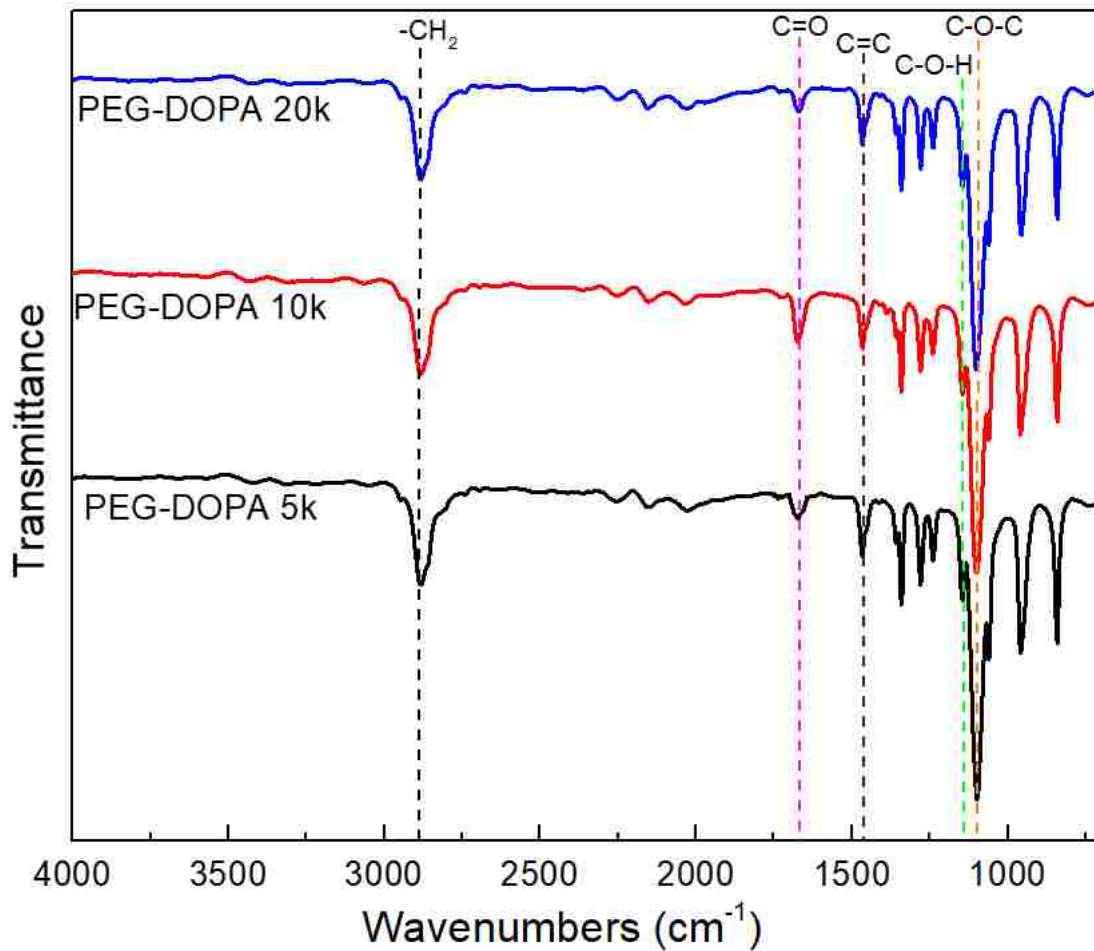
Figure 5.4. FTIR spectra of PEG-DOPA polymers

5.3.2. Nanoparticles characterization

Nanoparticle properties are summarized in table 5.1. The hydrodynamic size of the particles was measured using DLS and reported main peak was the average value of peak 1 (more than 95%). The uncoated particles were 138 nm with PDI of 0.23 while the crystal size of iron oxide particle calculated from XRD pattern was about 10 nm. After coating with PEG polymer, particle sizes increased from approximately 160 nm to 350 nm. The increase in size of coated particles may be due to the coatings or the aggregation of particles during the coating and washing steps. When the coating process temperature increased from 25° to $60^{\circ}C$, particles sizes also increased with PEG-DOPA 5k and PEG-

DOPA 20k coated particle, but the size of PEG 10k coated particles was unchanged. With the increasing of PEG molecular weight from 5k to 20k, the particle size increased significantly. The heating capacity of the nanoparticles in AMF was examined and specific absorption rate (SAR) is presented in table 1. The SAR value of uncoated particles was determined to be 380 W/g, and that of PEG-DOPA 5k and 10k coated particles were quite similar to the uncoated while the PEG-DOPA 20k coated particles exhibited a much lower SAR value, about 270-280 W/g). This could be due to the larger size of those coated particles.

TGA was used to determine the amount of coating present on the particle surface and reported as mass loss. These values were used to calculate the coating density of polymers on the nanoparticles with the assumptions that the particles were spherical, and a uniform layer of coating presented of the surface of nanoparticles. The mass loss along with the surface coverage were presented in table 5.1. The reported mass loss of coated particles was subtracted the mass loss of uncoated particles due to bound water on particles surface. The amount of polymer present on particle surface did not change much between nanoparticles coated by PEG-DOPA with different molecular weights or coating process temperatures. Surface coverage of PEG-DOPA 5k coated particles was about 1 chain per nanometer square, while that of PEG-DOPA 10k and 20k were 0.6 and 0.3 chain per nanometer square. Coating temperature did not affect much on particle mass loss and surface coverage.

Table 5.1. Nanoparticles properties of uncoated and PEG-DOPA (1mM) coated particles

Samples (1mM PEG)	Main peak (d, nm)	PDI	Mass loss (%)	SAR (W/g)	Surface coverage (chains/nm^2)
UC IONP	138.4 ± 2.4	0.23 ± 0.01	3.2	379.4 ± 8.4	-
PEG-DOPA 5k-25-4h	156.2 ± 3.5	0.23 ± 0.01	6.3	343.3 ± 31.2	0.98
PEG-DOPA 5k-60-4h	168.3 ± 3.5	0.2 ± 0.02	7.2	311.4 ± 22.8	1.13
PEG-DOPA 10k-25-4h	169.5 ± 4.2	0.21 ± 0.01	7.9	381.3 ± 40.8	0.62
PEG-DOPA 10k-60-4h	166.3 ± 3.6	0.18 ± 0.03	8.2	351.4 ± 35.5	0.65
PEG-DOPA 20k-25-4h	201.4 ± 8.7	0.17 ± 0.01	8.1	267.4 ± 9.1	0.32
PEG-DOPA 20k-60-4h	347.9 ± 28.9	0.19 ± 0.02	8.4	275.7 ± 24.6	0.33

Table 5.2 contains a summary of properties of PEG-DOPA 5k and 10k coated particles with varying feeding polymer concentrations. With the increasing PEG 10k concentration from 1 mM to 6 mM, the size of particles increased from 170 nm to 225 nm while the SAR values were decreased from 350 W/g to 307 W/g. Similarly, there was a big increase in particle size from 156 nm to 1240 nm when the PEG 5k concentration increased from 1 mM to 10 mM. This indicated an aggregation with the increase of PEG concentration during coating process. And the SAR value decreased from 343 W/g in 1 mM PEG-DOPA 5k coated particles to 233 W/g in 10 mM PEG coated particles. The mass loss of PEG-DOPA 10k increased from 8% with 1 mM of PEG to 11.6% with 6 mM of PEG. Similarly, the surface coverage also increased with the increase of feeding polymer, from 0.62 to 0.95 chain per nanometer square. With the increase of PEG-DOPA 5k

concentration from 1 mM to 10 mM, the amount of mass loss increased more than 2 times from 6.3% to 13.1%. Surface coverage also increase significantly from 0.98 chain to 2.2 chains per nanometer square.

Table 5.2. Summary of properties of PEG-DOPA 5k and 10k coated particles with varying PEG concentrations

Samples	Main peak (d, nm)	PDI	Mass loss (%)	SAR (W/g)	Surface coverage (chains/nm^2)
PEG-DOPA 10k-25-4h 1mM	169.5 ± 4.2	0.21 ± 0.01	7.9	351.4 ± 35.5	0.62
PEG-DOPA 10k-25-4h 4mM	179.1 ± 6.4	0.29 ± 0.03	9.3	323.9 ± 23.8	0.75
PEG-DOPA 10k-25-4h 6mM	224.7 ± 12.0	0.37 ± 0.01	11.6	306.9 ± 9.1	0.95
PEG-DOPA 5k-25-4 1mM	156.2 ± 3.5	0.23 ± 0.01	6.3	343.3 ± 31.2	0.98
PEG-DOPA 5k-25-4 10mM	1240.3 ± 143.2	0.24 ± 0.05	13.1	233.2 ± 16.7	2.19

The coating of PEG-DOPA polymer onto particle surface was confirmed using FTIR which is presented in fig. 5.5. The appearance of characteristic peaks at 1670 cm^{-1}; 1485 cm^{-1} and 1105 cm^{-1} corresponds to C = O, C = C and C – O – C vibrations confirmed the present of PEG-DOPA coating on the surface of nanoparticles. There was no big difference in FTIR spectrum of PEG-DOPA coated particles with different molecular weights or coating process temperatures.
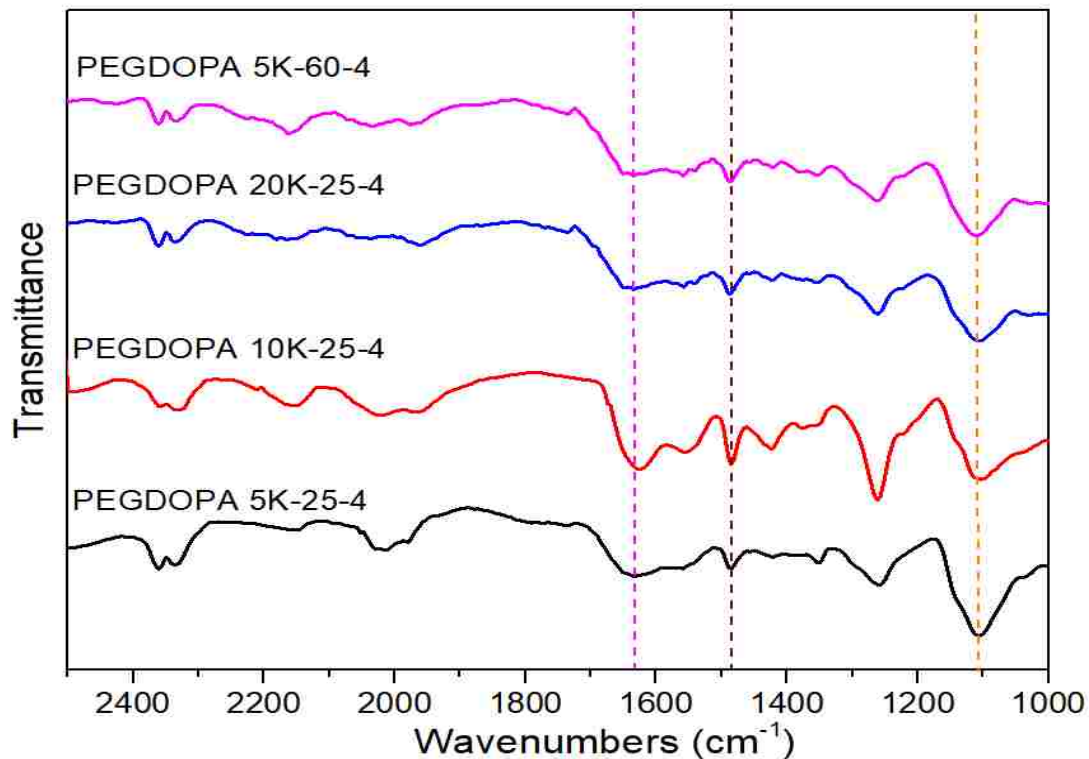
Figure 5.5. FTIR spectrum of different PEG-DOPA coated systems

5.3.3. Surface ROS generation

The generation of surface reactive oxygen species induced by PEG-DOPA coated particles was studied through methylene blue decolorization. The amount of methylene blue degraded is corresponded to the amount of generated ROS. Figure 5.6 presents the normalized absorbance of methylene blue after 30 minutes exposed to different PEG-DOPA coated IONP systems (1mM of initial polymer) upon AMF present. The concentration of iron oxide nanoparticles was kept at 75 µg/ml at which the temperature was oscillated around 37°C. It is worth mentioning that the effects of nanoparticles, hydrogen peroxide alone or the adsorption of methylene blue onto particle surface were negligible. The uncoated nanoparticles displayed nearly 50% degradation in methylene blue absorbance. PEG-DOPA 5k coated particles exhibited a similar behavior with the

uncoated particles. However, there was a decrease in surface ROS generation as the molecular weight of PEG increased from 5k to 10k and 20k. PEG 10k coated particles degraded about 60% of methylene blue while PEG 20k coated one degraded only 15%. This is on the contrary to our hypothesis that the higher molecular weight polymers would have less anchor sites on nanoparticles surface thus allowing for more reactive surface to be exposed. However, it has been shown that long chain polymers can form a thicker barrier which blocks the access of the molecules to nanoparticle surface, resulting in a lower surface interaction [23, 25]. This is in consistent with DLS data as well as TGA mass loss and surface coverage values discussed previously. As increasing polymer molecular weight, the calculated surface coverage decreased while the particle size increased gradually indicating a thicker layer of polymer coating was formed, thus leading to a decrease in surface reactivity.

Besides, higher coating process temperature was expected to allow more mobility or re-arrangement of polymer during coating process leading to a denser coating and lowering surface reactivity. Nevertheless, there was no significant change in methylene blue degradation induced by PEG-DOPA 5k and 20k coated particles when reaction temperature increased from 25° to 60°C, but a remarkable decrease in methylene blue degradation was observed in case of PEG-DOPA 10k coated particles, from 40% to 20%. One possible explanation is that a maximized coating was reached in case of PEG 5k at 1mM, therefore increasing reaction temperature did not yield a higher coating density. In case of PEG 20k, steric effect caused by long chain polymer limited the formation of denser coating, though the particle became much bigger.
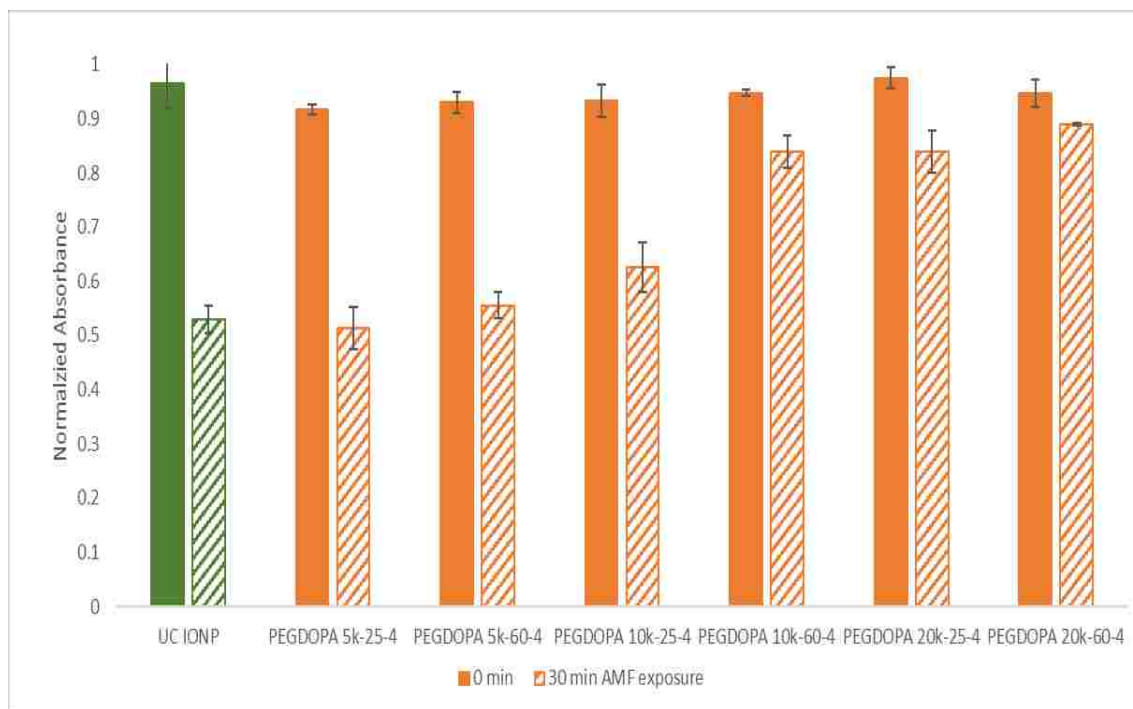
Figure 5.6. The absorbance of methylene blue after exposed to different PEG-DOPA (1 mM) coated systems under AMF present for 30 minutes

To investigate the effect of initial polymer concentration on surface reactivity, PEG-DOPA 5k and 10k coated iron oxide nanoparticles with varying feeding amounts of PEG was synthesized. The results are displayed in figure 5.7. When PEG-DOPA 10k concentration initial increased from 1 mM to 6 mM, there was a slight decrease in surface ROS generation. This is in agreement with DLS and TGA data since particle sizes and surface coverage increased as the polymer feeding concentration increased. The trend was more explicit in case of PEG-DOPA 5k. With 10 mM of PEG, there was a significant decrease in methylene blue decolorization in which only 10% methylene blue was degraded. In this case, particle size increased to 1240 nm and surface coverage was calculated to be 2.2 chains per nanometer square. This indicated a much more significant coating on the particle surface or aggregation of particles when higher concentration of PEG was used.
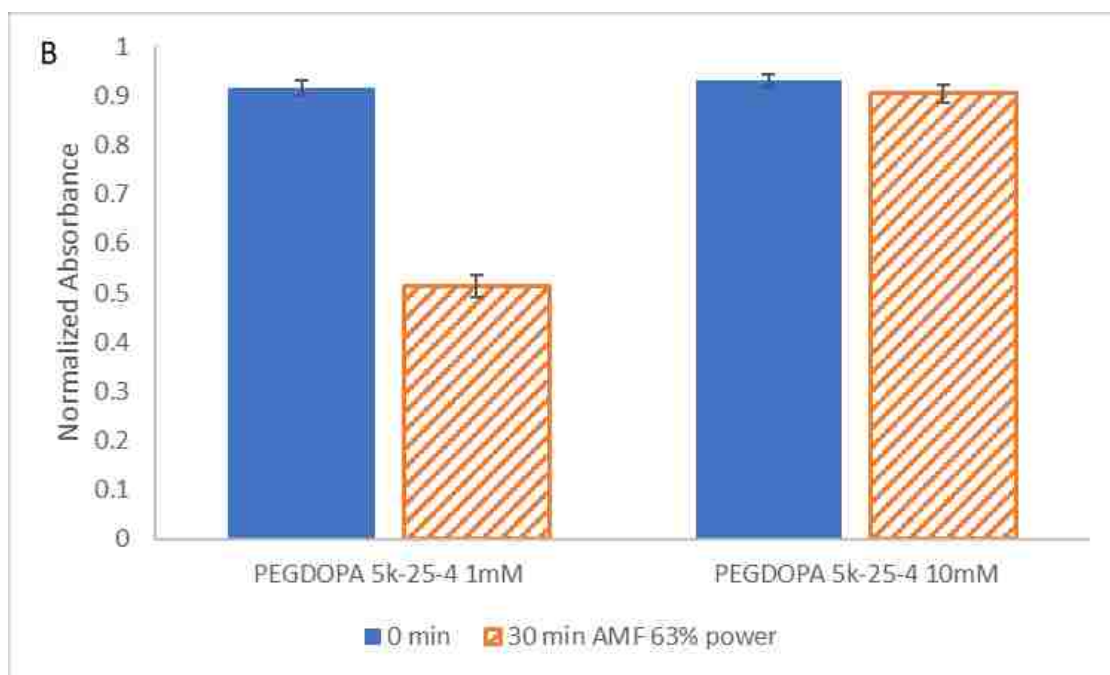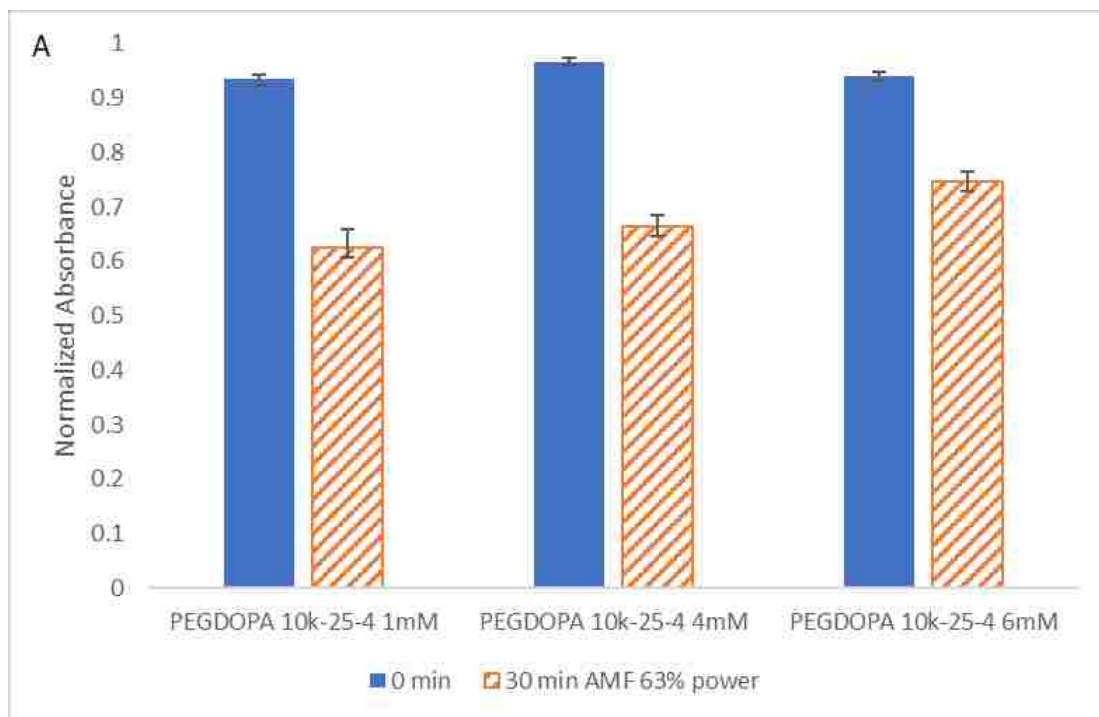
Figure 5.7. The extent of methylene blue degradation of PEG-DOPA 10k (a) and 5k (b) coated particles with varying polymer feeding concentrations over 30 min exposure to AMF

5.4. Conclusion

In this study, iron oxide nanoparticles were functionalized by PEG-dopamine polymers with varying molecular weights and concentrations. The effect of polymer coatings on surface reactive oxygen species generation was investigated through a methylene blue decolorization assay over 30 minutes exposure to an alternating magnetic field. The capacity to generate free radicals of the PEG coated nanoparticles decreased with the increase of polymer molecular weight as well as the initial polymer concentration. However, the effect of coating process temperature on surface reactive oxygen species generation was not significant. In general, PEG-DOPA 5k coated iron oxide nanoparticles seem to be the most reactive system which is comparable to uncoated particles. This result is very promising for future biomedical applications.

5.5. References

1.   Wu, W., Q. He, and C. Jiang, *Magnetic Iron Oxide Nanoparticles: Synthesis and Surface Functionalization Strategies.* Nanoscale Research Letter, 2008. **3**: p. 397-415.

2.   Wang, D., et al., *Superparamagnetic Fe2O3 Beads−CdSe/ZnS Quantum Dots Core−Shell Nanocomposite Particles for Cell Separation.* Nano Letters, 2004. **4**(3): p. 409-413.

3.   Lewin, M., et al., *Tat peptide-derivatized magnetic nanoparticles allow in vivo tracking and recovery of progenitor cells.* Nature Biotechnology, 2000. **18**(4): p. 410-414.

4.   Namdeo, M., et al., *Magnetic nanoparticles for drug delivery applications.* J Nanosci Nanotechnol, 2008. **8**(7): p. 3247-3271.

5.   Pankhurst, Q.A., et al., *Progress in applications of magnetic nanoparticles in biomedicine.* Journal of Physics D: Applied Physics, 2009. **42**(22): p. 224001.

6.   Kruse, A.M., et al., *Synthesis and characterization of CREKA-conjugated iron oxide nanoparticles for hyperthermia applications.* Acta Biomaterialia, 2014. **10**: p. 2622-2629.

7.   Weissleder, R., et al., *MR imaging of splenic metastases: ferrite-enhanced detection in rats.* AJR Am J Roentgenol, 1987. **149**(4): p. 723-6.

8.   Weissleder, R., et al., *Ultrasmall superparamagnetic iron oxide: characterization of a new class of contrast agents for MR imaging.* Radiology, 1990. **175**(2): p. 489-93.

9.   McCarthy, J.R. and R. Weissleder, *Multifunctional magnetic nanoparticles for targeted imaging and therapy.* Advanced Drug Delivery Reviews, 2008. **60**(11): p. 1241-51.

10.   Fu, P.P., et al., *Mechanisms of nanotoxicity: Generation of reactive oxygen species.* Journal of Food and Drug Analysis 2014. **22**: p. 64-75.

11.   Wydra, R.J., et al., *Accelerated generation of free radicals by iron oxide nanoparticles in the presence of an alternating magnetic field.* Royal Society of Chemistry Advances, 2015. **5**(25): p. 18888-18893.

12.   Cochran, D.B., et al., *Suppressing iron oxide nano particle toxicity by vascular targeted antioxidant polymer nanoparticles* Biomaterials, 2013. **34**: p. 9615-9622.

13. Ahamed, M., et al., *Selective killing of cancer cells by iron oxide nanoparticles mediated through reactive oxygen species via p53 pathway.* Journal of Nanoparticles Research, 2013. **15**: p. 1225-1235.

14. Huang, G., et al., *Superparamagnetic Iron Oxide Nanoparticles: Amplifying ROS Stress to Improve Anticancer Drug Efficacy.* Theranostics, 2013. **3**(2): p. 116-126.

15. Wydra, R.J., et al., *The role of ROS generation from magnetic nanoparticles in an alternating magnetic field on cytotoxicity.* Acta Biomaterialia, 2015. **25**: p. 284-292.

16. Hauser, A.M., et al., *Targeted iron oxide nanoparticles for the enhancement of radiation therapy.* Biomaterials, 2016. **105**: p. 127-135.

17. Gupta, A.K. and M. Gupta, *Synthesis and surface engineering of iron oxide nanoparticles for biomedical applications.* Biomaterials, 2005. **26**(18): p. 3995-4021.

18. Frimpong, R.A. and J.Z. Hilt, *Magnetic nanoparticles in biomedicine: synthesis, functionalization and applications.* Nanomedicine (Lond), 2010. **5**(9): p. 1401-14.

19. Amstad, E., M. Textor, and E. Reimhult, *Stabilization and functionalization of iron oxide nanoparticles for biomedical applications.* Nanoscale, 2011. **3**(7): p. 2819-2843.

20. Lind, K., et al., *A Novel Formulation for Superparamagnetic Iron Oxide (SPIO) Particles Enhancing MR Lymphography: Comparison of Physicochemical Properties and The In Vivo Behaviour.* Journal of Drug Targeting, 2002. **10**(3): p. 221-230.

21.   Larsen, E.K.U., et al., *Size-Dependent Accumulation of PEGylated Silane-Coated Magnetic Iron Oxide Nanoparticles in Murine Tumors.* ACS Nano, 2009. **3**(7): p. 1947-1951.

22.   Barrera, C., A.P. Herrera, and C. Rinaldi, *Colloidal dispersions of monodisperse magnetite nanoparticles modified with poly(ethylene glycol).* Journal of Colloid and Interface Science, 2009. **329**: p. 107-113.

23.   Barrera, C., et al., *Effect of poly(ethylene oxide)-silane graft molecular weight on the colloidal properties of iron oxide nanoparticles for biomedical applications.* Journal of Colloid and Interface Science, 2012. **377**: p. 40-50.

24.   Huang, L. and k. Nishinari, *Interaction between poly(ethylene glycol) and water as studied by differential scanning calorimetry.* Journal of Polymer Science B: Polymer Physics, 2001. **39**: p. 496-506.

25.   Miles, W.C., et al., *Synthesis and Colloidal Properties of Polyether−Magnetite Complexes in Water and Phosphate-Buffered Saline.* Langmuir, 2009. **25**(2): p. 803-813.

26.   Veiseh, O., J. Gunn, and M. Zhang, *Design and fabrication of magnetic nanoparticles for targeted drug delivery and imaging.* Advanced drug delivery reviews, 2010. **62**(3): p. 284-304.

27.   Vadala, M.L., et al., *Heterobifunctional Poly(ethylene oxide) Oligomers Containing Carboxylic Acids.* Biomacromolecules, 2008. **9**(3): p. 1035-1043.

28.   Goff, J.D., et al., *Novel Phosphonate-Functional Poly(ethylene oxide)-Magnetite Nanoparticles Form Stable Colloidal Dispersions in Phosphate-Buffered Saline.* Chemistry of Materials, 2009. **21**(20): p. 4784-4795.

29.   Amstad, E., et al., *Ultrastable Iron Oxide Nanoparticle Colloidal Suspensions Using Dispersants with Catechol-Derived Anchor Groups.* Nano Letters, 2009. **9**(2): p. 4042-4048.

30.   Amstad, E., M. Textora, and E. Reimhult, *Stabilization and functionalization of iron oxide nanoparticles for biomedical applications.* Nanoscale, 2011. **3**: p. 2819-2843.

31.   Davis, K., et al., *Quantitative Measurement of Ligand Exchange on Iron Oxides via Radiolabeled Oleic Acid.* Langmuir, 2014. **30**: p. 10918-10925.

32.   Saville, S.L., et al., *Investigation of the stability of magnetite nanoparticles functionalized with catechol based ligands in biological media.* Journal of Materials Chemistry, 2012. **22**: p. 24909-24917.

33.   Frimpong, R.A., et al., *Enhancing remote controlled heating characteristics in hydrophilic magnetite nanoparticles via facile co-precipitation.* Journal of Magnetism and Magnetic Materials 2010. **332**: p. 326-331.

Chapter 6: Enhancement of surface reactivity of iron oxide nanoparticles by the addition of hydroxylamine in Fenton reaction

Abstract. Iron oxide nanoparticles (IONPs) can generate highly reactive oxygen species (ROS) such as hydroxyl radicals via Fenton reactions. Exposure to alternating magnetic field (AMF) has been demonstrated to effectively enhance the production of surface ROS. However, the limitation of the Fenton systems is the accumulation of Fe (III) and narrow pH range, etc. It has been shown that NH_2OH can react with Fe (III) to regenerate Fe (II), thus alleviating Fe (III) accumulation and accelerating the redox cycle of Fe (II)/Fe (III) leading to an enhanced surface reactivity of nanoparticle via Fenton reaction. In this study, the ability to generate ROS of the uncoated and coated iron oxide nanoparticles was investigated under the presence of alternating magnetic field and hydroxylamine as a catalyst. We observed an increase in surface reactivity of nanoparticle with the addition of hydroxylamine (NH_2OH) in both cases. Moreover, the kinetic data was fit to pseudo-first-order model and the rate constants increased at least 3.4 times with the presence of hydroxylamine in the Fenton reaction.

6.1. Introduction

Fenton processes have been widely studied and proved to be potential as advanced oxidation processes (AOPs) for wastewater treatments [1-3]. Hydroxyl radical (HO·) is one of the most reactive species which can oxidize most organic substrate unselectively [1, 4]. It has been shown that iron oxide nanoparticles (IONPs) can be generated hydroxyl radical from Fenton/Haber-Weiss reactions with presence of hydrogen peroxide [1, 5]. Nevertheless, the environmental application of Fenton systems is still limited due to strict pH range, accumulation of sludges [6, 7].

Consequently, recent research has focused on the improvement of these shortcomings of the Fenton reactions. Heterogeneous catalysts using solid iron oxides and other transition metal oxides have been studied to enlarge pH application range and prevent the formation of sludges [8-11]. Adding chelating agents into Fenton systems to reduce the accumulation of ferric irons has also been studied by Sun et al. [12]. Another method is to combine Fenton system with other technologies such as UV radiation or ultrasonic to enhance hydroxyl radical generation [13-17]. In addition, several catalysts have been shown that can facilitate the transformation of Fe (III) to Fe (II) [18, 19]. Hydroxylamine (NH_2OH), a reductant and antioxidant, has been frequently used to determine total iron concentration [20] and to activate catalyst and polyacrylonitrile fiber in advanced oxidation [21, 22]. It has been demonstrated that it can effectively accelerate the transformation of Fe (III) to Fe (II) and enhance the Fe (III)/Fe (II) redox cycle [23].

The objective of this work was to study the effect of hydroxylamine on Fenton reactions induced by iron oxide nanoparticles upon alternating magnetic field exposure. Surface reactivity of uncoated particles via methylene blue dye decolorization with different hydroxylamine concentration was examined. The dye decolorization of coated systems (citric acid- and PEG- coated particles) was also studied with addition of 4 mM of hydroxylamine. The kinetic decolorization profiles of uncoated and coated nanoparticles under AMF presence was also investigated.

6.2. Materials and methods:

6.2.1. Materials

Iron (III) chloride hexahydrate ($FeCl_3 \cdot 6H_2O$), iron (II) chloride tetrahydrate ($FeCl_2 \cdot 6H_2O$), hydrogen peroxide, hydroxylamine hydrochloride and methylene blue were obtained from Sigma Aldrich (St. Louis MO). Citric acid monohydrate was from Fisher

Scientific. Ammonium hydroxide was purchased from EMD chemicals (Gibbstown, NJ). PEG-Dopamine 10k was from Mefford's group at Clemson University. All materials were used without any modification.

6.2.2. Nanoparticles synthesis

The uncoated iron oxide nanoparticles (UC IONP) were synthesized via co-precipitation process as mentioned previously [24]. Briefly, a mixture of $FeCl_3$ and $FeCl_2$ aqueous solution was prepared with a molar ratio of 2: 1 and heated to 85°C under nitrogen flow. Once the temperature reached 80°C, 5 ml of NH_4OH was added into the mixture and the reaction was performed for one hour at 85°C. The particles were then magnetically decanting and washed three time with deionized (DI) water. The final particles suspension in DI water was dialyzed against DI water for 24 hours and water was changed every 3 hours.

Citric acid coated particles (CA-IONP) were synthesized through a similar process with a slight modification in which 4ml of 2M citric acid solution in DI water was injected right after the addition of ammonium hydroxide. The reaction was carried out for 1 hour at 85°C and the final product was dialyzed against water for 48 hours with water changing every 3 hours.

PEG-Dopamine (PEG-DA) coated particles were prepared at 25°C for 4 hours and PEG with molecular weight of 10k was used. PEG-DA 10k polymer was dissolved in DI water at concentration of 1mM and added to particle suspension while ultrasonicating for 10 minutes. The coating process was done in a shaker at 150rpm. The product was centrifuged, washed 3 times with DI water and the final particles were dried and kept in desiccator until use.

6.2.3. Particle characterization

Dynamic light scattering (DLS) was done to analyze size distribution of nanoparticles Nanoparticles suspension was prepared at 0.2 mg/ml through ultrasonication for 10 min. Measurements were performed triplicate using Malvern Zetasizer, Nano ZS90 instrument.

Thermogravimetric analysis (TGA) was used to determine the amount of polymer coating in nanoparticles using Q50 TGA/DSC system. Approximate 5-10 mg of dried particles were heated at 5°/min to 500°C and held isothermally at 120°C and 500°C for 20 min. The mass loss was normalized to the mass after isothermal heating at 120°C.

Alternating magnetic field (AMF) heating was performed to measure heating profiles of the nanoparticles using a Taylor Winfield magnetic induction source. Temperature was measured using a fiber optic temperature sensor (Luxtron FOT Lab kit). Nanoparticles suspension was prepared at 3 mg/ml. One ml of the solution was exposed to magnetic field of 58 kA/m and 292 kHz for 5 min. The specific adsorption rate (SAR) values were calculated using the following equation (1)

$$SAR = \frac{C_{p,Fe}m_{Fe} + C_{p,H_2O}m_{H_2O}}{m_{Fe}} \frac{\Delta T}{\Delta t} \tag{1}$$

where C_p is the specific heat capacity (0.65 and 4.18 J/g*K for iron oxide and water, respectively), m_{Fe}, m_{H_2O} is the mass of iron and water respectively. $\Delta T/\Delta t$ is the initial slope of the heating profile which is calculated from 20 and 30 second time point.

6.2.4. Surface reactive oxygen species generation via methylene blue decolorization assay

The production of ROS induced by the as-synthesized nanoparticles was examined using methylene blue decolorization assay with a small modification [25]. Hydoxylamine was added as a catalyst for the Fenton process with concentration varying from 2mM to 6mM. Methylene blue was set at concentration of 5 µg/ml while 75 µg/ml of iron oxide nanoparticles was used in DI water. The samples were placed in the water bath at 37°C for 10 minutes to equilibrate to the set temperature. Then a certain amount of 80mM NH_2OH was added following by addition of 25 µl of 30% H_2O_2 and the mixture was immediately exposed the AMF field (58.0 kA/m; 292 kHz). Temperature was measured with a Luxtron FOT Lab Kit. After 30 minutes, excess amount of methanol was added to the mixture to quench the reaction and the samples were centrifuged for 2 minutes using a Phenix Quickspin Centrifuge, magnetically decanted for 30 seconds. The absorbance of supernatants was measured using UV-visible spectroscopy with maximum absorbance at 665 nm. The absorbance of nanoparticles only was also measured and subtracted out from the sample absorbance. The absorbance of sample after 0- and 30- minute exposure was normalized to that of methylene blue control with the same amount of hydroxylamine.

6.3.   Results and discussions

6.3.1. Methylene blue decolorization with and without the presence of hydroxylamine

Particle properties were discussed in previous chapters and summarized in table 6.1 below. The size of the uncoated particles was 106 nm with the mass loss of 3.2% corresponding to bound water on particle surface. After coated with PEG-DA polymer, particle size increased to 165 nm and the coating is about 8%. The citric acid coating did not change particle size significantly and remained about 102 nm and the coating is 3.2%, much smaller than that of PEG polymer coating. This could be explained by the adsorption of citric acid onto particle surface during synthesis process inhibiting the growth of nuclei

[24]. The heating capacity of the uncoated and PEG-DA coated particles were quite close while CA-IONP exhibited a lower SAR value.

Table 6.1 Nanoparticles properties

Samples	Main peak (d, nm)	PDI	Mass loss (%)	SAR (W/g)
UC IONP	106.4 ± 2.1	0.29 ± 0.01	3.2	379.4 ± 8.4
CA-IONP	102.4 ± 1.3	0.32 ± 0.01	5.5	305.7 ± 15.8
PEG-DA 10k-25-4h 1mM	165.3 ± 4.2	0.21 ± 0.01	7.9	381.3 ± 40.8

Hydroxylamine has been shown that it could increase Fenton reaction rates and expand pH range by accelerating the redox cycle of Fe (III) and Fe (II) [23, 26]. Fenton reactions with the presence of NH_2OH was illustrated in figure 1 below [23]. As shown in figure 6.1, NH_2OH reacts with Fe^{3+} to regenerate Fe^{2+} and release N_2O and NO_3^- as products. Hence, the addition of NH_2OH can eliminate the Fe (III) accumulation, enhance the formation of Fe (II), consequently increase reaction rates.
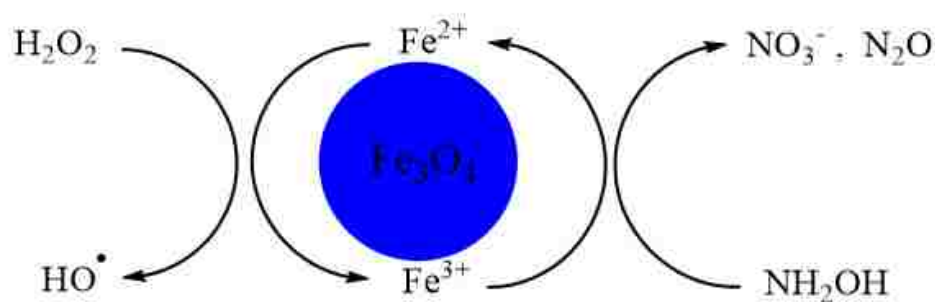
Figure 6.1. Illustration of Fenton reactions induced by iron oxide nanoparticles with the addition of hydroxylamine

To study the effect of NH_2OH on surface ROS generation induced by IONPs, methylene blue degradation, experiments were performed using uncoated particles with

varying NH_2OH concentrations from 0 to 6 mM upon AMF exposure and the results were shown in figure 6.2. Without the addition of NH_2OH, about 47% of methylene blue was degraded. With the increasing of NH_2OH concentration from 2 mM to 6 mM, the degradation of methylene blue also increased to 60% to 90%. However, there was no different in methylene blue degradation between 4 mM and 6 mM of NH_2OH, thus 4 mM NH_2OH was used for the upcoming experiments.
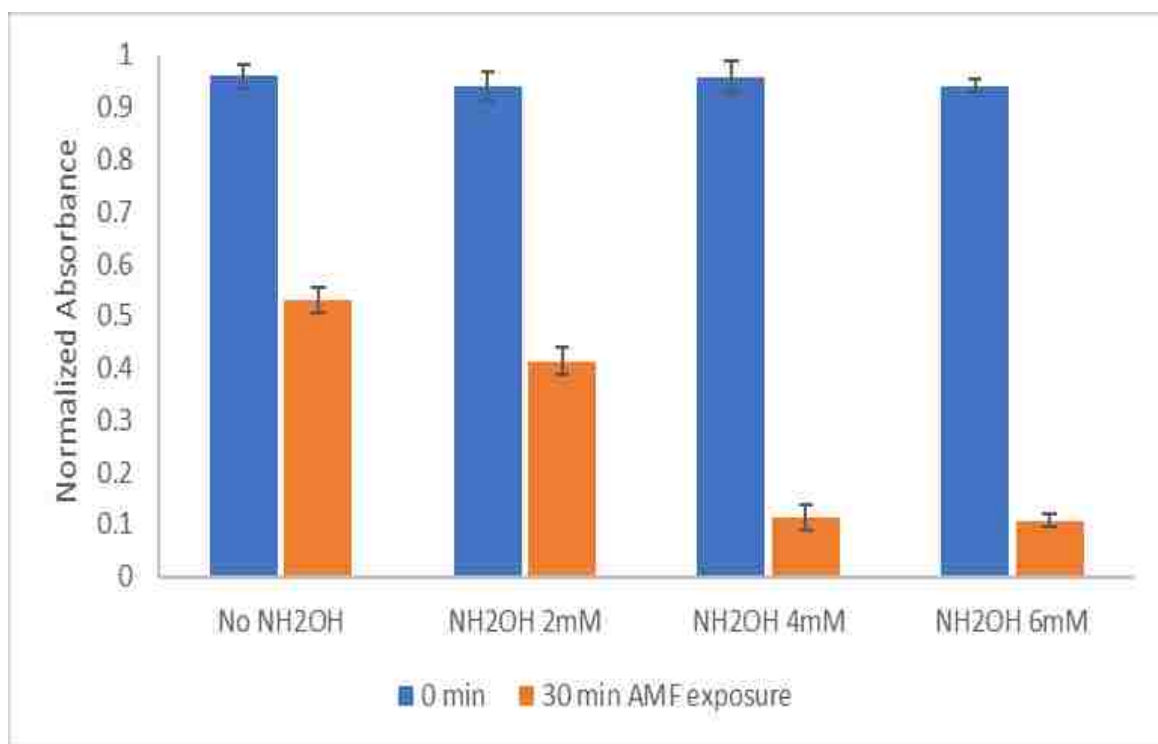
Figure 6.2. Methylene blue degradation of UC IONP with varying NH_2OH concentrations from 0 to 6 mM under 30 minutes AMF exposure

Figure 6.3 presents the degradation of methylene blue by the uncoated; CA- and PEG-DA- coated particles without and with 4mM of NH_2OH. As seen from figure 6.3, without the IONPs but 4mM NH_2OH, there was about 13% degradation in methylene blue absorbance since NH_2OH has been demonstrated that it can activate H_2O_2 to produce HO· without transition metal [150]. As discussed in previous chapters, citric acid coated

particles inhibited almost of the surface ROS generation due to a dense coating layer while PEGDA 10k coated particles degraded about 40% of methylene blue. However, with the addition of NH_2OH at 4 mM, about 95% of methylene blue was degraded in both CA-IONP and PEGDA 10k coated particles which was even higher than that of uncoated system. Besides the acceleration of Fe (II)/Fe (III) redox cycles thus enhancing the production of reactive radicals in Fenton reactions, the interaction mechanism of citric acid and PEG-dopamine coatings and NH_2OH is still unknown.
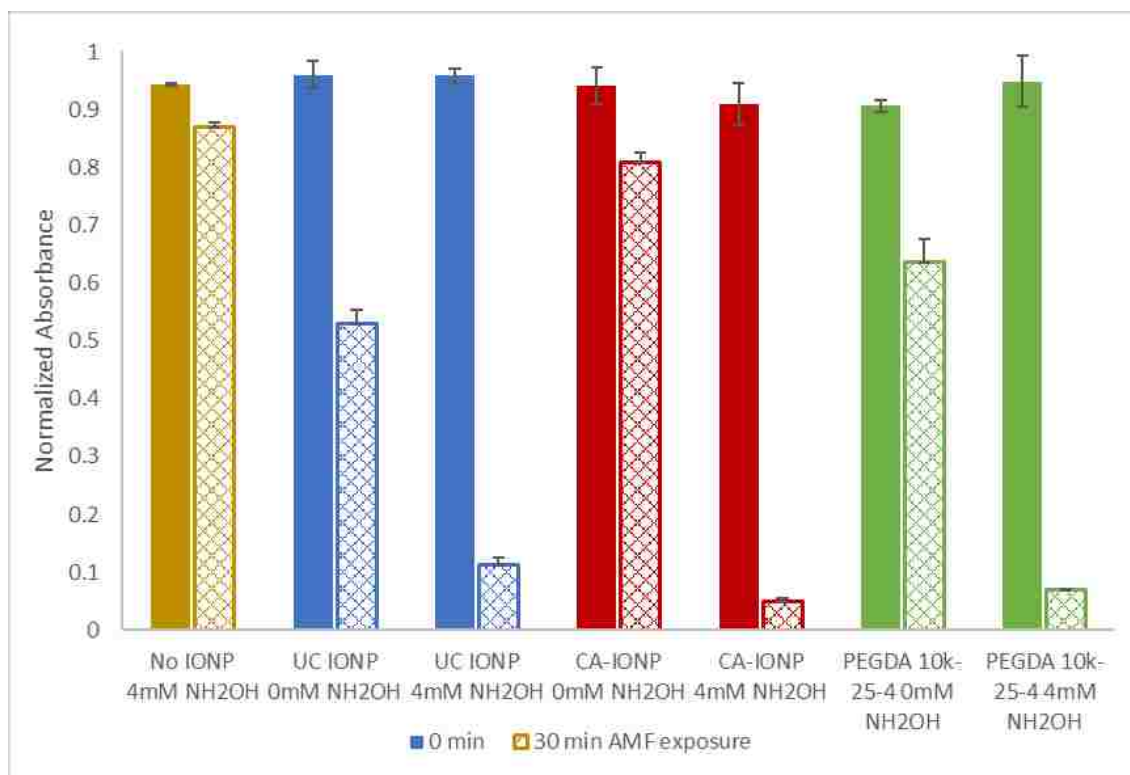
Figure 6.3. Methylene blue dye decolorization of UC IONP, CA-IONP and PEGDA 10k coated IONP without and with 4 mM of NH_2OH with the exposure of AMF for 30 minutes.

6.3.2. Kinetics study

The kinetics of methylene blue decolorization was studied with and without the addition of NH_2OH with the exposure to AMF at 37°C. The data was fit to both pseudo-first-order and second-order models as previously explored in literature [28, 29]. The following rate equations were used [30]

$$\ln(A_t/A_o) = -k_1 t \qquad (2)$$

$$1/(A_t/A_o) = k_2 t + 1 \qquad (3)$$

Where k_1 and k_2 are the first and second order rate constants, A_t is the absorbance measured at a given time while A_o is the initial absorbance of methylene blue
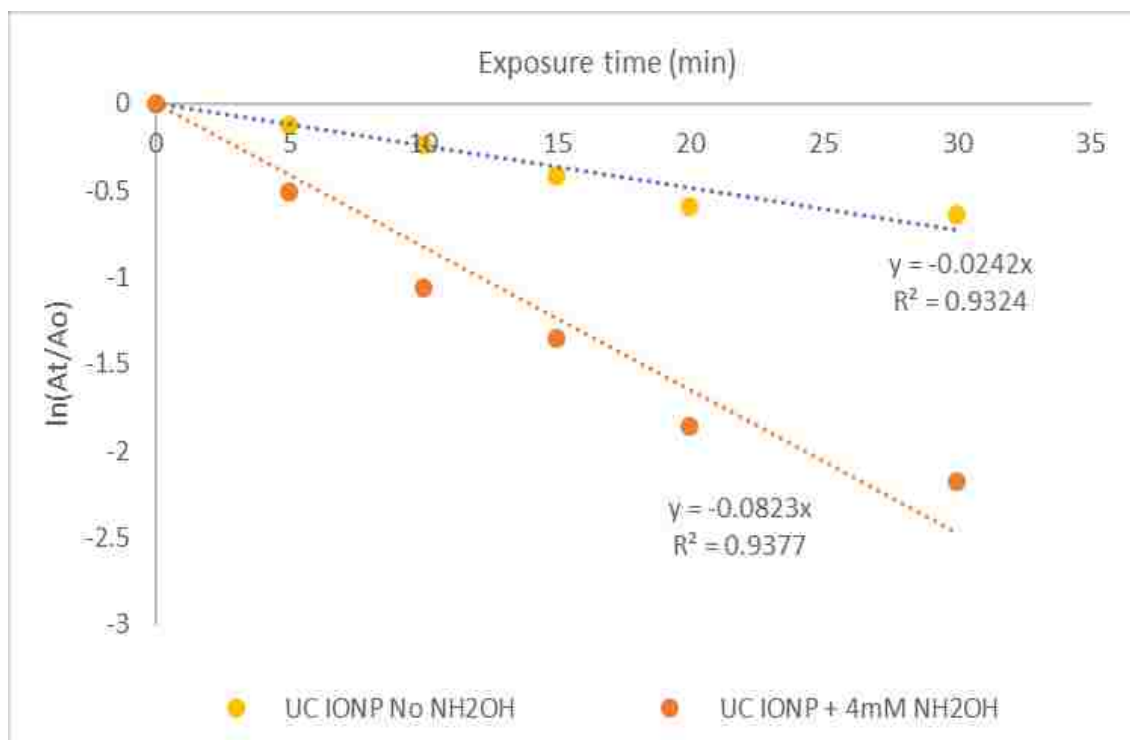
Figure 6.4. The pseudo-first-order kinetic plots of uncoated particles without and with the addition of 4 mM of NH_2OH with the presence of alternating magnetic field

The methylene blue decolorization data was fit using the above equations with linear regression and the respective rate constants was determined. The pseudo-first-order model was presented in figure 6.4 since it fit better to majority of the tested systems with the correlation coefficient (R^2) of approximately 0.93. This result is also similar to what reported in literature [29]. With the addition of NH_2OH, the rate constant increased 3.4 times compared to that of system with no NH_2OH (presented in table 6.2). Similarly, the kinetic data of coated particles with 4 mM of NH_2OH presented in figure 6.5 also fit to pseudo-first-order model with correlation coefficient of 0.93 or higher. The rate constants of citric acid and PEG-DA coated systems was 1.4 and 2.1 times, respectively, higher than that of uncoated system (presented in table 6.2). Hence, the addition of NH_2OH could effectively accelerate the regeneration of Fe (II) in Fenton reaction, alleviate the accumulation of Fe (III), resulting in increased surface reactivity of all tested nanoparticle systems under AMF exposure. Further experiments should be done to understand the possible interaction between the citric acid/ PEG coatings and the hydroxylamine.
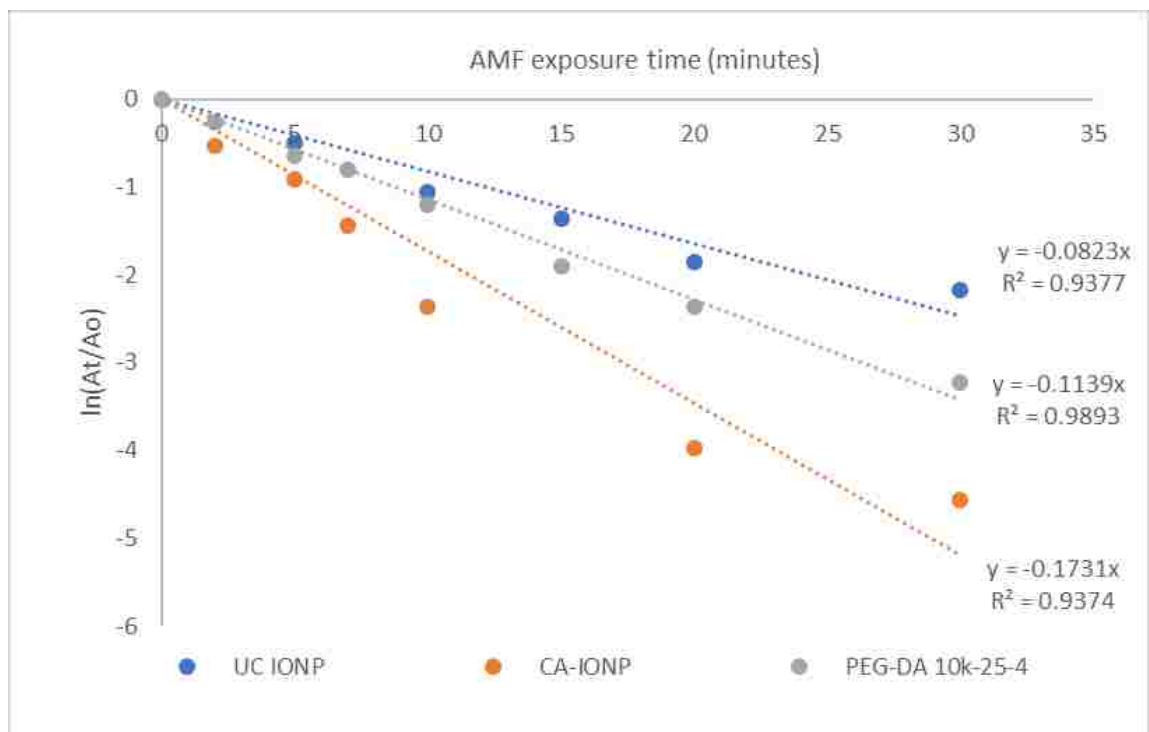
Figure 6.5. The pseudo-first-order kinetic plots of uncoated particles, citric acid and PEG-dopamine coated particles with 4 mM of NH_2OH upon alternating magnetic field exposure

Table 6.2. Summary of the pseudo-first-order rate constants

Samples	NH_2OH concentration (mM)	Rate constant (min^{-1})
UC IONP	0	0.0242
UC IONP	4	0.0823
CA-IONP	4	0.1731
PEG-DA 10k-25-4	4	0.1139

6.4. Conclusion

This study reported the enhanced decolorization of methylene blue by reactive oxygen species induced by iron oxide nanoparticles with the addition of hydroxylamine upon alternating magnetic field presence. The degradation of methylene blue increased with the increase of hydroxylamine concentration. The kinetics data of methylene blue decolorization was fit using pseudo-first-order model. With 4 mM of hydroxylamine, the reaction rate constant of uncoated particles increased about 3.4 times. Moreover, with the presence of hydroxylamine also significantly enhanced surface reactivity of citric acid and PEG-dopamine coated particles in which approximately 95% of methylene blue was degraded.

6.5. References

1.   Hartmann, M., S. Kullmann, and H. Keller, *Wastewater treatment with heterogeneous Fenton-type catalysts based on porous materials.* Journal of Materials Chemistry, 2010. **20**(41): p. 9002.

2.   Wang, B., et al., *Physicochemical Origin for Free Radical Generation of Iron Oxide Nanoparticles in Biomicroenvironment: Catalytic Activities Mediated by Surface Chemical States.* The Journal of Physical Chemistry C, 2012. **117**(1): p. 383-392.

3.   Wang, C., H. Liu, and Z. Sun, *Heterogeneous Photo-Fenton Reaction Catalyzed by Nanosized Iron Oxides for Water Treatment.* International Journal of Photoenergy, 2012. **2012**: p. 1-10.

4.   Goldstone, J.V., et al., *Reactions of Hydroxyl Radical with Humic Substances: Bleaching, Mineralization, and Production of Bioavailable Carbon Substrates.* Environmental Science & Technology, 2002. **36**(3): p. 364-372.

5.   Enami, S., Y. Sakamoto, and A.J. Colussi, *Fenton chemistry at aqueous interfaces.* Proc Natl Acad Sci U S A, 2014. **111**(2): p. 623-8.

6.   Pignatello, J.J., E. Oliveros, and A. MacKay, *Advanced Oxidation Processes for Organic Contaminant Destruction Based on the Fenton Reaction and Related Chemistry.* Critical Reviews in Environmental Science and Technology, 2006. **36**(1): p. 1-84.

7.   Descorme, C., *Catalytic wastewater treatment: Oxidation and reduction processes. Recent studies on chlorophenols.* Catalysis Today, 2017. **297**: p. 324-334.

8.   Qin, Q., et al., *Enhanced heterogeneous Fenton-like degradation of methylene blue by reduced CuFe2O4.* RSC Advances, 2018. **8**(2): p. 1071-1077.

9.   Hassanpour, M., H. Safardoust-Hojaghan, and M. Salavati-Niasari, *Degradation of methylene blue and Rhodamine B as water pollutants via green synthesized Co 3 O 4 /ZnO nanocomposite.* Journal of Molecular Liquids, 2017. **229**: p. 293-299.

10.   Ramirez, J.H., et al., *Azo-dye Orange II degradation by heterogeneous Fenton-like reaction using carbon-Fe catalysts.* Applied Catalysis B: Environmental, 2007. **75**(3-4): p. 312-323.

11.   Hua, Z., et al., *Heterogeneous Fenton degradation of bisphenol A catalyzed by efficient adsorptive Fe3O4/GO nanocomposites.* Environ Sci Pollut Res Int, 2014. **21**(12): p. 7737-45.

12.   Sun, Y. and J.J. Pignatello, *Chemical treatment of pesticide wastes. Evaluation of iron(III) chelates for catalytic hydrogen peroxide oxidation of 2,4-D at circumneutral pH.* Journal of Agricultural and Food Chemistry, 1992. **40**(2): p. 322-327.

13.   C, W. and Z. S, *Optimization and Interpretation of Fenton and UV/Fenton Processes for Degradation of Syringyl Lignin.* Journal of Environmental Analytical Chemistry, 2014. **01**(02).

14.   Huang, R., et al., *Ultrasonic Fenton-like catalytic degradation of bisphenol A by ferroferric oxide (Fe(3)O(4)) nanoparticles prepared from steel pickling waste liquor.* J Colloid Interface Sci, 2014. **436**: p. 258-66.

15.   Lakshmi Prasanna, V. and R. Vijayaraghavan, *Simultaneous Fenton–Photocatalytic Reactions through a New Single Catalyst (Nano ZnO2 /Fe2+) for Dye Degradation.* The Journal of Physical Chemistry C, 2017. **121**(34): p. 18557-18563.

16.   Li, M., et al., *Accelerated methylene blue (MB) degradation by Fenton reagent exposed to UV or VUV/UV light in an innovative micro photo-reactor.* Applied Catalysis B: Environmental, 2016. **187**: p. 83-89.

17.   Ojha, D.P., M.K. Joshi, and H.J. Kim, *Photo-Fenton degradation of organic pollutants using a zinc oxide decorated iron oxide/reduced graphene oxide nanocomposite.* Ceramics International, 2017. **43**(1): p. 1290-1297.

18.   Duesterberg, C.K. and T.D. Waite, *Kinetic Modeling of the Oxidation of p-Hydroxybenzoic Acid by Fenton's Reagent: Implications of the Role of Quinones in the Redox Cycling of Iron.* Environmental Science & Technology, 2007. **41**(11): p. 4103-4110.

19.   Paciolla, M.D., S. Kolla, and S.A. Jansen, *The reduction of dissolved iron species by humic acid and subsequent production of reactive oxygen species.* Advances in Environmental Research, 2002. **7**(1): p. 169-178.

20. Viollier, E., et al., *The ferrozine method revisited: Fe(II)/Fe(III) determination in natural waters.* Applied Geochemistry, 2000. **15**(6): p. 785-790.

21. Dong, Y., et al., *Preparation and photocatalytic performance of Fe (III)-amidoximated PAN fiber complex for oxidative degradation of azo dye under visible light irradiation.* Science of The Total Environment, 2010. **408**(10): p. 2245-2253.

22. Huling, S.G., et al., *Repeated Reductive and Oxidative Treatments of Granular Activated Carbon.* Journal of Environmental Engineering, 2005. **131**(2): p. 287-297.

23. Chen, L., et al., *Strong enhancement on fenton oxidation by addition of hydroxylamine to accelerate the ferric and ferrous iron cycles.* Environ Sci Technol, 2011. **45**(9): p. 3925-30.

24. Frimpong, R.A., et al., *Enhancing remote controlled heating characteristics in hydrophilic magnetite nanoparticles via facile co-precipitation.* Journal of Magnetism and Magnetic Materials 2010. **332**: p. 326-331.

25. Wydra, R.J., et al., *The role of ROS generation from magnetic nanoparticles in an alternating magnetic field on cytotoxicity.* Acta Biomaterialia, 2015. **25**: p. 284-292.

26. Zou, J., et al., *Rapid Acceleration of Ferrous Iron/Peroxymonosulfate Oxidation of Organic Pollutants by Promoting Fe(III)/Fe(II) Cycle with Hydroxylamine.* Environmental Science & Technology, 2013. **47**(20): p. 11685-11691.

27. Chen, L., et al., *Production of Hydroxyl Radical via the Activation of Hydrogen Peroxide by Hydroxylamine.* Environ Sci Technol, 2015. **49**(17): p. 10373-9.

28. Shahwan, T., et al., *Green synthesis of iron nanoparticles and their application as a Fenton-like catalyst for the degradation of aqueous cationic and anionic dyes.* Chemical Engineering Journal, 2011. **172**(1): p. 258-266.

29. Hsieh, S. and P.-Y. Lin, *FePt nanoparticles as heterogeneous Fenton-like catalysts for hydrogen peroxide decomposition and the decolorization of methylene blue.* Journal of Nanoparticle Research, 2012. **14**(6).

30. Wydra, R.J., et al., *Accelerated generation of free radicals by iron oxide nanoparticles in the presence of an alternating magnetic field.* Royal Society of Chemistry Advances, 2015. **5**(25): p. 18888-18893.

Chapter 7: Organic contaminants degradation via Fenton reaction induced by magnetite nanoparticle in the presence of alternating magnetic field

Abstract. In this work, the degradation of organic contaminants via Fenton reaction were studied and bisphenol A (BPA) was used as a model compound. The Fenton process was induced by iron oxide nanoparticles with the presence of H_2O_2 and enhanced by the addition of NH_2OH catalyst as well as upon alternating magnetic field (AMF) exposure. Moreover, key factors of the degradation such as pH, IONP concentration and catalyst concentration was also studied. The degradation process achieved a 57% degradation of BPA after 30 min exposure to AMF. For the parameters studied, optimum conditions for this degradation were determined to be at pH 3, 75 µg/ml of iron oxide nanoparticles, 20 mM of hydrogen peroxide and 6 mM of hydroxylamine. The BPA degradation was determined to follow 2nd order kinetics, and the rate constant was increased 1.4 time with AMF exposure compared to that of water bath exposure the same temperature (37 °C). These results suggested the potential application of iron oxide nanoparticles in organic contaminant degradation through Fenton process under AMF exposure.

7.1. Introduction

Organic wastewater pollutants have paid much interest recently due to their presence and persistence in the environment and the low efficacy in removal by conventional treatments. These organic contaminants are usually from industrial processes, municipal and agricultural activities. These substances have been shown to have biodegradability by conventional biological methods [1, 2], but these pollutants remain in the effluents of wastewater treatment plants and municipal solid waste landfill leachates [3-7]. Among many different pollutants encountered from the industrial wastewater, bisphenol A (2,2-bis(4-hydroxyphenyl) propane, BPA) is one of the most

widely manufactured chemicals [8]. It has been used as raw materials for the productions of polycarbonate, polysulphone plastics and eposy resins which can be found in plastic bottles, food cans, containers, composite dental filling and adhesives [4, 9-11]. This compound is not easily degradable with conventional biological methods which usually take a long time of treatment, thus it still remain in the environment leading to the contamination of superficial and ground water [12].

BPA has been detected in all kinds of environmental water from high level in specific industrial (up to several hundreds of mg/L) [13, 14] and urban wastewater (21.5 µg/L) [15], landfill leachates (17.2 mg/L) [4], to lower concentrations in effluents of stream water (12µg/L) [16] and even in drinking water (0.5-2 ng/L) [17]. As an endocrine disrupting compound (EDC), it is reported that BPA can simulate the effect of estrogen leading animals to female precocious and prostate hyperplasia [18, 19]. Several studies demonstrated that BPA can lead to embryonic malformation and increase the incidence of ovarian cancer, leukemia and other diseases at low does [20, 21]. Therefore, it is urgent to develop an effective method for the decomposition and removal of BPA in water.

Various methods have been developed for the removal of BPA from water, including physical adsorption [22], biological methods [9, 23-25], chemical and sonochemical oxidation [25, 26], electrochemical oxidation [27, 28], photocatalytic methods [11, 29-31], etc. It was demonstrated that 90% of BPA was degraded photocatalytically by nitrogen-doped TiO_2 hollow sphere after 2 hours irradiated to blue light [29]. It was also reported that UV-mediated heterogeneous photocatalysis was able to remove 99.7% of BPA at concentration of 20 mg/L with the addition of 0.5 g/L TiO_2 in 1 hour [11]. Ultrasonic irradiation at 300 kHz, 80 W was demonstrated to be able to eliminate BPA with oxygen as saturating gas while remain 50% of chemical oxygen demand (COD) and 80% of total organic carbon (TOC) in the solution after 9 hours of irradiation [26].

However, it is still necessary to find a rapid, more efficient and simpler method for wastewater treatment.

Advanced oxidation processes (AOPs), have been demonstrated to be effective and inexpensive for the decomposition of wastewater contaminants such as aromatics, pesticides, petroleum constituents and organic compounds [32]. AOPs are based on highly reactive radicals which can react with the organic compound and mineralize the contaminants into stable inorganic compounds [33]. These methods include photocatalysis, sonocatalysis, Fenton process and ozonation [34]. Recent studies using AOPs for the removal of BPA have showed some promising results [8, 30, 35-37]. Among these approaches, Fenton process is probably one of the most effective and common AOPs for wastewater treatment [38] . This process involves with the production of hydroxyl radicals ($\cdot$OH) and perhydroxyl radicals ($\cdot$HO$_2$) as oxidizing species via the following equations [39, 40]

$$Fe^{2+} + H_2O_2 = Fe^{3+} + \cdot OH + OH^- \qquad k = 76 \text{ M}^{-1}\text{s}^{-1} \qquad (1)$$

$$Fe^{3+} + H_2O_2 = Fe^{2+} + \cdot HO_2 + H^+ \qquad k = 0.003 \text{ M}^{-1}\text{s}^{-1} \qquad (2)$$
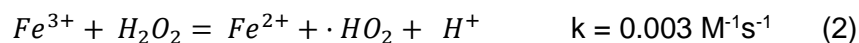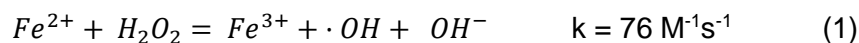
The hydroxyl radicals, with a high oxidation potential (2.8 V), is a very powerful oxidant which can react non-selectively with almost all organic compounds (except perfluorinated alkanes) at or near diffusion-controlled rates (10^9-10^{10} M^{-1}s^{-1}) [38, 41]. However, the application of Fenton reaction for wastewater treatments is still limited due to narrow pH requirement and the production of sludge after treatment [40]. To overcome these limitations and enhance catalytic activity of Fenton process, many researches have been carried out to develop heterogeneous Fenton-like catalysts such as iron oxides, nano-zero valent iron, iron- immobilized clays and Fe-containing zeolites, etc. to generate hydroxyl radicals from hydrogen peroxide [42-46]. Moreover, recent study by Wydra et al.

has shown that the generation of reactive oxygen species induced by magnetite nanoparticles can be enhanced under the presence of an alternating magnetic field [47].

The overall objective of this study is to study the degradation of bisphenol A via Fenton reaction induced by iron oxide nanoparticles under exposure to an alternating magnetic field. Several key experimental factors of Fenton process including pH, H_2O_2 and iron oxide nanoparticles concentration. In addition, the effect of hydroxylamine as a catalyst for the Fenton process was also discussed. Moreover, the kinetics of bisphenol A degradation at optimum conditions in this study will be also determined.

7.2. Materials and Method

7.2.1. Materials

Iron (III) chloride hexahydrate ($FeCl_3 \cdot 6H_2O$), iron (II) chloride tetrahydrate ($FeCl_2 \cdot 6H_2O$), hydrogen peroxide, and bisphenol A were obtained from Sigma Aldrich (St. Louis MO). Hydroxylamine hydrochloride was from Fisher Scientific. Ammonium hydroxide was purchased from EMD chemicals (Gibbstown, NJ). All materials were used without any modification.

7.2.2. Nanoparticle synthesis

The synthesis of uncoated iron oxide nanoparticles (UC IONP) was done using coprecipitation method as described previously. In short, iron salts were mixed at a molar ratio of Fe (III): Fe (II) of 2: 1 in DI water. The mixture was then heated to 85°C under nitrogen flow. When the temperature reaches 80°C, 5 mL of 30% NH_4OH were injected drop wise into the solution and the reaction was carried out for 1 hour under continuously stirring. After 1 hour, the solution was washed through magnetic decantation 2 to 3 times, and then dialyzed against DI water for 24 hours, changing water periodically.

7.2.3. Characterization of nanoparticles

Hydrodynamic size of nanoparticles was measured using dynamic light scattering which was performed on Malvern Zetasizer, Nano ZS90 instrument at particles concentration of 0.2 mg/ml. The heating capapcity of the nanoparticles was tested under alternating magnetic field (AMF) exposure at 58 kA/m and 292 kHz for 5 min at concentration of 3 mg/ml. The study was performed using a Taylor Winfield magnetic induction source and temperature was measured using a fiber optic sensor (Luxtron FOT Lab kit). The specific adsorption rate (SAR) values were calculated using the following equation (3)

$$SAR = \frac{C_{p,Fe}m_{Fe} + C_{p,H_2O}m_{H_2O}}{m_{Fe}} \frac{\Delta T}{\Delta t} \qquad (3)$$

where C_p is the specific heat capacity (0.65 and 4.18 J/g*K for iron oxide and water, respectively), m_{Fe}, m_{H_2O} is the mass of iron and water respectively. $\Delta T/\Delta t$ is the initial slope of the heating profile which is calculated from 20 and 30 second time point.

7.2.4. Bisphenol A degradation

The degradation of BPA was performed in a 1ml microtube at 37°C. Aqueous BPA solution was prepared at concentration of 50 ppm from aqueous stock solution (200ppm). The pH was adjusted to pH 3 using 0.1M HCl. Various amounts of IONPs (50; 75; 100 µg/ml) were added to the BPA solutions. The reactant mixture was placed into a preheated water bath at 37°C for 10 min. The degradation was initiated by the addition of hydroxylamine at concentration of 6 mM followed by spiking hydrogen peroxide 3% (20 mM). The sample was then immediately exposed to AMF at frequency of 292 kHz and 58 kA/m. After a certain time, the sample was transferred to a centrifuge tube with a 0.45µm

cellulose acetate filter and centrifuged for 3 minutes at 13,400 rpm to remove IONP particles. The absorbance of the supernatant was measured using UV-Vis spectroscopy (Varian Cary 50 UV-Vis spectrophotometer) with maximum absorption at 277 nm. To account for the present of any remaining particle in the supernatant, the absorbance of particle alone was measured using a similar procedure and subtracted from the results. The experiments were repeated three times and the recorded absorbance was normalized to initial absorbance of bisphenol A.

To optimize the experiment conditions, the effect of pH, IONP concentration and NH_2OH on BPA degradation was also studied. Initial pH of the reactant mixture was about 7 and pH 3 was achieved with the addition of 5 μl of 0.1M HCl. The concentration of IONPs was varied from 50 μg/ml and 100 μg/ml, but the equilibrium temperature was remained at 37-38°C. The NH_2OH concentration was tested at 6 mM and 10 mM. Moreover, kinetics of the BPA degradation was also investigated at pH 3 over 30 minutes exposure.

7.3.   Results and discussion

7.3.1. BPA degradation via Fenton reaction

Nanoparticle properties are summarized in table 7.1. The hydrodynamic size of the particles was measured using DLS and reported main peak was the value of peak 1 (more than 95%). The uncoated particles were 138 nm with PDI of 0.23 while the crystal size of iron oxide particle calculated from XRD pattern was about 10 nm. The SAR value of uncoated particles was determined to be 380 W/g which indicated a significant heating capacity.

Table 7.1. Nanoparticle properties

Samples	Main peak (d, nm)	PDI	SAR (W/g)
UC IONP	138.4 ± 2.4	0.23 ± 0.01	379.4 ± 8.4

The effect of pH on BPA degradation was studied with exposure to water bath or AMF at 37°C for 30 minutes with the present of 6 mM of NH_2OH. Figure 1 presents the degradation at pH 3 and pH 7. As shown in fig. 7.1, water bath exposure at pH 7 degraded about 34% of BPA while degradation with AMF exposure at the same pH was about 48%. Similar trend was also observed at pH 3, degradation of BPA with water bath and AMF was 44% and 52%, respectively. Therefore, AMF exposure did enhance the degradation of BPA induced by iron oxide particles at both pH 3 and pH 7. The maximum catalytic performance of Fenton process has been demonstrated to occur at pH 3 [33, 48]. In this experiment, there was about 4% increase in BPA degradation at pH 3 compared to pH 7. Though this was not a big enhancement, the future experiments were performed at pH 3 to maximize the degradation process.
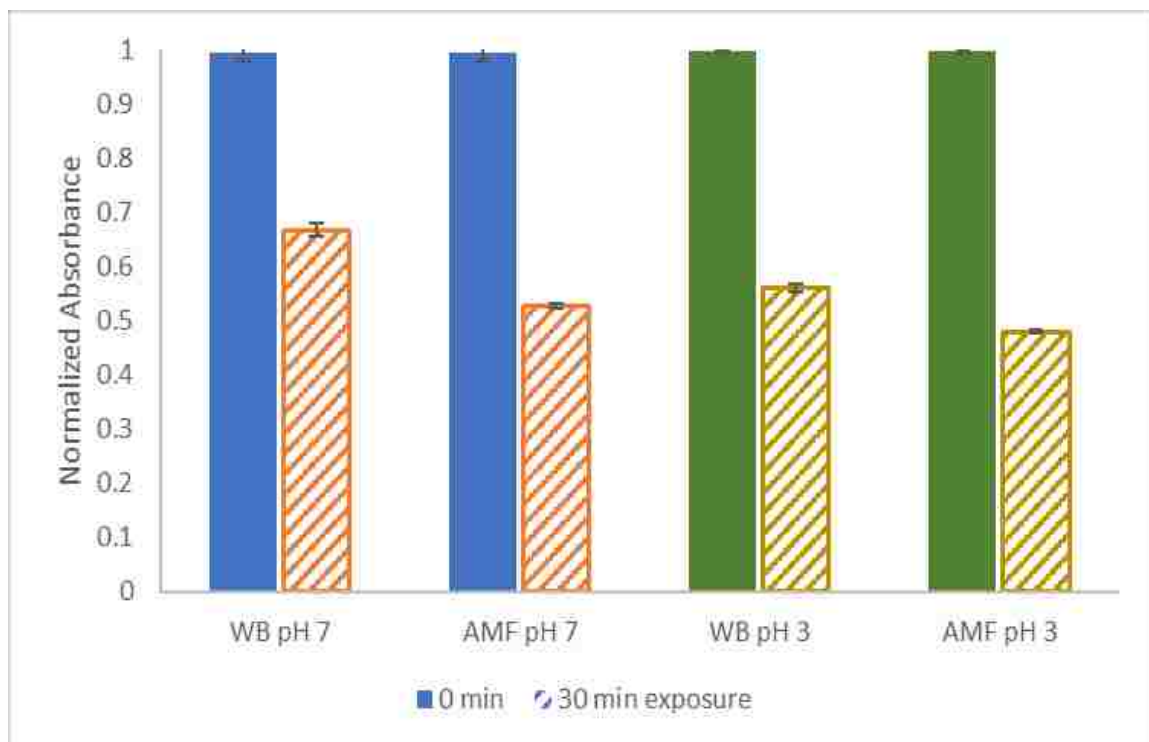
Figure 7.1. The BPA degradation induced by uncoated particles (75 μ/ml) at pH 3 and pH 7 under water bath and alternating magnetic field exposure (37°C) over 30 minutes exposure with the present of 6 mM NH_2OH

To study the effect of hydrogen peroxide on the degradation of BPA, the amount of H_2O_2 was varied from 5 mM to 40 mM and the experiments were performed under the presence of AMF at pH 7 without the addition of NH_2OH. As seen in figure 7.2, the degradation of BPA was increased gradually when increasing the H_2O_2 concentration from 5 mM to 40 mM. However, at concentration higher than 20 mM, no significant enhancement in BPA degradation was observed. It is also worth-mentioning that the presence of high H_2O_2 concentration had some influence on measuring the absorbance of BPA. With these data and observation, 20 mM of H_2O_2 seemed to be the optimum condition in this study.
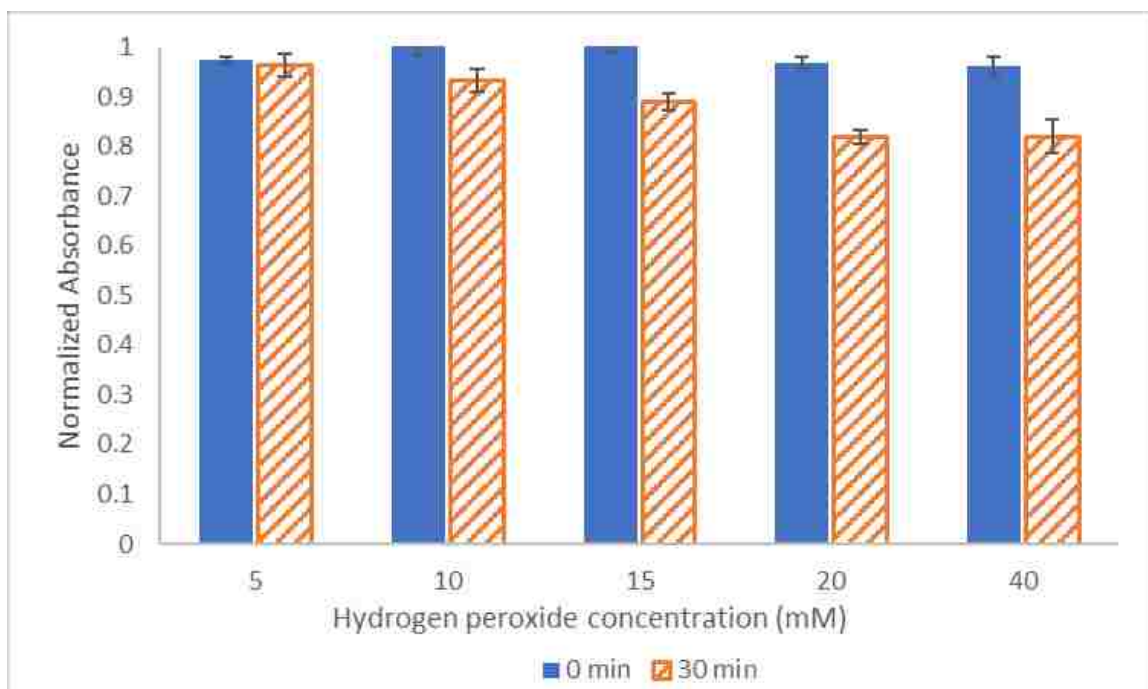
Figure 7.2. The absorbance of BPA exposed to 75 µg/ml of nanoparticles with varying concentration of hydrogen peroxide at pH 7 without the addition of NH_2OH upon AMF exposure

Hydroxylamine (NH_2OH) was added as a catalyst to accelerate the redox cycle of Fe (III)/Fe (II) returning in an enhanced surface reactivity of the particles. The BPA degradation induced by Fenton reactions was studied without and with 6 mM of NH_2OH at pH 7 and the data was summarized in figure 7.3. Without the addition of hydroxylamine, about 10% of BPA was degraded with water bath exposure at $37^{\circ}C$ while that of AMF exposure was nearly 20%. Similarly, the BPA degradation increased from 34% to 48% with the presence of 6 mM NH_2OH. These results endorsed the role of hydroxylamine as a catalyst for Fenton reaction. It is also clearly that the exposure to alternating magnetic field enhanced the BPA degradation induced by IONP in both cases. Moreover, the concentrations of NH_2OH was tested at 6 mM and 10 mM and the results are presented in figure 7.4. When increasing NH_2OH concentration from 6 mM to 10 mM, there was a

slight enhancement, about 6%, in BPA degradation with water bath exposure. However,

there was no difference in the degradation of BPA with AMF exposure between 6 mM and

10 mM of NH$_2$OH. Hence, the optimum concentration of NH$_2$OH from this study is 6 mM.
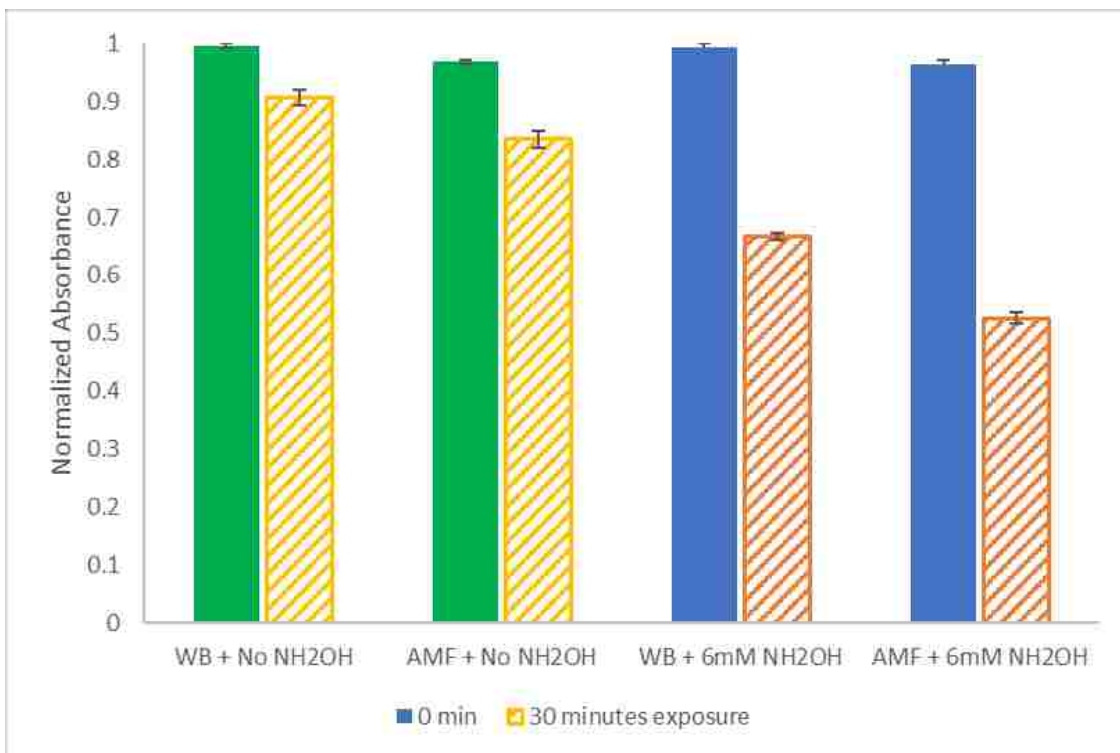
Figure 7.3. BPA degradation induced by IONP (75 µg/ml) without and with 6 mM of

NH$_2$OH at pH 7
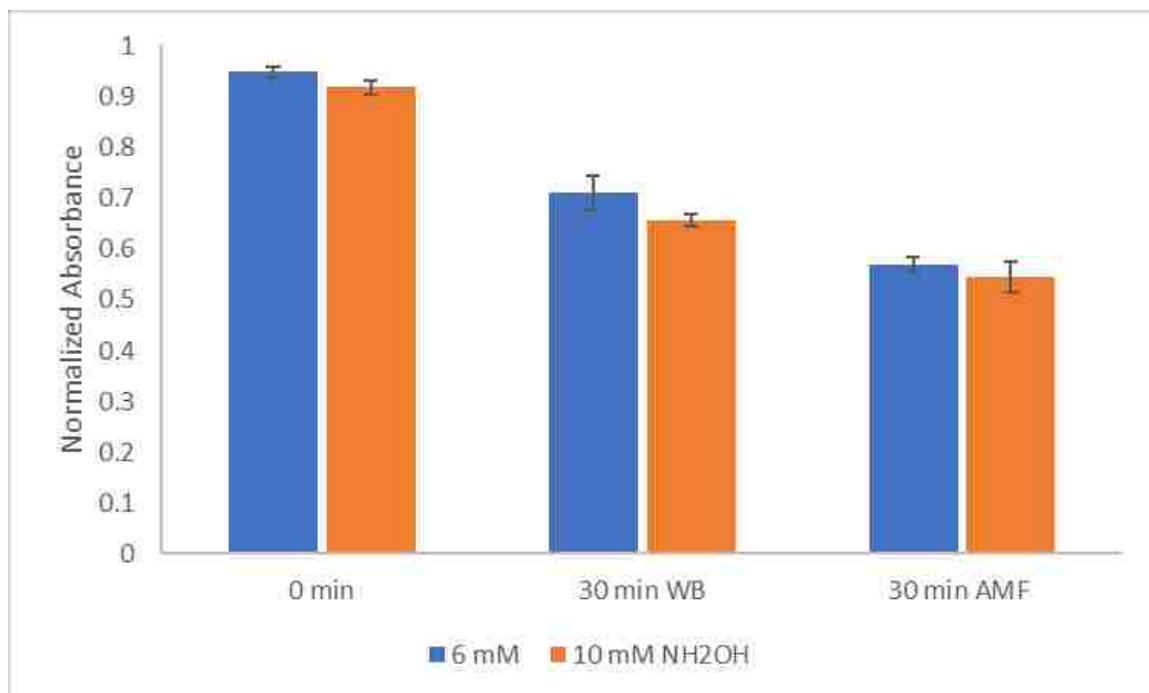
Figure 7.4. The degradation of BPA with NH_2OH concentration of 6 mM and 10 mM while the concentration of IONP was kept at 75 µg/ml and pH remained at 3. The exposure to water bath and AMF was at 37°C for 30 minutes.

Figure 7.5 showed the effect of IONP concentration on degradation of BPA. The amounts of particles were varied from 50 to 100 µg/ml while the equilibrium temperature remained at 37°C. In general, the degradation of BPA increased with the increase of IONP concentration with both AMF and water bath exposure due to the increase of surface area corresponded to the amounts of particles used. However, there was no difference in BPA degradation between 75 and 100 µg/ml of IONP with AMF exposure. This situation was also reported by Wydra et al. in which no significant enhancement in surface ROS generation was observed when IONP concentration increased from 75 to 150 µg/ml. It has been explained by either the pronounced effect of nanoscale heating at lower magnetite nanoparticle concentrations or the enhanced agglomeration of nanoparticles under AMF exposure [47]. With these results, 75 µg/ml of IONP was used for future experiments.
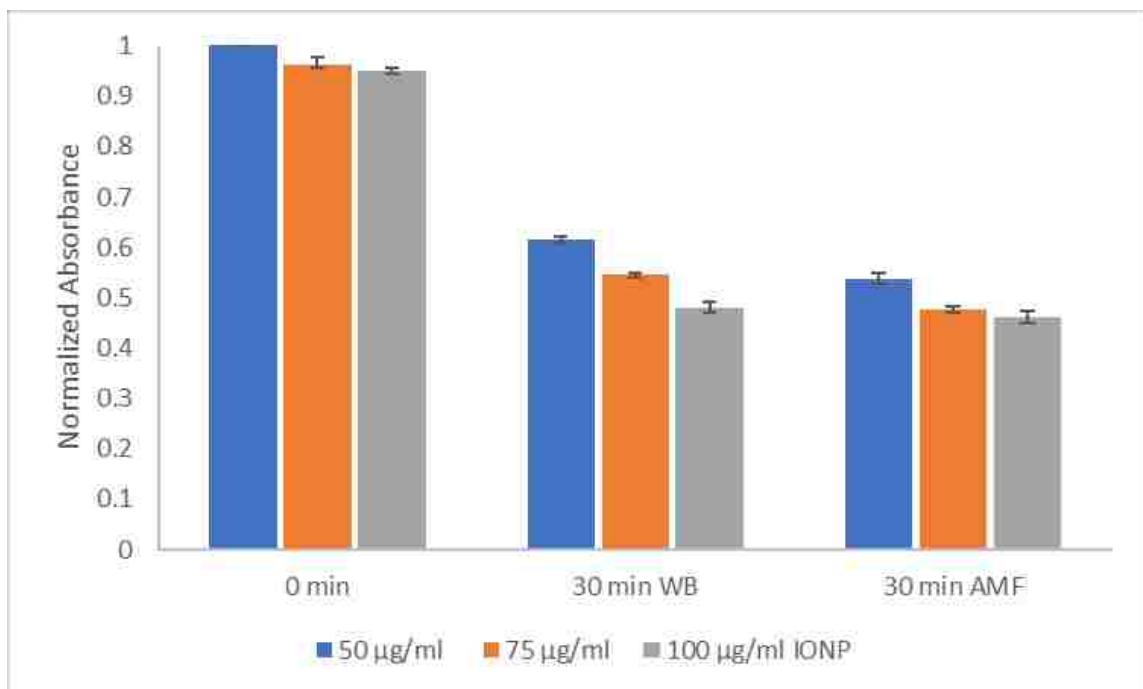
Figure 7.5. The normalized absorbance of BPA after 30 min exposure to water bath and AMF with various concentrations of IONP (50-100 µg/ml). The study was done at pH 3 with 6mM of NH_2OH.

7.3.2. Kinetics study:

The kinetics of BPA degradation was investigated at pH 3 with 75 µg/ml of IONP, 6 mM of NH_2OH over a 30 minutes exposure to water bath and AMF at 37°C which was showed in figure 7.6. The displayed data is the average of three measurements for each time point. The kinetic data was fit to pseudo-first-order and second-order models using these two following rate models [49, 50]

$$\ln(A_t/A_o) = -k_1 t \ (4)$$

$$1/(A_t/A_o) = k_2 t + 1 \ (5)$$

Where k_1 and k_2 are the first and second order rate constants, A_t is the absorbance measured at a given time while A_o is the initial absorbance of BPA at 277 nm.

The BPA degradation data was fit to these above two equations with linear regression and the second-order model seems to fit better (R^2 = 0.95 to 0.98) which was presented in figure 7.7. With the AMF exposure the rate constant increased 1.4 times, 0.0379 and 0.0266 $ppm^{-1}min^{-1}$ for AMF and water bath exposure, respectively.
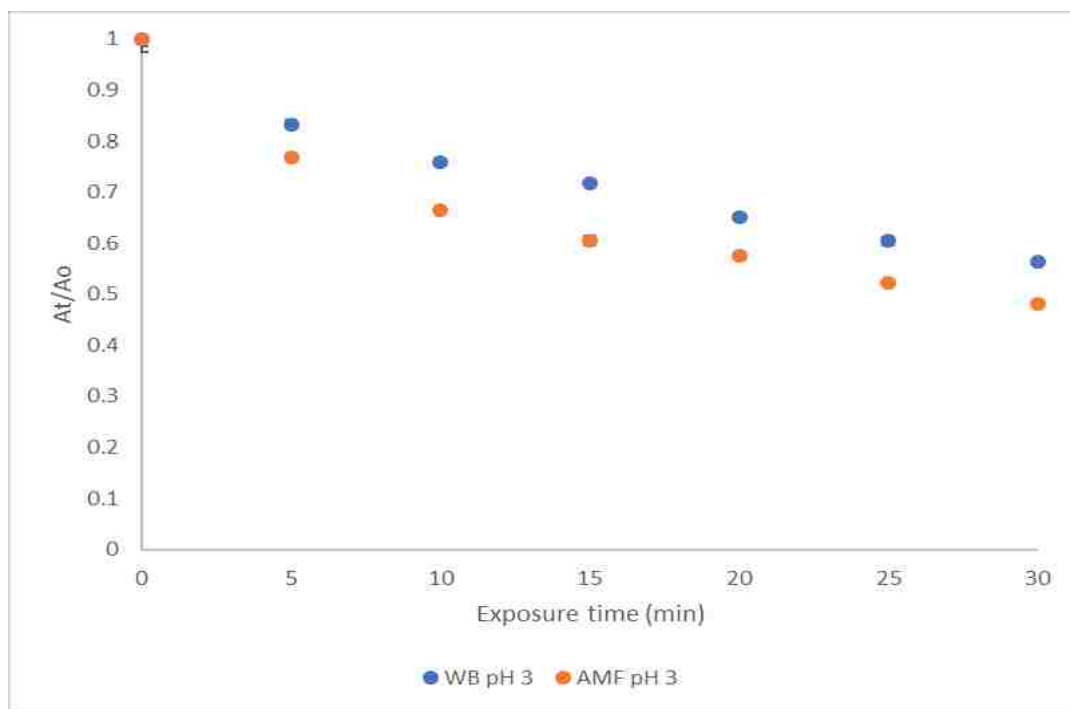
Figure 7.6. The absorbance of BPA after a certain time exposed to magnetite nanoparticles (75 μg/ml) at pH 3 with 6 mM of NH_2OH
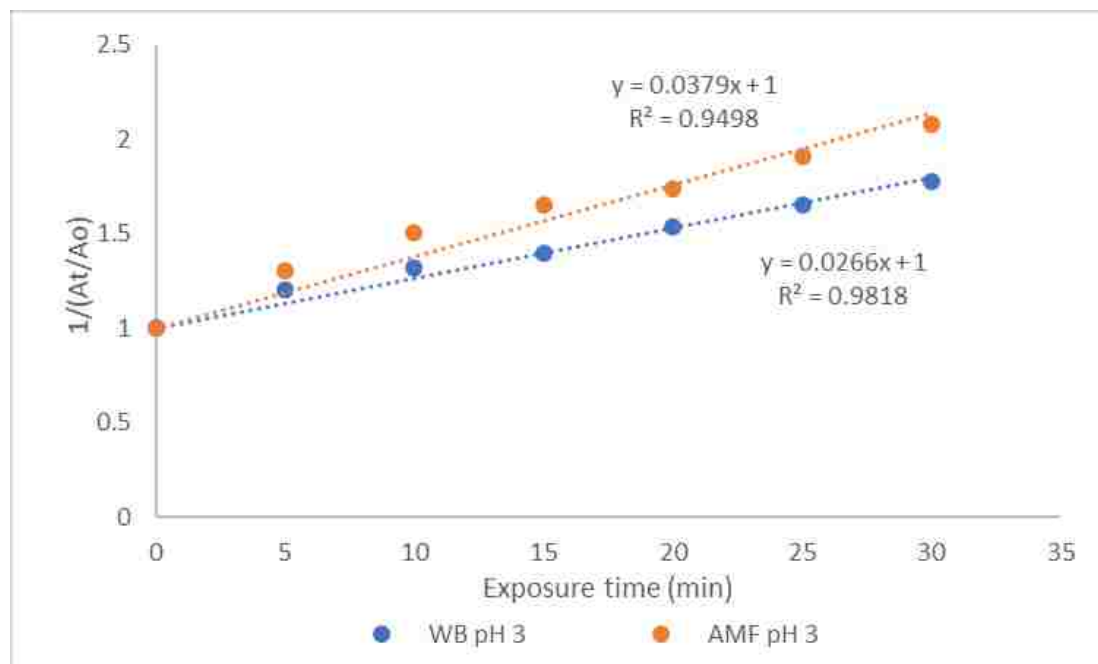
Figure 7.7. The second-order kinetic plots of BPA degradation with 75 µg/ml of IONP at pH 3 with 6 mM NH_2OH in water bath and AMF exposure.

Although the degradation pathway as well as the intermediates and oxidative products were not the scope of this study, it has been shown that hydroquinone, 4'-hydroxyacetophenone, 4'-isoproenylphenone and catechol are the major products of BPA oxidation by Fenton process. Besides, some ring opened compounds including oxalic acid, lactic acid and fumaric acid have been also detected at high H_2O_2 concentration [41, 51]. Figure 7.8 below is the proposed pathway of BPA oxidation via Fenton process using carbon nanotube-supported Fe_3O4 reported by Cleveland et al. [52]
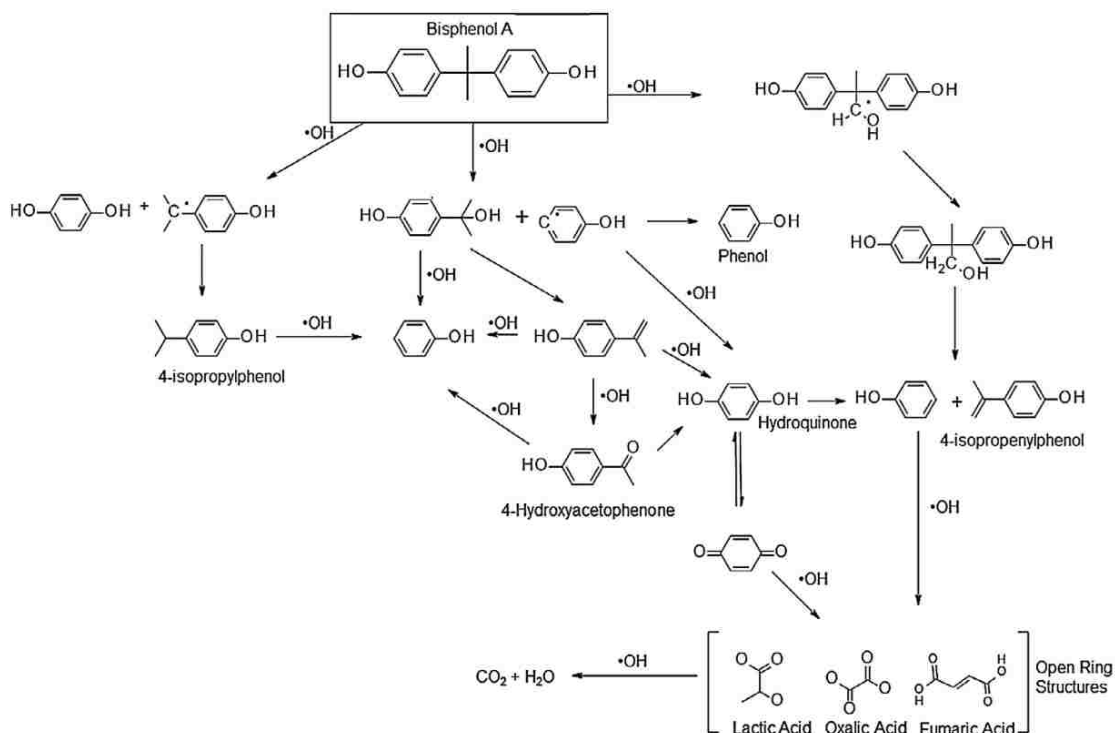
Figure 7.8. BPA degradation pathway via Fenton process reported by Cleveland et al. [52] (Reprint with permission from Elsevier)

7.4. Conclusion

In this study, co-precipitated iron oxide nanoparticles with approximate size of 140 nm were used as heterogeneous Fenton catalyst for BPA degradation upon the exposure of alternating magnetic field. The magnetite nanoparticles displayed a promising catalytic ability in the degradation of BPA in the presence of hydrogen peroxide and hydroxylamine. The BPA degradation was enhanced with the exposure of the alternating magnetic field. Moreover, several key experiment factors including pH, nanoparticle concentration and hydroxylamine concentration on Fenton process was also investigated. Acidic condition (pH 3) showed a slight improvement in the degradation of BPA compared to neutral pH 7. More than 50%

131

of BPA degradation was achieved after 30 min exposure to AMF at 75 μg/ml of iron oxide nanoparticles, 6 mM of NH_2OH and 20 mM of H_2O_2. The kinetics of BPA degradation was also studied, and the data was fit to second-order model. The rate constant increased by 1.4 times upon exposure to an alternating magnetic field compared to that of water bath exposure at the same temperature.

7.5. References

1.   Tekin, H., et al., *Use of Fenton oxidation to improve the biodegradability of a pharmaceutical wastewater.* Journal of Hazardous Materials, 2006. **136**(2): p. 258-265.

2.   Rivero, M.J., et al., *Kinetic analysis and biodegradability of the Fenton mineralization of bisphenol A.* Journal of Chemical Technology & Biotechnology, 2014. **89**(8): p. 1228-1234.

3.   Melcer, H. and G. Klecka, *<Treatment of Wastewaters Containing Bisphenol A-State of the Science Review.pdf>.* Water Environment Research, 2011. **83**(7): p. 650-666.

4.   Yamamoto, T., et al., *Bisphenol A in hazardous waste landfill leachates.* Chemosphere, 2001. **42**(4): p. 415-418.

5.   Gorga, M., M. Petrovic, and D. Barceló, *Multi-residue analytical method for the determination of endocrine disruptors and related compounds in river and waste water using dual column liquid chromatography switching system coupled to mass spectrometry.* Journal of Chromatography A, 2013. **1295**: p. 57-66.

6.   Boonyaroj, V., et al., *Toxic organic micro-pollutants removal mechanisms in long-term operated membrane bioreactor treating municipal solid waste leachate.* Bioresource Technology, 2012. **113**: p. 174-180.

7. Umar, M., et al., *Application of ozone for the removal of bisphenol A from water and wastewater – A review.* Chemosphere, 2013. **90**(8): p. 2197-2207.

8. Katsumata, H., et al., *Degradation of bisphenol A in water by the photo-Fenton reaction.* Journal of Photochemistry and Photobiology A: Chemistry, 2004. **162**(2): p. 297-305.

9. Staples, C.A., et al., *A review of the environmental fate, effects, and exposures of bisphenol A.* Chemosphere, 1998. **36**(10): p. 2149-2173.

10. Chiang, K., et al., *Photocatalytic degradation and mineralization of bisphenol A by TiO2 and platinized TiO2.* Applied Catalysis A: General, 2004. **261**(2): p. 225-237.

11. Guo, C., et al., *Directed Synthesis of Mesoporous TiO2 Microspheres: Catalysts and Their Photocatalysis for Bisphenol A Degradation.* Environmental Science & Technology, 2010. **44**(1): p. 419-425.

12. Limam, I., et al., *Evaluation of biodegradability of phenol and bisphenol A during mesophilic and thermophilic municipal solid waste anaerobic digestion using 13C-labeled contaminants.* Chemosphere, 2013. **90**(2): p. 512-520.

13. Fürhacker, M., S. Scharf, and H. Weber, *Bisphenol A: emissions from point sources.* Chemosphere, 2000. **41**(5): p. 751-756.

14. Sanchez-Avila, J., et al., *Determination and occurrence of phthalates, alkylphenols, bisphenol A, PBDEs, PCBs and PAHs in an industrial sewage grid discharging to a Municipal Wastewater Treatment Plant.* Sci Total Environ, 2009. **407**(13): p. 4157-67.

15. Jackson, J. and R. Sutton, *Sources of endocrine-disrupting chemicals in urban wastewater, Oakland, CA.* Sci Total Environ, 2008. **405**(1-3): p. 153-60.

16. Kolpin, D.W., et al., *Pharmaceuticals, Hormones, and Other Organic Wastewater Contaminants in U.S. Streams, 1999−2000: A National Reconnaissance.* Environmental Science & Technology, 2002. **36**(6): p. 1202-1211.

17. Kuch, H.M. and K. Ballschmiter, *Determination of endocrine-disrupting phenolic compounds and estrogens in surface and drinking water by HRGC-(NCI)-MS in the picogram per liter range.* Environ Sci Technol, 2001. **35**(15): p. 3201-6.

18. Chen, W., et al., *The experimental investigation of bisphenol A degradation by Fenton process with different types of cyclodextrins.* Journal of Industrial and Engineering Chemistry, 2017. **56**: p. 428-434.

19. Rebuli, M.E., et al., *Investigation of the Effects of Subchronic Low Dose Oral Exposure to Bisphenol A (BPA) and Ethinyl Estradiol (EE) on Estrogen Receptor Expression in the Juvenile and Adult Female Rat Hypothalamus.* Toxicological Sciences, 2014. **140**(1): p. 190-203.

20. Lee, M.S., et al., *Human endometrial cell coculture reduces the endocrine disruptor toxicity on mouse embryo development.* J Occup Med Toxicol, 2012. **7**(1): p. 7.

21. Hussain, I., et al., *Bisphenol-A induces expression of HOXC6, an estrogen-regulated homeobox-containing gene associated with breast cancer.* Biochimica et Biophysica Acta (BBA) - Gene Regulatory Mechanisms, 2015. **1849**(6): p. 697-708.

22. Pan, B., et al., *Adsorption and Hysteresis of Bisphenol A and 17α-Ethinyl Estradiol on Carbon Nanomaterials.* Environmental Science & Technology, 2008. **42**(15): p. 5480-5485.

23. Zhao, J., et al., *Sorption and degradation of bisphenol A by aerobic activated sludge.* Journal of Hazardous Materials, 2008. **155**(1): p. 305-311.

24. Kang, J.H. and F. Kondo, *Bisphenol a degradation by bacteria isolated from river water.* Arch Environ Contam Toxicol, 2002. **43**(3): p. 265-9.

25. Xuan, Y.J., Y. Endo, and K. Fujimoto, *Oxidative degradation of bisphenol a by crude enzyme prepared from potato.* J Agric Food Chem, 2002. **50**(22): p. 6575-8.

26.   Torres, R.A., et al., *Ultrasonic cavitation applied to the treatment of bisphenol A. Effect of sonochemical parameters and analysis of BPA by-products.* Ultrason Sonochem, 2008. **15**(4): p. 605-11.

27.   Kuramitz, H., M. Matsushita, and S. Tanaka, *Electrochemical removal of bisphenol A based on the anodic polymerization using a column type carbon fiber electrode.* Water Res, 2004. **38**(9): p. 2330-7.

28.   Yang, C.-w., *Degradation of bisphenol A using electrochemical assistant Fe(II)-activated peroxydisulfate process.* Water Science and Engineering, 2015. **8**(2): p. 139-144.

29.   Subagio, D.P., et al., *Photocatalytic degradation of bisphenol-A by nitrogen-doped TiO2 hollow sphere in a vis-LED photoreactor.* Applied Catalysis B: Environmental, 2010. **95**(3): p. 414-422.

30.   Wang, R., et al., *Photocatalytic degradation of Bisphenol A (BPA) using immobilized TiO2 and UV illumination in a horizontal circulating bed photocatalytic reactor (HCBPR).* Journal of Hazardous Materials, 2009. **169**(1): p. 926-932.

31.   Fukahori, S., et al., *Capturing of bisphenol A photodecomposition intermediates by composite TiO2–zeolite sheets.* Applied Catalysis B: Environmental, 2003. **46**(3): p. 453-462.

32.   Duesterberg, C.K., S.E. Mylon, and T.D. Waite, *pH Effects on Iron-Catalyzed Oxidation using Fenton's Reagent.* Environmental Science & Technology, 2008. **42**(22): p. 8522-8527.

33.   Hartmann, M., S. Kullmann, and H. Keller, *Wastewater treatment with heterogeneous Fenton-type catalysts based on porous materials.* Journal of Materials Chemistry, 2010. **20**(41): p. 9002.

34. Descorme, C., *Catalytic wastewater treatment: Oxidation and reduction processes. Recent studies on chlorophenols.* Catalysis Today, 2017. **297**: p. 324-334.

35. Garoma, T. and S. Matsumoto, *Ozonation of aqueous solution containing bisphenol A: Effect of operational parameters.* Journal of Hazardous Materials, 2009. **167**(1): p. 1185-1191.

36. Rosenfeldt, E.J. and K.G. Linden, *Degradation of Endocrine Disrupting Chemicals Bisphenol A, Ethinyl Estradiol, and Estradiol during UV Photolysis and Advanced Oxidation Processes.* Environmental Science & Technology, 2004. **38**(20): p. 5476-5483.

37. Chen, P.-J., et al., *Biological assessment of bisphenol A degradation in water following direct photolysis and UV advanced oxidation.* Chemosphere, 2006. **65**(7): p. 1094-1102.

38. Qin, Q., et al., *Enhanced heterogeneous Fenton-like degradation of methylene blue by reduced CuFe2O4.* RSC Advances, 2018. **8**(2): p. 1071-1077.

39. Enami, S., Y. Sakamoto, and A.J. Colussi, *Fenton chemistry at aqueous interfaces.* Proc Natl Acad Sci U S A, 2014. **111**(2): p. 623-8.

40. Zhang, X., et al., *Degradation of bisphenol A by hydrogen peroxide activated with CuFeO2 microparticles as a heterogeneous Fenton-like catalyst: Efficiency, stability and mechanism.* Chemical Engineering Journal, 2014. **236**: p. 251-262.

41. Poerschmann, J., U. Trommler, and T. Gorecki, *Aromatic intermediate formation during oxidative degradation of Bisphenol A by homogeneous sub-stoichiometric Fenton reaction.* Chemosphere, 2010. **79**(10): p. 975-86.

42. Xu, L. and J. Wang, *A heterogeneous Fenton-like system with nanoparticulate zero-valent iron for removal of 4-chloro-3-methyl phenol.* J Hazard Mater, 2011. **186**(1): p. 256-64.

43. Lin, S.-S. and M.D. Gurol, *Catalytic Decomposition of Hydrogen Peroxide on Iron Oxide: Kinetics, Mechanism, and Implications.* Environmental Science & Technology, 1998. **32**(10): p. 1417-1423.

44. Zhang, S., et al., *Superparamagnetic Fe3O4 nanoparticles as catalysts for the catalytic oxidation of phenolic and aniline compounds.* Journal of Hazardous Materials, 2009. **167**(1): p. 560-566.

45. Zhang, G., et al., *Fe2O3-Pillared Rectorite as an Efficient and Stable Fenton-Like Heterogeneous Catalyst for Photodegradation of Organic Contaminants.* Environmental Science & Technology, 2010. **44**(16): p. 6384-6389.

46. Gonzalez-Olmos, R., et al., *Fe-zeolites as heterogeneous catalysts in solar Fenton-like reactions at neutral pH.* Applied Catalysis B: Environmental, 2012. **125**: p. 51-58.

47. Wydra, R.J., et al., *Accelerated generation of free radicals by iron oxide nanoparticles in the presence of an alternating magnetic field.* Royal Society of Chemistry Advances, 2015. **5**(25): p. 18888-18893.

48. De Laat, J. and H. Gallard, *Catalytic Decomposition of Hydrogen Peroxide by Fe(III) in Homogeneous Aqueous Solution: Mechanism and Kinetic Modeling.* Environmental Science & Technology, 1999. **33**(16): p. 2726-2732.

49. Shahwan, T., et al., *Green synthesis of iron nanoparticles and their application as a Fenton-like catalyst for the degradation of aqueous cationic and anionic dyes.* Chemical Engineering Journal, 2011. **172**(1): p. 258-266.

50. Hsieh, S. and P.-Y. Lin, *FePt nanoparticles as heterogeneous Fenton-like catalysts for hydrogen peroxide decomposition and the decolorization of methylene blue.* Journal of Nanoparticle Research, 2012. **14**(6).

51.   Hua, Z., et al., *Heterogeneous Fenton degradation of bisphenol A catalyzed by efficient adsorptive Fe3O4/GO nanocomposites.* Environ Sci Pollut Res Int, 2014. **21**(12): p. 7737-45.

52.   Cleveland, V., J.-P. Bingham, and E. Kan, *Heterogeneous Fenton degradation of bisphenol A by carbon nanotube-supported Fe3O4.* Separation and Purification Technology, 2014. **133**: p. 388-395.

Chapter 8: Conclusions

In this dissertation, iron oxide nanoparticles were surface functionalized with several types of coatings including small molecules (citric acid, sodium phosphate, aminosilane and dopamine); degradable poly (beta amino ester) polymers and non-degradable PEG-based polymers. Iron oxide nanoparticles can induce the formation of reactive oxygen species (ROS) via Fenton/Haber-Weiss reactions which is one of the key mechanisms of nanoparticle toxicity. The ability to generate ROS using these functionalized nanoparticles was investigated under the exposure of alternating magnetic field (AMF). Once exposed to the AMF, the iron oxide nanoparticles absorb the energy and convert it into other forms such as local heat, rotational work and chemical effect (Fenton reaction) without significantly increasing the bulk temperature. This energy dissipation can enhance the surface reactivity of the nanoparticle via ROS generation which can be utilized in biomedical and environmental applications. Coatings are essential for improving biostability, biocompatibility in biomedical applications, though they can also inhibit surface ROS generation which occurs at the surface of the nanoparticles. With small molecule coatings, almost all of the surface reactivity of the nanoparticles was inhibited due to a dense coating onto particle surface. Degradable polymer coatings showed some retention in surface ROS generation before the polymer coating was degraded, though the formation of ROS was inhibited by the binding of degradation by-products onto particle surface. Non-degradable PEG-based polymer coated IONPs displayed a comparable surface reactivity to uncoated particles in some cases which is promising for biomedical applications. Moreover, the surface ROS generation induced by IONPs can be utilized as heterogeneous catalyst in advanced oxidation processed for the degradation of organic contaminants.

8.1. **Significant findings**

There are several findings in this work that contribute to the understandings and utilizing iron oxide nanoparticles for biomedical and environmental applications. The use of iron oxide nanoparticles with the exposure to alternating magnetic field to enhance surface reactivity is relatively new in literature, therefore, our findings contribute directly to a growing field. The specific conclusions of this work are presented below.

- The exposure to alternating magnetic field enhanced the surface reactive oxygen species generation induced by iron oxide nanoparticles via Fenton/Haber-Weiss reactions.

- Small molecule coatings including citric acid, sodium phosphate, aminosilane and dopamine significantly inhibited surface reactivity of the nanoparticles due to a dense coating layer onto particle surface.

- Degradable poly (beta amino ester) (PBAE) coatings retained some surface reactivity of the nanoparticles before the coating was hydrolyzed, but the surface reactivity was lost once the coating was degraded because of the binding of degradation products onto the particle surface.

- PEG-based polymer coated iron oxide nanoparticles displayed a quite comparable surface reactivity compared to uncoated nanoparticles in some cases (PEG 5k).

- The surface ROS generation of PEG coated nanoparticles decreased with the increase of polymer molecular weight and initial concentration while the effect of coating process temperature was not significant.

- The addition of hydroxylamine as a catalyst for Fenton process accelerated the redox cycle of Fe (III)/Fe (II), thus significantly enhanced the generation of surface ROS induced by nanoparticles.

- The ability to generate surface ROS of iron oxide nanoparticles was promising for the degradation of bisphenol A upon alternating magnetic field exposure.

- Iron oxide nanoparticles as heterogeneous catalysts for Fenton reaction can expand the working pH of the conventional Fenton process.

Appendix 1: Methylene blue dye decolorization via Fenton reaction induced by iron oxide nanoparticles

Surface reactive oxygen species (ROS) generation induced by iron oxide nanoparticles was determined via methylene blue decolorization. We observed an enhanced surface reactivity with the exposure to alternating magnetic field (AMF) at 37°C. However, the effect of other important factors towards Fenton reaction such as pH, temperature and exposure time under AMF exposure was not mentioned yet. In this study, the surface ROS generation of iron oxide nanoparticles with the presence of AMF was investigated in various pH, temperature and exposure time. Moreover, the scavenging effect of methanol on hydroxyl radicals in the degradation of methylene blue was also studied.

A1.1. Introduction

Iron oxide nanoparticles (IONP) are capable to generate reactive oxygen species (ROS) at the surface of the particles via Fenton/ Haber-Weiss reaction (equations 1-3) [1-3]. The ROS generated from this process have been utilized as one of the advanced oxidation processes (AOPs) for the removal of wastewater contaminants [4, 5]. The conventional Fenton process involves with the reaction of hydrogen peroxide and ferrous iron (Fe^{2+}) to form hydroxyl radicals and ferric ions (Fe^{3+}) at acidic conditions. The generated radicals can react with organic pollutants and oxidize them to CO_2 and H_2O and possible inorganic salts [3]. Though the Fenton process has shown the efficiency in a variety of wastewater treatments [6-11], its application is still limited due to the narrow working pH and sludge generation [12]. Heterogeneous Fenton oxidation have demonstrated to be potential alternative for the convention Fenton process in extended pH range and reduced sludge formation [13].

$$Fe^{2+} + H_2O_2 \rightarrow Fe^{3+} + OH^- + OH^{\cdot} \tag{1}$$

$$Fe^{3+} + O_2^{\cdot-} \rightarrow Fe^{2+} + O_2 \tag{2}$$

$$O_2^{\cdot-} + H_2O_2 \rightarrow O_2 + OH^- + OH^{\cdot} \tag{3}$$
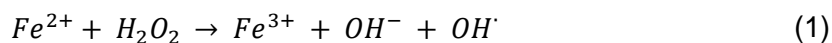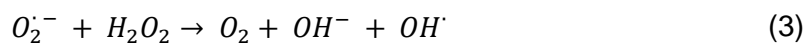
Magnetite nanoparticles (Fe_3O_4) have been shown to be a good candidate as a heterogeneous Fenton catalyst thanks to the low cost and simple synthesis as well as magnetic properties [14]. Furthermore, it is suggested that magnetite nanoparticles should have a greater ROS generation since they contain both ferrous and ferric iron [15, 16]. Magnetite nanoparticles have presented some promising results in the oxidation of many organic pollutants such as phenols, tetrabromobisphenol A, various dyes, etc [17-22]. In addition, the exposure of alternating magnetic field can enhance the surface ROS generation induced by IONPs [23].

In this work, surface reactive oxygen species generation induced by iron oxide nanoparticles upon alternating magnetic field (AMF) was studied via methylene blue decolorization assay. To optimize the experiment conditions, the effects of AMF exposure time and amplitude as well as pH was also investigated. Moreover, the addition of methanol to the methylene blue degradation as a quencher to stop Fenton reaction was also performed.

A1.2. Materials and method

A1.2.1. Materials

Iron (III) chloride hexahydrate ($FeCl_3 \cdot 6H_2O$), iron (II) chloride tetrahydrate ($FeCl_2 \cdot 6H_2O$), hydrogen peroxide, hydroxylamine hydrochloride and methylene blue were obtained from Sigma Aldrich (St. Louis MO). Methanol was from Fisher Scientific while ammonium hydroxide was purchased from EMD chemicals (Gibbstown, NJ). 3-aminopropyl trimethoxysilane was from Gelest Inc. (Morrisville, PA). All materials were used without any modification.

A1.2.2. Iron oxide nanoparticles synthesis

Uncoated iron oxide nanoparticles (UC IONP) were synthesized via co-precipitation method [24]. Briefly, a 2: 1 molar ratio mixture of $FeCl_3 \cdot 6H_2O$ and $FeCl_2 \cdot 6H_2O$ was prepared in aqueous solution. The mixture was heated to 85^oC while vigorous stirring under nitrogen flow. 5 ml of NH_4OH was added into the mixture at 80^oC and the reaction was performed for one hour. The product was then magnetically decanting and washed three time with deionized (DI) water. The final nanoparticles were then dialyzed against DI water for 24 hours while water was changed every 3 hours.

A1.2.3. Methylene blue decolorization

Methylene blue dye decolorization assay was used to determine the surface reactive oxygen species generation [25]. The experiments were performed at either 37^oC controlled water bath or exposed to an AMF. Methylene blue was diluted to concentration of 5 µg/ml from aqueous stock solution while iron oxide nanoparticle concentration was kept at 75 µg/ml. The samples were placed in the water bath at 37^oC for 10 min to equilibrate to the set temperature. The degradation was initiated by spiking the samples with 25 µl of H_2O_2. After a certain time exposed to either water bath or AMF, the samples were centrifuged at 13,400rpm for 3 minutes, magnetically decanted and the absorbance of supernatants was measured using UV-visible spectroscopy (maximum absorbance at 665 nm) with a Varian Cary. To account for nanoparticle scattering from the nanoparticles that remain in suspension, samples containing nanoparticles alone were measured and subtracted out from the sample absorbance. The experiment was repeated 3 times and the reported data is the absorbance of methylene blue after exposure at 665nm normalized to the initial absorbance of methylene blue. The effect of exposure time and AMF power on the degradation as well as working pH was also investigated.

To study the scavenging effect of methanol to the Fenton process, 0.5 mL of methanol was added right after water bath and AMF exposure time. The absorbance of methylene blue with and without the addition of methanol was measured using a similar procedure as mentioned above. The absorbance of nanoparticles control was also measured with the presence of methanol.

A1.3. Results and discussion

One of the drawbacks of the conventional Fenton process is pH limitation. It has been suggested that the optimum pH for homogeneous Fenton reaction is around pH 3. At higher pH, the decrease in iron ions concentration and the precipitation of ferric oxyhydroxide were observed. In addition, the potential of hydroxyl radicals also decreased with the increase of pH [5]. Though, recent studies showed that heterogeneous catalysts can help extending the efficient working pH of Fenton process, pH is still an important parameter since it can impact the stability and the leaching of the catalysts. In this study, pH of the samples was controlled at 3.0; 5.0 and 7.0 by adding 0.1M of HCl while ionic strengths remained at 0.05 (adjusted by NaCl). It should be noted that a similar experiment was done without pH controlling, so-called DI water, therefore, its pH was pH of the methylene blue aqueous solution which was determined to be around 7. Figure A1.1 displayed the absorbance of methylene blue after exposure to AMF for 30 minutes at different pH. Though, it was suggested that highest reactivity of Fenton reaction was observed at around pH, there was no big difference in the amount of methylene blue degradation in all tested pH. This could be due to the short exposure time that makes no changes in particle stability and surface reactivity of the particles. This indicated that iron oxide nanoparticles as heterogeneous Fenton catalyst can expand the working pH of the Fenton process, therefore no pH control was used in future experiments.
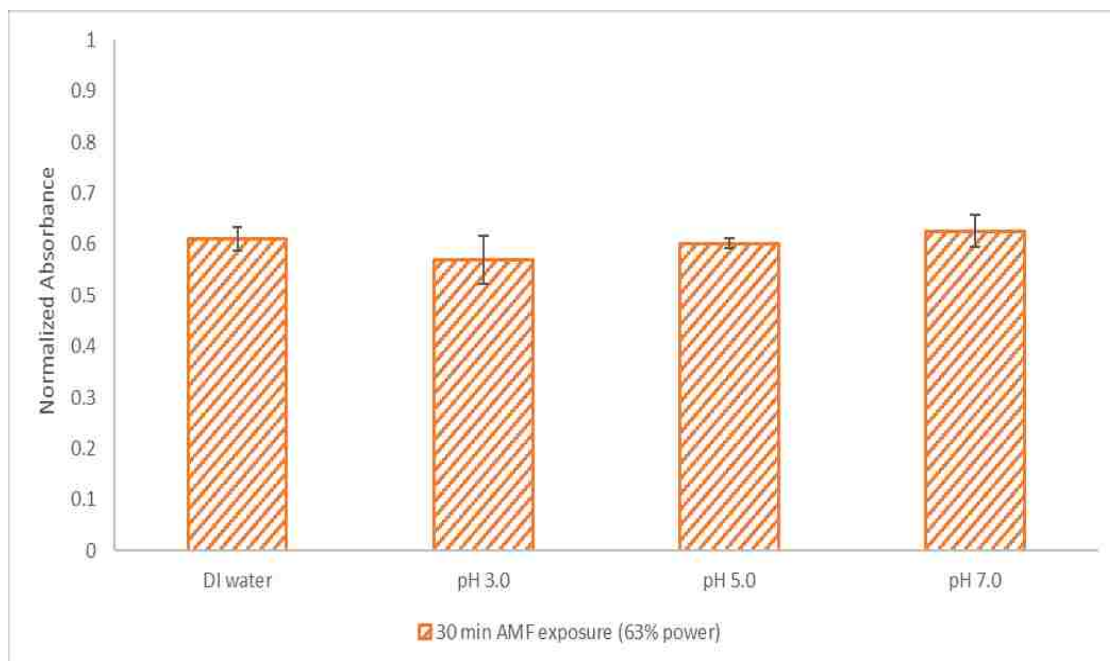
Figure A1.1. The normalized absorbance of methylene blue exposed to IONP (75 µg/ml) at different pH upon AMF exposure at 63% power (37°C)

Temperature is also an important factor which can affect Fenton process. It has been shown that once the temperature is higher than 40°C, hydrogen peroxide begins to degrade into oxygen and water which in turn limits the Fenton reaction [26]. The exposure of an alternating magnetic field can increase the temperature of magnetite nanoparticle suspension through Neel and Brownian relaxation [27]. To study the effect of temperature to Fenton process induced by IONPs, different AMF powers were applied so that the temperature of the sample varied from 31°C to 42°C. Figure A1.2 presented the absorbance of methylene blue after exposed to temperature for 30 minutes. It should be mentioned that no pH control was performed during this experiment, so pH of the sample was pH of methylene blue solution at this concentration which was around 7. At around 37°C, there was about 40% of methylene blue was degraded after 30 minutes exposure of AMF at 63% power. The amount of ROS generation decreased when reaction temperature is at 40°C or higher. This is consistent with literature report. At temperature

146

lower than 37ºC, there was not a big difference in surface ROS generation at 34ºC and 31ºC.

Exposure time is another important factor on the degradation of methylene blue. In this study, the exposure time to alternating magnetic field was varied from 0 to 60 minutes and results were summarized in figure A1.3. At 0 minute, there was about 2-3% degradation in methylene blue absorbance. It should be noted that after a certain time exposed to the field, the samples were centrifuged and decanted for more than 3 minutes before the absorbance was measured, so the actual reaction time was about 3.5 minutes instead of 0 minute. The degradation of methylene blue at 0 minute was could be due to this delay in measuring the absorbance. With the increase of exposure time, the methylene blue degradation increased gradually and reached 48% degradation after 60 minutes exposed to the AMF. However, there was about 44% of methylene blue degraded after 30 minutes which was not a big increase in degradation after 30 minutes exposure. This indicated that most of the degradation was achieved at the first 30 minutes of the AMF exposure and the exposure time was kept at 30 minutes for later experiments.
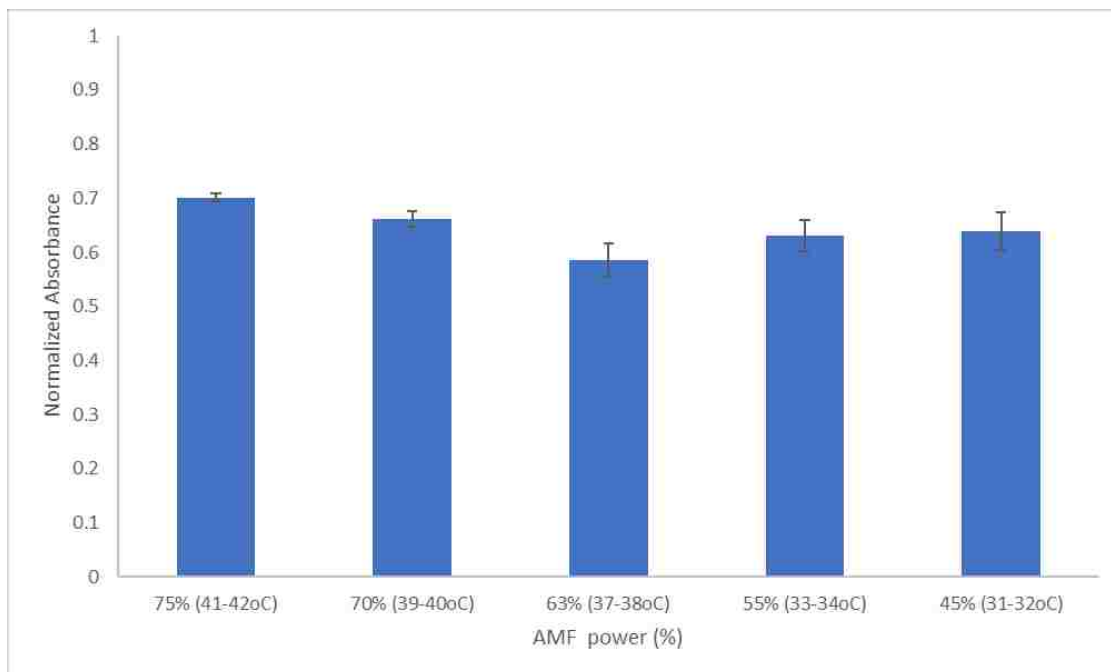
Figure A1.2. The absorbance of methylene blue after 30 minutes exposed to AMF with 75μg/ml of IONP at different powers
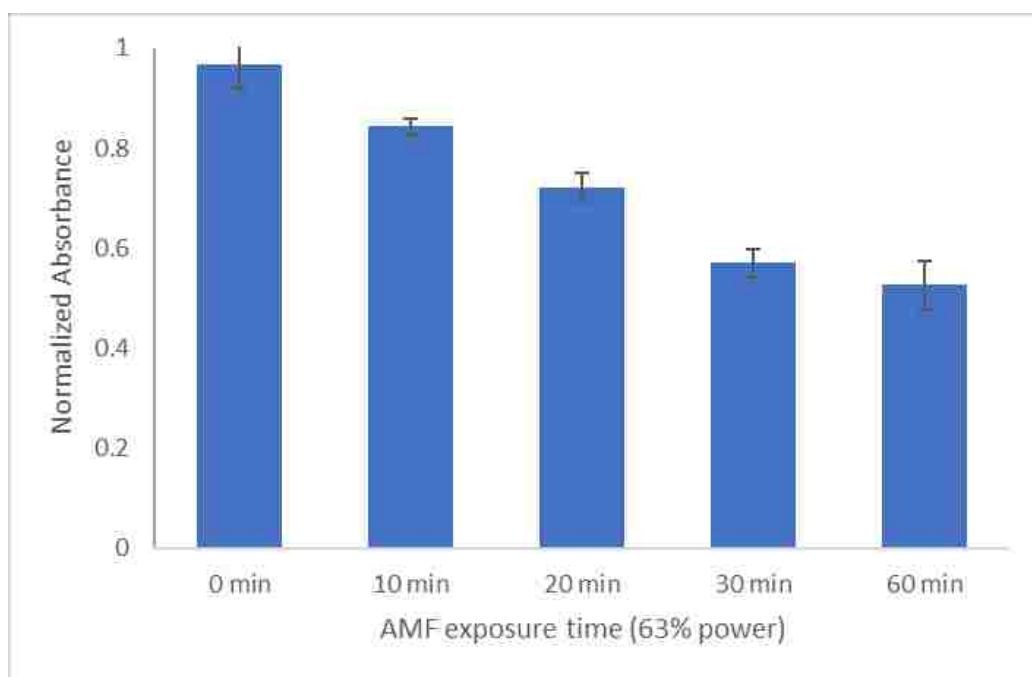
Figure A1.3. Methylene blue absorbance at 665 nm after exposure to AMF at 63% power corresponded to 37°C for various time intervals.

As mentioned above, the actual reaction time was about 3 minutes more than the real exposed time causing a difference in the absorbance of methylene blue. To overcome this issue, methanol, a hydroxyl radical scavenger [28-31], was added in excess to the reaction to capture ·OH in the degradation of methylene blue. Figure A1.4 presented methylene blue degradation data at 0 minute with the addition of excess methanol. It was clear that the addition of methanol did not affect the absorbance of methylene blue alone. With the addition of methanol, the degradation of methylene blue exposed to nanoparticles at 0 minute decreased from about 7% to almost 0%. When 4 mM of hydroxylamine was added to the reaction mixture, about 40% of methylene blue was degraded at 0 minute which reduced significantly to approximately 5% once methanol was added right after the addition of hydroxylamine and hydrogen peroxide. These results confirmed the scavenging effect of methanol in Fenton reaction. The addition of methanol in the degradation of methylene blue can stop reaction of organic dye and hydroxyl radicals generated via Fenton reaction induced by iron oxide nanoparticles. Methanol was able to quench the degradation of methylene blue by hydroxyl radicals generated from Fenton reaction and provided more accurate results.
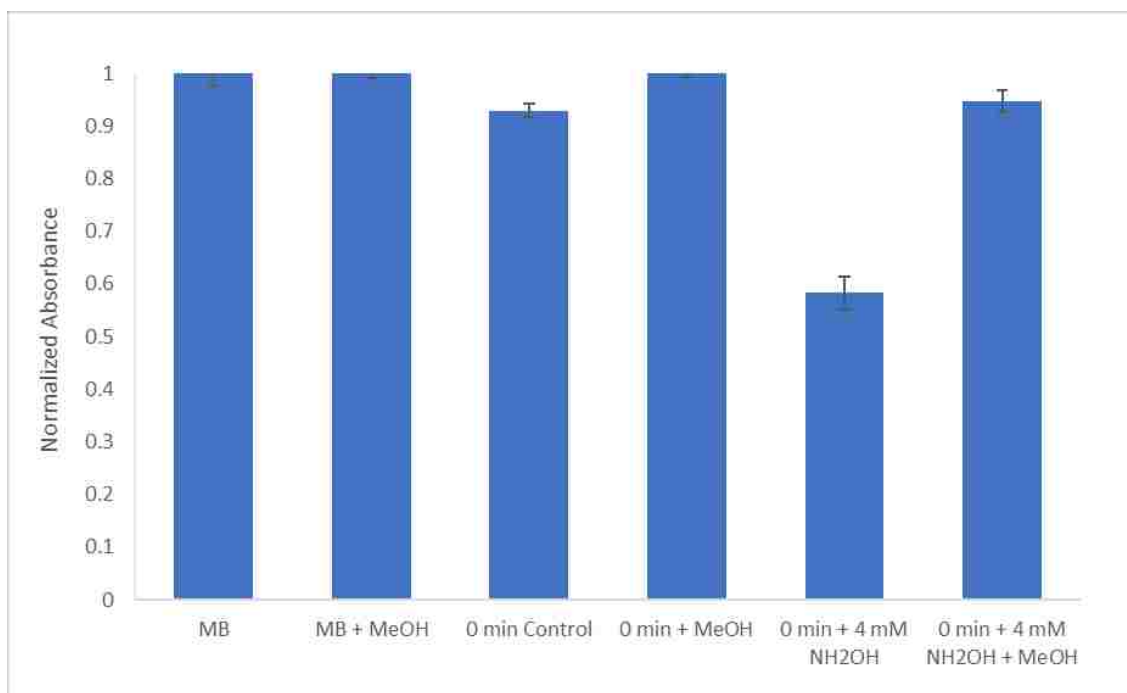
Figure A1.4. The quenching effect of methanol on methylene blue degradation exposed to iron oxide nanoparticles at 0 minute with and without the addition of hydroxylamine.

A1.4. Conclusion

In this study, the methylene blue degradation via Fenton reaction induced by iron oxide nanoparticles was performed. The effect of several experimental factors including pH, temperature, exposure time on the degradation of methylene blue was investigated. There was no big difference in methylene blue degradation at various pH while temperature at or above 40°C displayed a reduction in surface reactive oxygen species generation. The addition of methanol as a hydroxyl radical scavenger was able to stop the Fenton reaction after AMF exposure and provide more accurate data.

A1.5. References

1.   Wang, B., et al., *Physicochemical Origin for Free Radical Generation of Iron Oxide Nanoparticles in Biomicroenvironment: Catalytic Activities Mediated by Surface Chemical States.* The Journal of Physical Chemistry C, 2012. **117**(1): p. 383-392.

2.   Enami, S., Y. Sakamoto, and A.J. Colussi, *Fenton chemistry at aqueous interfaces.* Proc Natl Acad Sci U S A, 2014. **111**(2): p. 623-8.

3.   Munoz, M., et al., *Preparation of magnetite-based catalysts and their application in heterogeneous Fenton oxidation – A review.* Applied Catalysis B: Environmental, 2015. **176-177**: p. 249-265.

4.   Hartmann, M., S. Kullmann, and H. Keller, *Wastewater treatment with heterogeneous Fenton-type catalysts based on porous materials.* Journal of Materials Chemistry, 2010. **20**(41): p. 9002.

5.   Descorme, C., *Catalytic wastewater treatment: Oxidation and reduction processes. Recent studies on chlorophenols.* Catalysis Today, 2017. **297**: p. 324-334.

6.   Pliego, G., et al., *Treatment of Highly Polluted Hazardous Industrial Wastewaters by Combined Coagulation–Adsorption and High-Temperature Fenton Oxidation.* Industrial & Engineering Chemistry Research, 2012. **51**(7): p. 2888-2896.

7.   Pérez, M., et al., *Removal of organic contaminants in paper pulp effluents by AOPs: an economic study.* Journal of Chemical Technology & Biotechnology, 2002. **77**(5): p. 525-532.

8.   Bautista, P., et al., *An overview of the application of Fenton oxidation to industrial wastewaters treatment.* Journal of Chemical Technology & Biotechnology, 2008. **83**(10): p. 1323-1338.

9.   Bautista, P., et al., *Application of Fenton oxidation to cosmetic wastewaters treatment.* J Hazard Mater, 2007. **143**(1-2): p. 128-34.

10.   Rivas, F.J., et al., *Treatment of Olive Oil Mill Wastewater by Fenton's Reagent.* Journal of Agricultural and Food Chemistry, 2001. **49**(4): p. 1873-1880.

11. Lucas, M.S. and J.A. Peres, *Removal of COD from olive mill wastewater by Fenton's reagent: Kinetic study.* Journal of Hazardous Materials, 2009. **168**(2): p. 1253-1259.

12. Garrido-Ramírez, E.G., B.K.G. Theng, and M.L. Mora, *Clays and oxide minerals as catalysts and nanocatalysts in Fenton-like reactions — A review.* Applied Clay Science, 2010. **47**(3): p. 182-192.

13. Zhang, X., et al., *Degradation of bisphenol A by hydrogen peroxide activated with CuFeO2 microparticles as a heterogeneous Fenton-like catalyst: Efficiency, stability and mechanism.* Chemical Engineering Journal, 2014. **236**: p. 251-262.

14. Pereira, M.C., E. Murad, and L.C.A. Oliveira, *Iron oxide catalysts: Fenton and Fenton-like reactions - a review.* Clay Minerals, 2012. **47**(3): p. 285-302.

15. Aranda, A., et al., *Dichloro-dihydro-fluorescein diacetate (DCFH-DA) assay: A quantitative method for oxidative stress assessment of nanoparticle-treated cells.* Toxicology in Vitro, 2013. **27**(2): p. 954-963.

16. Neyens, E. and J. Baeyens, *A review of classic Fenton's peroxidation as an advanced oxidation technique.* J Hazard Mater, 2003. **98**(1-3): p. 33-50.

17. Matta, R., K. Hanna, and S. Chiron, *Fenton-like oxidation of 2,4,6-trinitrotoluene using different iron minerals.* Sci Total Environ, 2007. **385**(1-3): p. 242-51.

18. Xue, X., et al., *Effect of chelating agent on the oxidation rate of PCP in the magnetite/H2O2 system at neutral pH.* Journal of Molecular Catalysis A: Chemical, 2009. **311**(1): p. 29-35.

19. Hanna, K., T. Kone, and C. Ruby, *Fenton-like oxidation and mineralization of phenol using synthetic Fe(II)-Fe(III) green rusts.* Environ Sci Pollut Res Int, 2010. **17**(1): p. 124-34.

20. Zhong, Y., et al., *Heterogeneous UV/Fenton degradation of TBBPA catalyzed by titanomagnetite: catalyst characterization, performance and degradation products.* Water Res, 2012. **46**(15): p. 4633-44.

21. Liang, X., et al., *The decolorization of Acid Orange II in non-homogeneous Fenton reaction catalyzed by natural vanadium–titanium magnetite.* Journal of Hazardous Materials, 2010. **181**(1): p. 112-120.

22. Usman, M., et al., *Application of magnetite catalyzed chemical oxidation (Fenton-like and persulfate) for the remediation of oil hydrocarbon contamination.* Fuel, 2012. **96**: p. 270-276.

23. Wydra, R.J., et al., *Accelerated generation of free radicals by iron oxide nanoparticles in the presence of an alternating magnetic field.* Royal Society of Chemistry Advances, 2015. **5**(25): p. 18888-18893.

24. Frimpong, R.A., et al., *Enhancing remote controlled heating characteristics in hydrophilic magnetite nanoparticles via facile co-precipitation.* Journal of Magnetism and Magnetic Materials 2010. **332**: p. 326-331.

25. Wydra, R.J., et al., *The role of ROS generation from magnetic nanoparticles in an alternating magnetic field on cytotoxicity.* Acta Biomaterialia, 2015. **25**: p. 284-292.

26. Ghosh, P., et al., *Comparison of a new immobilized Fe3+ catalyst with homogeneous Fe3+–H2O2 system for degradation of 2,4-dinitrophenol.* Journal of Chemical Technology & Biotechnology, 2012. **87**(7): p. 914-923.

27. Rosensweig, R.E., *Heating magnetic fluid with alternating magnetic field.* Journal of Magnetism and Magnetic Materials, 2002. **252**: p. 370-374.

28. Tabaï, A., O. Bechiri, and M. Abbessi, *Degradation of organic dye using a new homogeneous Fenton-like system based on hydrogen peroxide and a recyclable Dawson-type heteropolyanion.* International Journal of Industrial Chemistry, 2017. **8**(1): p. 83-89.

29.   Tadolini, B. and L. Cabrini, *On the mechanism of OH. scavenger action.* Biochem J, 1988. **253**(3): p. 931-2.

30.   Lindsey, M.E. and M.A. Tarr, *Quantitation of hydroxyl radical during Fenton oxidation following a single addition of iron and peroxide.* Chemosphere, 2000. **41**(3): p. 409-417.

31.   Overend, R. and G. Paraskevopoulos, *Rates of hydroxyl radical reactions. 4. Reactions with methanol, ethanol, 1-propanol, and 2-propanol at 296 K.* The Journal of Physical Chemistry, 1978. **82**(12): p. 1329-1333.

References

Ahamed, M., M. J. Akhtar, H. A. Alhadlaq, M. A. M. Khan and S. A. Alrokayan (2015). "Comparative cytotoxic response of nickel ferrite nanoparticles in human liver HepG2 and breast MFC-7 cancer cells." Chemosphere **135**: 278-288.

Ahamed, M., M. J. Akhtar, M. A. Siddiqui, J. Ahmad, J. Musarrat, A. A. Al-Khedhairy, M. S. AlSalhi and S. A. Alrokayan (2011). "Oxidative stress mediated apoptosis induced by nickel ferrite nanoparticles in cultured A549 cells." Toxicology **283**: 101-108.

Ahamed, M., H. A. Alhadlaq, M. A. M. Khan and M. J. Akhtar (2013). "Selective killing of cancer cells by iron oxide nanoparticles mediated through reactive oxygen species via p53 pathway." Journal of Nanoparticles Research **15**: 1225-1235.

Ahmad, J., H. A. Alhadlaq, M. A. Siddiqui, Q. Saquib, A. A. Al-Khedhairy, J. Musarrat and M. Ahamed (2013). "Concentration dependant induction of ROS, cell cycle arrest and apoptosis in human liver cells after nickel nanoparticles exposure " Experimental Toxicology **30**(2): 137-148.

Akhtar, M. J., M. Ahamed, S. Kumar, M. M. Khan, J. Ahmad and S. A. Alrokayan (2012). "Zinc oxide nanoparticles selectively induce apoptosis in human cancer cells through reactive oxygen species." International Journal of Nanomedicine **7**: 845-857.

Alhadlaq, H. A., M. J. Akhtar and M. Ahame (2015). "Zinc ferrite nanoparticle-induced cytotoxicity and oxidative stress in diffrent human cells." Cell and Bioscience **5**(1): 1-11.

Aljarrah, K., N. M. Mhaidat, M. A. H. Al-Akhras, A. N. Aldaher, B. A. Albiss, K. Aledealat and F. M. Alsheyab (2012). "Magnetic nanoparticles sensitize MCF-7 breast cancer cells to doxorubicin-induced apoptosis." World Journal of Surgical Oncology **10**: 62-62.

Amstad, E., T. Gillich, I. Bilecka, M. Textor and E. Reimhult (2009). "Ultrastable Iron Oxide Nanoparticle Colloidal Suspensions Using Dispersants with Catechol-Derived Anchor Groups." Nano Letters **9**(2): 4042-4048.

Amstad, E., M. Textora and E. Reimhult (2011). "Stabilization and functionalization of iron oxide nanoparticles for biomedical applications." Nanoscale **3**: 2819-2843.

Anderson, D. G., C. A. Tweedie, N. Hossain, S. M. Navarro, D. M. Brey, K. J. V. Vliet, R. Langer and J. A. Burdick (2006). "A combinatorial library of photocrosslinkable and degradable materials." Advanced Materials **18**: 2614-2618.

Aranda, A., L. Sequedo, L. Tolosa, G. Quintas, E. Burello, J. V. Castell and L. Gombau (2013). "Dichloro-dihydro-fluorescein diacetate (DCFH-DA) assay: A quantitative method for oxidative stress assessment of nanoparticle-treated cells." Toxicology in Vitro **27**(2): 954-963.

Auffan, M., W. Achouak, J. Rose, M.-A. Roncato, C. Chanéac, D. T. Waite, A. Masion, J. C. Woicik, M. R. Wiesner and J.-Y. Bottero (2008). "Relation between the Redox State of Iron-Based Nanoparticles and Their Cytotoxicity toward Escherichia coli." Environmental Science & Technology **42**(17): 6730-6735.

Barrera, C., A. P. Herrera, N. Bezares, E. Fachini, R. Olayo-Valles, J. P. Hinestroza and C. Rinaldi (2012). "Effect of poly(ethylene oxide)-silane graft molecular weight on the colloidal properties of iron oxide nanoparticles for biomedical applications." Journal of Colloid and Interface Science **377**: 40-50.

Barrera, C., A. P. Herrera and C. Rinaldi (2009). "Colloidal dispersions of monodisperse magnetite nanoparticles modified with poly(ethylene glycol)." Journal of Colloid and Interface Science **329**: 107-113.

Bautista, P., A. F. Mohedano, J. A. Casas, J. A. Zazo and J. J. Rodriguez (2008). "An overview of the application of Fenton oxidation to industrial wastewaters treatment." Journal of Chemical Technology & Biotechnology **83**(10): 1323-1338.

Bautista, P., A. F. Mohedano, M. A. Gilarranz, J. A. Casas and J. J. Rodriguez (2007). "Application of Fenton oxidation to cosmetic wastewaters treatment." J Hazard Mater **143**(1-2): 128-134.

Berry, C. C. (2009). "Progress in functionalization of magnetic nanoparticles for applications in biomedicine." Journal of Physics D: Applied Physics **42**(22): 224003.

Bini, R. A., R. F. C. Marques, F. J. Santos, J. A. Chaker and M. Jafelicci Jr (2012). "Synthesis and functionalization of magnetite nanoparticles with different amino-functional alkoxysilanes." Journal of Magnetism and Magnetic Materials **324**(4): 534-539.

Boonyaroj, V., C. Chiemchaisri, W. Chiemchaisri, S. Theepharaksapan and K. Yamamoto (2012). "Toxic organic micro-pollutants removal mechanisms in long-term operated membrane bioreactor treating municipal solid waste leachate." Bioresource Technology **113**: 174-180.

Brey, D. M., J. L. Ifkovits, R. I. Mozia, J. S. Katz and J. A. Burdick (2008). "Controlling PBAE network properties through macromer branching." Acta Biomaterialia **4**: 207-217.

Chen, L., X. Li, J. Zhang, J. Fang, Y. Huang, P. Wang and J. Ma (2015). "Production of Hydroxyl Radical via the Activation of Hydrogen Peroxide by Hydroxylamine." Environ Sci Technol **49**(17): 10373-10379.

Chen, L., J. Ma, X. Li, J. Zhang, J. Fang, Y. Guan and P. Xie (2011). "Strong enhancement on fenton oxidation by addition of hydroxylamine to accelerate the ferric and ferrous iron cycles." Environ Sci Technol **45**(9): 3925-3930.

Chen, M., S. Yamamuro, D. Farrell and S. A. Majetich (2003). "Gold-coated iron nanoparticles for biomedical applications." Journal of Applied Physics **93**(10): 7551-7553.

Chen, P.-J., K. G. Linden, D. E. Hinton, S. Kashiwada, E. J. Rosenfeldt and S. W. Kullman (2006). "Biological assessment of bisphenol A degradation in water following direct photolysis and UV advanced oxidation." Chemosphere **65**(7): 1094-1102.

Chen, T.-J., J.-Y. Jeng, C.-W. Lin, C.-Y. Wu and Y.-C. Chen (2006). "Quercetin inhibition of ROS-dependent and -independent apoptosis in rat glioma C6 cell." Toxicology **223**: 113-126.

Chen, W., C. Zou, Y. Liu and X. Li (2017). "The experimental investigation of bisphenol A degradation by Fenton process with different types of cyclodextrins." Journal of Industrial and Engineering Chemistry **56**: 428-434.

Chiang, K., T. M. Lim, L. Tsen and C. C. Lee (2004). "Photocatalytic degradation and mineralization of bisphenol A by TiO2 and platinized TiO2." Applied Catalysis A: General **261**(2): 225-237.

Cleveland, V., J.-P. Bingham and E. Kan (2014). "Heterogeneous Fenton degradation of bisphenol A by carbon nanotube-supported Fe3O4." Separation and Purification Technology **133**: 388-395.

Cochran, D. B., P. P. Wattamwar, Robert Wydra, J. Z. Hilt, K. W. Anderson, R. E. Eitel and T. D. Dziubla (2013). "Suppressing iron oxide nano particle toxicity by vascular targeted antioxidant polymer nanoparticles " Biomaterials **34**: 9615-9622.

Connord, V., P. Clerc, N. Hallali, D. El Hajj Diab, D. Fourmy, V. Gigoux and J. Carrey (2015). "Real-Time Analysis of Magnetic Hyperthermia Experiments on Living Cells under a Confocal Microscope." Small **11**(20): 2437-2445.

Creixell, M., A. C. Bohorquez, M. Torres-Lugo and C. Rinaldi (2011). "EGFR-Targeted Magnetic Nanoparticle Heaters Kill Cancer Cells Without A Sensible Temperature Rise." ACS Nano **5**(9): 7124–7129.

Davis, K., B. Qi, M. Witmer, C. L. Kitchens, B. A. Powell and O. T. Mefford (2014). "Quantitative Measurement of Ligand Exchange on Iron Oxides via Radiolabeled Oleic Acid." Langmuir **30**: 10918-10925.

De Laat, J. and H. Gallard (1999). "Catalytic Decomposition of Hydrogen Peroxide by Fe(III) in Homogeneous Aqueous Solution: Mechanism and Kinetic Modeling." Environmental Science & Technology **33**(16): 2726-2732.

de Sousa, M. E., M. B. Fernández van Raap, P. C. Rivas, P. Mendoza Zélis, P. Girardin, G. A. Pasquevich, J. L. Alessandrini, D. Muraca and F. H. Sánchez (2013). "Stability and

Relaxation Mechanisms of Citric Acid Coated Magnetite Nanoparticles for Magnetic Hyperthermia." The Journal of Physical Chemistry C **117**(10): 5436-5445.

Dennis, C. L., A. J. Jackson, J. A. Borchers, P. J. Hoopes, R. Strawbridge, A. R. Foreman, J. van Lierop, C. Gruttner and R. Ivkov (2009). "Nearly complete regression of tumors via collective behavior of magnetic nanoparticles in hyperthermia." Nanotechnology **20**(39): 395103.

Descorme, C. (2017). "Catalytic wastewater treatment: Oxidation and reduction processes. Recent studies on chlorophenols." Catalysis Today **297**: 324-334.

Dong, Y., Z. Han, C. Liu and F. Du (2010). "Preparation and photocatalytic performance of Fe (III)-amidoximated PAN fiber complex for oxidative degradation of azo dye under visible light irradiation." Science of The Total Environment **408**(10): 2245-2253.

Duesterberg, C. K., S. E. Mylon and T. D. Waite (2008). "pH Effects on Iron-Catalyzed Oxidation using Fenton's Reagent." Environmental Science & Technology **42**(22): 8522-8527.

Duesterberg, C. K. and T. D. Waite (2007). "Kinetic Modeling of the Oxidation of p-Hydroxybenzoic Acid by Fenton's Reagent: Implications of the Role of Quinones in the Redox Cycling of Iron." Environmental Science & Technology **41**(11): 4103-4110.

Emerit, J., C. Beaumont and F. Trivin (2001). "Iron metabolism, free radicals, and oxidative injury." Biomed Pharmacother **55**(6): 333-339.

Enami, S., Y. Sakamoto and A. J. Colussi (2014). "Fenton chemistry at aqueous interfaces." Proc Natl Acad Sci U S A **111**(2): 623-628.

Erdal, H., M. Berndtsson, J. Castro, U. Brunk, M. C. Shoshan and S. Linder (2005). "Induction of lysosomal membrane permeabilization by compounds that activate p53-independent apoptosis." Proc Natl Acad Sci U S A **102**(1): 192-197.

Fang, C., F. M. Kievit, O. Veiseh, Z. R. Stephen, T. Wang, D. Lee, R. G. Ellenbogen and M. Zhang (2012). "Fabrication of magnetic nanoparticles with controllable drug loading

and release through a simple assembly approach." Journal of Controlled Release **162**: 233-241.

Frimpong, R. A., J. Dou, M. Pechan and J. Z. Hilt (2010). "Enhancing remote controlled heating characteristics in hydrophilic magnetite nanoparticles via facile co-precipitation." Journal of Magnetism and Magnetic Materials **332**: 326-331.

Frimpong, R. A. and J. Z. Hilt (2010). "Magnetic nanoparticles in biomedicine: synthesis, functionalization and applications." Nanomedicine (Lond) **5**(9): 1401-1414.

Fu, P. P., Q. Xia, H.-M. Hwang, P. C. Ray and H. Yu (2014). "Mechanisms of nanotoxicity: Generation of reactive oxygen species." Journal of Food and Drug Analysis **22**: 64-75.

Fukahori, S., H. Ichiura, T. Kitaoka and H. Tanaka (2003). "Capturing of bisphenol A photodecomposition intermediates by composite TiO2–zeolite sheets." Applied Catalysis B: Environmental **46**(3): 453-462.

Fürhacker, M., S. Scharf and H. Weber (2000). "Bisphenol A: emissions from point sources." Chemosphere **41**(5): 751-756.

Gao, F., H. Qu, Y. Duan, J. Wang, X. Song, T. Ji, L. Cao, G. Nieb and S. Sun (2014). "Dopamine coating as a general and facile route to biofunctionalization of superparamagnetic Fe3O4 nanoparticles for magnetic separation of proteins." RSC Advances **4**: 6657-6663.

Garoma, T. and S. Matsumoto (2009). "Ozonation of aqueous solution containing bisphenol A: Effect of operational parameters." Journal of Hazardous Materials **167**(1): 1185-1191.

Garrido-Ramírez, E. G., B. K. G. Theng and M. L. Mora (2010). "Clays and oxide minerals as catalysts and nanocatalysts in Fenton-like reactions — A review." Applied Clay Science **47**(3): 182-192.

Ghosh, P., C. Kumar, A. N. Samanta and S. Ray (2012). "Comparison of a new immobilized Fe3+ catalyst with homogeneous Fe3+–H2O2 system for degradation of 2,4-dinitrophenol." Journal of Chemical Technology & Biotechnology **87**(7): 914-923.

Goff, J. D., P. P. Huffstetler, W. C. Miles, N. Pothayee, C. M. Reinholz, S. Ball, R. M. Davis and J. S. Riffle (2009). "Novel Phosphonate-Functional Poly(ethylene oxide)-Magnetite Nanoparticles Form Stable Colloidal Dispersions in Phosphate-Buffered Saline." Chemistry of Materials **21**(20): 4784-4795.

Goldstone, J. V., M. J. Pullin, S. Bertilsson and B. M. Voelker (2002). "Reactions of Hydroxyl Radical with Humic Substances: Bleaching, Mineralization, and Production of Bioavailable Carbon Substrates." Environmental Science & Technology **36**(3): 364-372.

Gonzalez-Olmos, R., M. J. Martin, A. Georgi, F.-D. Kopinke, I. Oller and S. Malato (2012). "Fe-zeolites as heterogeneous catalysts in solar Fenton-like reactions at neutral pH." Applied Catalysis B: Environmental **125**: 51-58.

Gordon, R. T., J. R. Hines and D. Gordon (1979). "Intracellular hyperthermia. A biophysical approach to cancer treatment via intracellular temperature and biophysical alterations." Med Hypotheses **5**(1): 83-102.

Gorga, M., M. Petrovic and D. Barceló (2013). "Multi-residue analytical method for the determination of endocrine disruptors and related compounds in river and waste water using dual column liquid chromatography switching system coupled to mass spectrometry." Journal of Chromatography A **1295**: 57-66.

Grazú, V., A. M. Silber, M. Moros, L. Asín, T. E. Torres, C. Marquina, M. R. Ibarra and G. F. Goya (2012). "Application of magnetically induced hyperthermia in the model protozoan Crithidia fasciculata as a potential therapy against parasitic infections." International Journal of Nanomedicine **7**: 5351-5360.

Guo, C., M. Ge, L. Liu, G. Gao, Y. Feng and Y. Wang (2010). "Directed Synthesis of Mesoporous TiO2 Microspheres: Catalysts and Their Photocatalysis for Bisphenol A Degradation." Environmental Science & Technology **44**(1): 419-425.

Guo, D., H. Bi, B. Liu, Q. Wu, D. Wang and Y. Cui (2013). "Reactive oxygen species-induced cytotoxic effects of zinc oxide nanoparticles in rat retinal ganglion cells." Toxicology in Vitro **27**: 731-738.

Guo, S., E. Bezard and B. Zhao (2005). "Protective effect of green tea polyphenols on the SH-SY5Y cells against 6-OHDA induced apoptosis through ROS – NO pathway." Free Radical Biology & Medicine **39**: 682-695.

Gupta, A. K. and M. Gupta (2005). "Synthesis and surface engineering of iron oxide nanoparticles for biomedical applications." Biomat **26**.

Guptaa, A. K. and M. Gupta (2005). "Synthesis and surface engineering of iron oxide nanoparticles for biomedical applications." Biomaterials **26**: 3995-4021.

Hanna, K., T. Kone and C. Ruby (2010). "Fenton-like oxidation and mineralization of phenol using synthetic Fe(II)-Fe(III) green rusts." Environ Sci Pollut Res Int **17**(1): 124-134.

Hartmann, M., S. Kullmann and H. Keller (2010). "Wastewater treatment with heterogeneous Fenton-type catalysts based on porous materials." Journal of Materials Chemistry **20**(41): 9002.

Hassanpour, M., H. Safardoust-Hojaghan and M. Salavati-Niasari (2017). "Degradation of methylene blue and Rhodamine B as water pollutants via green synthesized Co 3 O 4 /ZnO nanocomposite." Journal of Molecular Liquids **229**: 293-299.

Hauser, A. M., K. W. Anderson and J. Z. Hilt (2016). "Peptide conjugated magnetic nanoparticles for magnetically mediated energy delivery to lung cancer cells." Nanomedicine (Lond).

Hauser, A. M., M. I. Mitov, E. F. Daley, R. C. McGarry, K. W. Anderson and J. Z. Hilt (2016). "Targeted iron oxide nanoparticles for the enhancement of radiation therapy." Biomaterials **105**: 127-135.

Hawkins, A. M., M. E. Tolbert, B. Newton, T. A. Milbrandt, D. A. Puleo and J. Z. Hilt (2013). "Tuning biodegradable hydrogel properties via synthesis proce dure." Polymer **54**: 5.

He, F. and L. Zuo (2015). "Redox Roles of Reactive Oxygen Species in Cardiovascular Diseases." International Journal of Molecular Sciences **16**(11): 27770-27780.

Hsieh, H.-C., C.-M. Chen, W.-Y. Hsieh, C.-Y. Chen, C.-C. Liu and F.-H. Lin (2015). "ROS-induced toxicity: exposure of 3T3, RAW264.7, and MCF7 cells to superparamagnetic iron oxide nanoparticles results in cell death by mitochondriadependent apoptosis." Journal of Nanoparticles Research **17**: 70-83.

Hsieh, S. and P.-Y. Lin (2012). "FePt nanoparticles as heterogeneous Fenton-like catalysts for hydrogen peroxide decomposition and the decolorization of methylene blue." Journal of Nanoparticle Research **14**(6).

Hua, Z., W. Ma, X. Bai, R. Feng, L. Yu, X. Zhang and Z. Dai (2014). "Heterogeneous Fenton degradation of bisphenol A catalyzed by efficient adsorptive Fe3O4/GO nanocomposites." Environ Sci Pollut Res Int **21**(12): 7737-7745.

Huang, G., H. Chen, Y. Dong, X. Luo, H. Yu, Z. Moore, E. A. Bey, D. A. Boothman and J. Gao (2013). "Superparamagnetic Iron Oxide Nanoparticles: Amplifying ROS Stress to Improve Anticancer Drug Efficacy." Theranostics **3**(2): 116-126.

Huang, L. and k. Nishinari (2001). "Interaction between poly(ethylene glycol) and water as studied by differential scanning calorimetry." Journal of Polymer Science B: Polymer Physics **39**: 496-506.

Huang, R., Z. Fang, X. Fang and E. P. Tsang (2014). "Ultrasonic Fenton-like catalytic degradation of bisphenol A by ferroferric oxide (Fe(3)O(4)) nanoparticles prepared from steel pickling waste liquor." J Colloid Interface Sci **436**: 258-266.

Huling, S. G., P. K. Jones, W. P. Ela and R. G. Arnold (2005). "Repeated Reductive and Oxidative Treatments of Granular Activated Carbon." Journal of Environmental Engineering **131**(2): 287-297.

Hussain, I., A. Bhan, K. I. Ansari, P. Deb, S. A. M. Bobzean, L. I. Perrotti and S. S. Mandal (2015). "Bisphenol-A induces expression of HOXC6, an estrogen-regulated homeobox-containing gene associated with breast cancer." Biochimica et Biophysica Acta (BBA) - Gene Regulatory Mechanisms **1849**(6): 697-708.

Issa, B., I. M. Obaidat, B. A. Albiss and Y. Haik (2013). "Magnetic Nanoparticles: Surface effects and Properties Related to Biomedicine Applications." International Journal of Molecular Sciences **14**: 21266-21305.

Ito, A., M. Shinkai, H. Honda and T. Kobayashi (2005). "Medical application of functionalized magnetic nanoparticles." Journal of Bioscience and Bioengineering **100**(1): 1-11.

Jaattela, M. (2004). "Multiple cell death pathways as regulators of tumour initiation and progression." Oncogene **23**(16): 2746-2756.

Jackson, J. and R. Sutton (2008). "Sources of endocrine-disrupting chemicals in urban wastewater, Oakland, CA." Sci Total Environ **405**(1-3): 153-160.

Jordan, A., R. Scholz, P. Wust, H. Fähling and F. Roland (1999). "Magnetic fluid hyperthermia (MFH): Cancer treatment with AC magnetic field induced excitation of biocompatible superparamagnetic nanoparticles." Journal of Magnetism and Magnetic Materials **201**(1): 413-419.

Kang, J. H. and F. Kondo (2002). "Bisphenol a degradation by bacteria isolated from river water." Arch Environ Contam Toxicol **43**(3): 265-269.

Karihtala, P. and Y. Soini (2007). "Reactive oxygen species and antioxidant mechanisms in human tissues and their relation to malignancies." APMIS **115**: 81-103.

Katsumata, H., S. Kawabe, S. Kaneco, T. Suzuki and K. Ohta (2004). "Degradation of bisphenol A in water by the photo-Fenton reaction." Journal of Photochemistry and Photobiology A: Chemistry **162**(2): 297-305.

Klein, S., A. Sommer, L. V. R. Distel, W. Neuhuber and C. Kryschi (2012). "Superparamagnetic iron oxide nanoparticles as radiosensitizer via enhanced reactive oxygen species formation." Biochemical and Biophysical Research Communications **425**: 393-397.

Kolpin, D. W., E. T. Furlong, M. T. Meyer, E. M. Thurman, S. D. Zaugg, L. B. Barber and H. T. Buxton (2002). "Pharmaceuticals, Hormones, and Other Organic Wastewater Contaminants in U.S. Streams, 1999−2000: A National Reconnaissance." Environmental Science & Technology **36**(6): 1202-1211.

Kozissnik, B., A. C. Bohorquez, J. Dobson and C. Rinaldi (2013). "Magnetic fluid hyperthermia: Advances, challenges, and opportunity." International Journal of Hyperthermia **29**(8): 706-714.

Kruse, A. M., S. A. Meenach, K. W. Anderson and J. Z. Hilt (2014). "Synthesis and characterization of CREKA-conjugated iron oxide nanoparticles for hyperthermia applications." Acta Biomaterialia **10**: 2622-2629.

Kuch, H. M. and K. Ballschmiter (2001). "Determination of endocrine-disrupting phenolic compounds and estrogens in surface and drinking water by HRGC-(NCI)-MS in the picogram per liter range." Environ Sci Technol **35**(15): 3201-3206.

Kumar, P., S. Agnihotri and I. Roy (2016). "Synthesis of Dox drug conjugation and CA stabilized SPION for drug delivery." Biochemicstry & Physiology **5**(1): 1000194-1100199.

Kuramitz, H., M. Matsushita and S. Tanaka (2004). "Electrochemical removal of bisphenol A based on the anodic polymerization using a column type carbon fiber electrode." Water Res **38**(9): 2330-2337.

Lakshmi Prasanna, V. and R. Vijayaraghavan (2017). "Simultaneous Fenton–Photocatalytic Reactions through a New Single Catalyst (Nano ZnO_2 /Fe^{2+}) for Dye Degradation." The Journal of Physical Chemistry C **121**(34): 18557-18563.

Larsen, E. K. U., T. Nielsen, T. Wittenborn, H. Birkedal, T. Vorup-Jensen, M. H. Jakobsen, L. Østergaard, M. R. Horsman, F. Besenbacher, K. A. Howard and J. Kjems (2009). "Size-Dependent Accumulation of PEGylated Silane-Coated Magnetic Iron Oxide Nanoparticles in Murine Tumors." ACS Nano **3**(7): 1947-1951.

Laurent, S., S. Dutz, U. O. Häfeli and M. Mahmoudi (2011). "Magnetic fluid hyperthermia: Focus on superparamagnetic iron oxide nanoparticles." Advances in Colloid and Interface Science **166**(1): 8-23.

Laurent, S., D. Forge, M. Port, A. Roch, C. Robic, L. Vander Elst and R. N. Muller (2008). "Magnetic Iron Oxide Nanoparticles: Synthesis, Stabilization, Vectorization, Physicochemical Characterizations, and Biological Applications." Chemical Reviews **108**(6): 2064-2110.

Laurent, S. and M. Mahmoudi (2011). "Superparamagnetic iron oxide nanoparticles: promises for diagnosis and treatment of cancer." International Journal of Molecular Epidermiology and Genetics **2**(4): 367-390.

Lee, M. S., Y. S. Lee, H. H. Lee and H. Y. Song (2012). "Human endometrial cell coculture reduces the endocrine disruptor toxicity on mouse embryo development." J Occup Med Toxicol **7**(1): 7.

Lee, S. S., W. Song, M. Cho, H. L. Puppala, P. Nguyen, H. Zhu, L. Segatori and V. L. Colvin (2013). "Antioxidant properties of cerium oxide nanocrystal as a function of nanocrystal diameter and surface coating " ACS Nano **7**(11): 9693-9703.

Lewin, M., N. Carlesso, C. H. Tung, X. W. Tang, D. Cory, D. T. Scadden and R. Weissleder (2000). "Tat peptide-derivatized magnetic nanoparticles allow in vivo tracking and recovery of progenitor cells." Nature Biotechnology **18**(4): 410-414.

Lewinski, N., V. Colvin and R. Drezek (2008). "Cytotoxicity of nanoparticles." Small **4**(1): 26-49.

Li, M., Z. Qiang, C. Pulgarin and J. Kiwi (2016). "Accelerated methylene blue (MB) degradation by Fenton reagent exposed to UV or VUV/UV light in an innovative micro photo-reactor." Applied Catalysis B: Environmental **187**: 83-89.

Liang, X., Y. Zhong, S. Zhu, J. Zhu, P. Yuan, H. He and J. Zhang (2010). "The decolorization of Acid Orange II in non-homogeneous Fenton reaction catalyzed by natural vanadium–titanium magnetite." Journal of Hazardous Materials **181**(1): 112-120.

Limam, I., M. Mezni, A. Guenne, C. Madigou, M. R. Driss, T. Bouchez and L. Mazéas (2013). "Evaluation of biodegradability of phenol and bisphenol A during mesophilic and thermophilic municipal solid waste anaerobic digestion using 13C-labeled contaminants." Chemosphere **90**(2): 512-520.

Lin, S.-S. and M. D. Gurol (1998). "Catalytic Decomposition of Hydrogen Peroxide on Iron Oxide: Kinetics, Mechanism, and Implications." Environmental Science & Technology **32**(10): 1417-1423.

Lind, K., M. Kresse, N. P. Debus and R. H. Müller (2002). "A Novel Formulation for Superparamagnetic Iron Oxide (SPIO) Particles Enhancing MR Lymphography: Comparison of Physicochemical Properties and The In Vivo Behaviour." Journal of Drug Targeting **10**(3): 221-230.

Lindsey, M. E. and M. A. Tarr (2000). "Quantitation of hydroxyl radical during Fenton oxidation following a single addition of iron and peroxide." Chemosphere **41**(3): 409-417.

Lubbe, A. S., C. Alexiou and C. Bergemann (2001). "Clinical applications of magnetic drug targeting." J Surg Res **95**(2): 200-206.

Lucas, M. S. and J. A. Peres (2009). "Removal of COD from olive mill wastewater by Fenton's reagent: Kinetic study." Journal of Hazardous Materials **168**(2): 1253-1259.

Mahmoudi, M., A. Simchi, M. Imani, M. A. Shokrgozar, A. S. Milani, U. O. Hafeli and P. Stroeve (2010). "A new approach for the in vitro identification of the cytotoxicity of superparamagnetic iron oxide nanoparticles." Colloids Surf B Biointerfaces **75**(1): 300-309.

Malvindi, M. A., V. d. Matteis, A. Galeone, V. Brunetti, G. C. Anyfantis, A. Athannassiou, R. Cingolani and P. P. Pompa (2014). "Toxicity assessment of silica coated iron oxide nanoparticles and biocompatibility improvement by surface engineering." Plos one **9**(1): e85835.

Manke, A., L. Wang and Y. Rojanasakul (2013). "Mechanisms of Nanoparticle-Induced Oxidative Stress and Toxicity." Biomedical Research International: 1-15.

Matta, R., K. Hanna and S. Chiron (2007). "Fenton-like oxidation of 2,4,6-trinitrotoluene using different iron minerals." Sci Total Environ **385**(1-3): 242-251.

McCarthy, J. R. and R. Weissleder (2008). "Multifunctional magnetic nanoparticles for targeted imaging and therapy." Advanced Drug Delivery Reviews **60**(11): 1241-1251.

Meenach, S. A., C. G. Otu, K. W. Anderson and J. Z. Hilt (2012). "Controlled synergistic delivery of paclitaxel and heat from poly (beta-amino ester)/iron oxide-based hydrogel nanocomposites." Internation Journal of Pharmaceutics **427**: 177-184.

Melcer, H. and G. Klecka (2011). "Treatment of Wastewaters Containing Bisphenol A-State of the Science Review." Water Environment Research **83**(7): 650-666.

Mesárosová, M., K. Kozics, A. Bábelová, E. Regendová, M. Pastorek, D. Vnuková, B. Buliaková, F. Rázga and A. Gábelová (2014). "The role of reactive oxygen species in the genotoxicity of surface-modified magnetite nanoparticle." Toxicology Letters **226**: 303-313.

Miles, W. C., J. D. Goff, P. P. Huffstetler, C. M. Reinholz, N. Pothayee, B. L. Caba, J. S. Boyd, R. M. Davis and J. S. Riffle (2009). "Synthesis and Colloidal Properties of

Polyether−Magnetite Complexes in Water and Phosphate-Buffered Saline." Langmuir **25**(2): 803-813.

Min, K. H., J.-H. Kim, S. M. Bae, H. Shin, M. S. Kim, S. Park, H. Lee, R.-W. Park, I.-S. Kim, K. Kim, I. C. Kwon, S. Y. Jeong and D. S. Lee (2010). "Tumoral acidic pH-responsive MPEG-poly(β -amino ester) polymeric micelles for cancer targeting therapy." Journal of Controlled Release **144**: 259-266.

Moroz, P., S. K. Jones and B. N. Gray (2002). "Magnetically mediated hyperthermia: current status and future directions." Int J Hyperthermia **18**(4): 267-284.

Mumtaz, S., L.-S. Wang, M. Abdullah, S. Z. Hussain, Z. Iqbal, V. M. Rotello and I. Hussain (2017). "Facile method to synthesize dopamine-capped mixed ferrite nanoparticles and their peroxidase-like activity." Journal of Physics D: Applied Physics **50**: 11LT02-11LT10.

Munoz, M., Z. M. de Pedro, J. A. Casas and J. J. Rodriguez (2015). "Preparation of magnetite-based catalysts and their application in heterogeneous Fenton oxidation – A review." Applied Catalysis B: Environmental **176-177**: 249-265.

Muthukumaran, T. and J. Philip (2015). "A single pot approach for synthesis of phosphate coated iron oxide nanoparticles." Journal of Nanoscience and Nanotechnology **15**: 2715-2725.

Namdeo, M., S. Saxena, R. Tankhiwale, M. Bajpai, Y. M. Mohan and S. K. Bajpai (2008). "Magnetic nanoparticles for drug delivery applications." J Nanosci Nanotechnol **8**(7): 3247-3271.

Naqvi, S., M. Samim, M. Abdin, F. J. Ahmed, A. Maitra, C. Prashant and A. K. Dinda (2010). "Concentration-dependent toxicity of iron oxide nanoparticles mediated by increased oxidative stress." Int J Nanomedicine **5**: 983-989.

Nel, A., T. Xia, L. Madler and N. Li (2006). "Toxic Potential of Materials at the Nanolevel." Science **311**: 622-628.

Neyens, E. and J. Baeyens (2003). "A review of classic Fenton's peroxidation as an advanced oxidation technique." J Hazard Mater **98**(1-3): 33-50.

Novo, E. and M. Parola (2008). "Redox mechanisms in hepatic chronic wound healing and fibrogenesis." Fibrogenesis & Tissue Repair **1**(5): 1-58.

Ojha, D. P., M. K. Joshi and H. J. Kim (2017). "Photo-Fenton degradation of organic pollutants using a zinc oxide decorated iron oxide/reduced graphene oxide nanocomposite." Ceramics International **43**(1): 1290-1297.

Overend, R. and G. Paraskevopoulos (1978). "Rates of hydroxyl radical reactions. 4. Reactions with methanol, ethanol, 1-propanol, and 2-propanol at 296 K." The Journal of Physical Chemistry **82**(12): 1329-1333.

Paciolla, M. D., S. Kolla and S. A. Jansen (2002). "The reduction of dissolved iron species by humic acid and subsequent production of reactive oxygen species." Advances in Environmental Research **7**(1): 169-178.

Pan, B., D. Lin, H. Mashayekhi and B. Xing (2008). "Adsorption and Hysteresis of Bisphenol A and 17α-Ethinyl Estradiol on Carbon Nanomaterials." Environmental Science & Technology **42**(15): 5480-5485.

Pankhurst, Q. A., J. Connolly, S. K. Jones and J. Dobson (2003). "Applications of magnetic nanoparticles in biomedicine." Journal of Physics D: Applied Physics **36**: R167-R181.

Pankhurst, Q. A., N. T. K. Thanh, S. K. Jones and J. Dobson (2009). "Progress in applications of magnetic nanoparticles in biomedicine." Journal of Physics D: Applied Physics **42**(22): 224001.

Pereira, M. C., E. Murad and L. C. A. Oliveira (2012). "Iron oxide catalysts: Fenton and Fenton-like reactions - a review." Clay Minerals **47**(3): 285-302.

Pérez, M., F. Torrades, X. Domènech and J. Peral (2002). "Removal of organic contaminants in paper pulp effluents by AOPs: an economic study." Journal of Chemical Technology & Biotechnology **77**(5): 525-532.

Petri-Fink, A., M. Chastellain, L. Juillerat-Jeanneret, A. Ferrari and H. Hofmann (2005). "Development of functionalized superparamagnetic iron oxide nanoparticles for interaction with human cancer cells." Biomaterials **26**(15): 2685-2694.

Pignatello, J. J., E. Oliveros and A. MacKay (2006). "Advanced Oxidation Processes for Organic Contaminant Destruction Based on the Fenton Reaction and Related Chemistry." Critical Reviews in Environmental Science and Technology **36**(1): 1-84.

Pliego, G., J. A. Zazo, S. Blasco, J. A. Casas and J. J. Rodriguez (2012). "Treatment of Highly Polluted Hazardous Industrial Wastewaters by Combined Coagulation–Adsorption and High-Temperature Fenton Oxidation." Industrial & Engineering Chemistry Research **51**(7): 2888-2896.

Poerschmann, J., U. Trommler and T. Gorecki (2010). "Aromatic intermediate formation during oxidative degradation of Bisphenol A by homogeneous sub-stoichiometric Fenton reaction." Chemosphere **79**(10): 975-986.

Poljsak, B. (2011). "Strategies for Reducing or Preventing the Generation of Oxidative Stress." Oxidative Medicine and Cellular Longevity **2011**.

Poljsak, B., D. Šuput and I. Milisav (2013). "Achieving the Balance between ROS and Antioxidants: When to Use the Synthetic Antioxidants." Oxidative Medicine and Cellular Longevity **2013**: 1-11.

Polo-Corrales, L. and C. Rinaldi (2012). "Monitoring iron oxide nanoparticle surface temperature in an alternating magnetic field using thermoresponsive fluorescent polymers." Journal of Applied Physics **111**(7).

Qiao, Z.-Y., S.-L. i. Qiao, G. Fan, Y.-S. Fan, Y. Chen and H. Wang (2014). "One-pot synthesis of pH-sensitive poly(RGD-co-beta amino ester)s for targeted intracellular drug delivery." Polymer Chemistry of Materials **5**: 844-853.

Qin, Q., Y. Liu, X. Li, T. Sun and Y. Xu (2018). "Enhanced heterogeneous Fenton-like degradation of methylene blue by reduced CuFe2O4." RSC Advances **8**(2): 1071-1077.

Rabin, Y. (2002). "Is intracellular hyperthermia superior to extracellular hyperthermia in the thermal sense?" Int J Hyperthermia **18**(3): 194-202.

Racuciu, M., D. E. Creang and A. Airinei (2006). "Citric-acid–coated magnetite nanoparticles for biological applications." THE EUROPEAN PHYSICAL JOURNAL E **21**: 117-121.

Ramesh, V., P. Ravichandran, C. L. Copeland, R. Gopikrishnan, S. Biradar, V. Goornavar, G. T. Ramesh and J. C. Hall (2012). "Magnetite induces oxidative stress and apoptosis in lung epithelial cells." Molecular and Cellular Biochemistry **363**: 225-234.

Ramirez, J. H., F. J. Maldonado-Hódar, A. F. Pérez-Cadenas, C. Moreno-Castilla, C. A. Costa and L. M. Madeira (2007). "Azo-dye Orange II degradation by heterogeneous Fenton-like reaction using carbon-Fe catalysts." Applied Catalysis B: Environmental **75**(3-4): 312-323.

Rebuli, M. E., J. Cao, E. Sluzas, K. B. Delclos, L. Camacho, S. M. Lewis, M. M. Vanlandingham and H. B. Patisaul (2014). "Investigation of the Effects of Subchronic Low Dose Oral Exposure to Bisphenol A (BPA) and Ethinyl Estradiol (EE) on Estrogen Receptor Expression in the Juvenile and Adult Female Rat Hypothalamus." Toxicological Sciences **140**(1): 190-203.

Richard, P. U., J. T. Duskey, S. Stolarov, M. Spulber and C. G. Palivan (2015). "New concepts to fight oxidative stress: nanosized three dimensional supramolecular antioxidant assemblies." Expert Opinion on Drug Delivery **12**(19-27).

Richter, H. W. and W. H. Waddell (1983). "Mechanism of the oxidation of dopamine by the hydroxyl radical in aqueous solution." Journal of the American Chemical Society **105**(16): 5434-5440.

Rivas, F. J., F. J. Beltrán, O. Gimeno and J. Frades (2001). "Treatment of Olive Oil Mill Wastewater by Fenton's Reagent." Journal of Agricultural and Food Chemistry **49**(4): 1873-1880.

Rivero, M. J., E. Alonso, S. Dominguez, P. Ribao, R. Ibañez, I. Ortiz and A. Irabien (2014). "Kinetic analysis and biodegradability of the Fenton mineralization of bisphenol A." Journal of Chemical Technology & Biotechnology **89**(8): 1228-1234.

Rosenfeldt, E. J. and K. G. Linden (2004). "Degradation of Endocrine Disrupting Chemicals Bisphenol A, Ethinyl Estradiol, and Estradiol during UV Photolysis and Advanced Oxidation Processes." Environmental Science & Technology **38**(20): 5476-5483.

Rosensweig, R. E. (2002). "Heating magnetic fluid with alternating magnetic field." Journal of Magnetism and Magnetic Materials **252**: 370-374.

Sadeghi, L., F. Tanwir and V. Y. Babadi (2015). "In vitro toxicity of iron oxide nanoparticle: Oxidative damages on HepG2 cells." Experimental and Toxicologic Pathology **67**: 197-203.

Sahoo, Y., H. Pizem, T. Fried, D. Golodnitsky, L. Burstein, C. N. Sukenik and G. Markovich (2001). "Alkyl Phosphonate/Phosphate Coating on Magnetite Nanoparticles: A Comparison with Fatty Acids." Langmuir **17**(25): 7907-7911.

Sahu, N. K., J. Gupta and D. Bahadur (2015). "PEGylated FePt–Fe3O4 composite nanoassemblies (CNAs): in vitro hyperthermia, drug delivery and generation of reactive oxygen species (ROS)." Dalton Transactions **44**: 9103-9113.

Sanchez-Avila, J., J. Bonet, G. Velasco and S. Lacorte (2009). "Determination and occurrence of phthalates, alkylphenols, bisphenol A, PBDEs, PCBs and PAHs in an industrial sewage grid discharging to a Municipal Wastewater Treatment Plant." Sci Total Environ **407**(13): 4157-4167.

Sanchez, C., D. El Hajj Diab, V. Connord, P. Clerc, E. Meunier, B. Pipy, B. Payre, R. P. Tan, M. Gougeon, J. Carrey, V. Gigoux and D. Fourmy (2014). "Targeting a G-protein-coupled receptor overexpressed in endocrine tumors by magnetic nanoparticles to induce cell death." ACS Nano **8**(2): 1350-1363.

Saville, S. L., R. C. Stone, B. Qi and O. T. Mefford (2012). "Investigation of the stability of magnetite nanoparticles functionalized with catechol based ligands in biological media." Journal of Materials Chemistry **22**: 24909-24917.

Shahwan, T., S. Abu Sirriah, M. Nairat, E. Boyacı, A. E. Eroğlu, T. B. Scott and K. R. Hallam (2011). "Green synthesis of iron nanoparticles and their application as a Fenton-like catalyst for the degradation of aqueous cationic and anionic dyes." Chemical Engineering Journal **172**(1): 258-266.

Shen, Y., Y. Zhang, X. Zhang, X. Zhou, X. Teng, M. Yana and H. Bi (2015). "Horseradish peroxidase-immobilized magnetic mesoporous silica nanoparticles as a potential candidate to eliminate intracellular reactive oxygen species." Nanoscale **7**: 2941-2950.

Siddiqui, M. A., M. Ahamed, J. Ahmad, M. A. M. Khan, J. Musarrat, A. A. Al-Khedhairy and S. A. Alrokayan (2012). "Nickel oxide nanoparticles induce cytotoxicity, oxidative stress and apoptosis in cultured human cells that is abrogated by the dietary antioxidant curcumin." Food and chemical toxicology **50**: 641-647.

Song, W., Z. Tang, M. Li, S. Lv, H. Yu, L. Ma, X. Zhuang, Y. Huang and X. Chen (2012). "Tunable pH-Sensitive Poly(b-amino ester)s Synthesized from Primary Amines and Diacrylates for Intracellular Drug Delivery." Macromolecular Biosciences **12**: 1375-1383.

Staples, C. A., P. B. Dome, G. M. Klecka, S. T. Oblock and L. R. Harris (1998). "A review of the environmental fate, effects, and exposures of bisphenol A." Chemosphere **36**(10): 2149-2173.

Subagio, D. P., M. Srinivasan, M. Lim and T.-T. Lim (2010). "Photocatalytic degradation of bisphenol-A by nitrogen-doped TiO2 hollow sphere in a vis-LED photoreactor." Applied Catalysis B: Environmental **95**(3): 414-422.

Sun, C., J. S. H. Lee and M. Zhang (2008). "Magnetic nanoparticles in MR imaging and drug delivery." Advanced Drug Delivery Reviews **60**(11): 1252-1265.

Sun, Y. and J. J. Pignatello (1992). "Chemical treatment of pesticide wastes. Evaluation of iron(III) chelates for catalytic hydrogen peroxide oxidation of 2,4-D at circumneutral pH." Journal of Agricultural and Food Chemistry **40**(2): 322-327.

Tabaï, A., O. Bechiri and M. Abbessi (2017). "Degradation of organic dye using a new homogeneous Fenton-like system based on hydrogen peroxide and a recyclable Dawson-type heteropolyanion." International Journal of Industrial Chemistry **8**(1): 83-89.

Tadolini, B. and L. Cabrini (1988). "On the mechanism of OH. scavenger action." Biochem J **253**(3): 931-932.

Tartaj, P., T. González-Carreño and C. J. Serna (2002). "Synthesis of Nanomagnets Dispersed in Colloidal Silica Cages with Applications in Chemical Separation." Langmuir **18**(12): 4556-4558.

Tekin, H., O. Bilkay, S. S. Ataberk, T. H. Balta, I. H. Ceribasi, F. D. Sanin, F. B. Dilek and U. Yetis (2006). "Use of Fenton oxidation to improve the biodegradability of a pharmaceutical wastewater." Journal of Hazardous Materials **136**(2): 258-265.

Torres, R. A., C. Petrier, E. Combet, M. Carrier and C. Pulgarin (2008). "Ultrasonic cavitation applied to the treatment of bisphenol A. Effect of sonochemical parameters and analysis of BPA by-products." Ultrason Sonochem **15**(4): 605-611.

Trachootham, D., J. Alexandre and P. Huang (2009). "Targeting cancer cells by ROS-mediated mechanisms: a radical therapeutic approach." Nature review: drug discovery **8**: 579-591.

Tran, N. and T. J. Webster (2010). "Magnetic nanoparticles: biomedical applications and challenges." Journal of Materials Chemistry **20**(40): 8760-8767.

Tsuda, T., F. Horiob and T. Osaw (2000). "The role of anthocyanins as an antioxidant under oxidative stress in rat." BioFactors **13**: 133-139.

Umar, M., F. Roddick, L. Fan and H. A. Aziz (2013). "Application of ozone for the removal of bisphenol A from water and wastewater – A review." Chemosphere **90**(8): 2197-2207.

Usman, M., P. Faure, K. Hanna, M. Abdelmoula and C. Ruby (2012). "Application of magnetite catalyzed chemical oxidation (Fenton-like and persulfate) for the remediation of oil hydrocarbon contamination." Fuel **96**: 270-276.

Vadala, M. L., M. S. Thompson, M. A. Ashworth, Y. Lin, T. P. Vadala, R. Ragheb and J. S. Riffle (2008). "Heterobifunctional Poly(ethylene oxide) Oligomers Containing Carboxylic Acids." Biomacromolecules **9**(3): 1035-1043.

Veiseh, O., J. Gunn and M. Zhang (2010). "Design and fabrication of magnetic nanoparticles for targeted drug delivery and imaging." Advanced drug delivery reviews **62**(3): 284-304.

Villanueva, A., P. de la Presa, J. M. Alonso, T. Rueda, A. Martínez, P. Crespo, M. P. Morales, M. A. Gonzalez-Fernandez, J. Valdés and G. Rivero (2010). "Hyperthermia HeLa Cell Treatment with Silica-Coated Manganese Oxide Nanoparticles." The Journal of Physical Chemistry C **114**(5): 1976-1981.

Viollier, E., P. W. Inglett, K. Hunter, A. N. Roychoudhury and P. Van Cappellen (2000). "The ferrozine method revisited: Fe(II)/Fe(III) determination in natural waters." Applied Geochemistry **15**(6): 785-790.

Voinov, M. A., J. O. S. Pagán, E. Morrison, T. I. Smirnova and A. I. Smirnov (2011). "Surface-Mediated Production of Hydroxyl Radicals as a Mechanism of Iron Oxide Nanoparticle Biotoxicity." Journal of the American Chemical Society **133**(1): 35-41.

Wahab, R., S. Dwivedi, A. Umar, S. Singh, I. H. Hwang, H.-S. Shin, J. Musarrat, A. A. Al-Khedhairy and Y.-S. Kim (2013). "ZnO Nanopar ticles Induce Oxidative Stress in Cloudman S91 Melanoma Cancer Cells." Journal of Biomedical Nanotechnology **9**(3): 441-449.

Wang, B., J.-J. Yin, X. Zhou, I. Kurash, Z. Chai, Y. Zhao and W. Feng (2012). "Physicochemical Origin for Free Radical Generation of Iron Oxide Nanoparticles in

Biomicroenvironment: Catalytic Activities Mediated by Surface Chemical States." The Journal of Physical Chemistry C **117**(1): 383-392.

Wang, C., H. Liu and Z. Sun (2012). "Heterogeneous Photo-Fenton Reaction Catalyzed by Nanosized Iron Oxides for Water Treatment." International Journal of Photoenergy **2012**: 1-10.

Wang, C., S. Zhang, Z. Zhang, M. Zeng and S. Yuji (2014). "Optimization and Interpretation of Fenton and UV/Fenton Processes for Degradation of Syringyl Lignin." Journal of Environmental Analytical Chemistry **01**(02).

Wang, D., J. He, N. Rosenzweig and Z. Rosenzweig (2004). "Superparamagnetic Fe2O3 Beads−CdSe/ZnS Quantum Dots Core−Shell Nanocomposite Particles for Cell Separation." Nano Letters **4**(3): 409-413.

Wang, R., D. Ren, S. Xia, Y. Zhang and J. Zhao (2009). "Photocatalytic degradation of Bisphenol A (BPA) using immobilized TiO2 and UV illumination in a horizontal circulating bed photocatalytic reactor (HCBPR)." Journal of Hazardous Materials **169**(1): 926-932.

Wattamwar, P. P., Y. Mo, R. Wan, R. Palli, Q. Zhang and T. D. Dziubla (2010). "Antioxidant activity of degradable polymer poly(trolox ester) to suppress oxidative stress injury in the cells " Advanced Functional Materials **20**: 147-154.

Weissleder, R., G. Elizondo, J. Wittenberg, C. A. Rabito, H. H. Bengele and L. Josephson (1990). "Ultrasmall superparamagnetic iron oxide: characterization of a new class of contrast agents for MR imaging." Radiology **175**(2): 489-493.

Weissleder, R., P. F. Hahn, D. D. Stark, E. Rummeny, S. Saini, J. Wittenberg and J. T. Ferrucci (1987). "MR imaging of splenic metastases: ferrite-enhanced detection in rats." AJR Am J Roentgenol **149**(4): 723-726.

Wenzel, U., A. Nickel, S. Kuntz and H. Daniel (2004). "Ascorbic acid suppresses drug-induced apoptosis in human colon cancer cells by scavenging mitochondrial superoxide anions." Carcinogenesis **25**(5): 703-712.

Wu, W., Q. He and C. Jiang (2008). "Magnetic Iron Oxide Nanoparticles: Synthesis and Surface Functionalization Strategies." Nanoscale Research Letter **3**: 397-415.

Wydra, R. J., A. M. Kruse, Y. Bae, K. W. Anderson and J. Z. Hilt (2013). "Synthesis and characterization of PEG-iron oxide core-shell composite nanoparticles for thermal therapy." Materials Science and Engineering C **33**: 4660-4667.

Wydra, R. J., C. E. Oliver, K. W. Anderson, T. D. Dziubla and J. Z. Hilt (2015). "Accelerated generation of free radicals by iron oxide nanoparticles in the presence of an alternating magnetic field." Royal Society of Chemistry Advances **5**(25): 18888-18893.

Wydra, R. J., P. G. Rychahou, B. M. Evers, K. W. Anderson, T. D. Dziubla and J. Z. Hilt (2015). "The role of ROS generation from magnetic nanoparticles in an alternating magnetic field on cytotoxicity." Acta Biomaterialia **25**: 284-292.

Xia, T., M. Kovochich, M. Liong, L. Madler, B. Gilbert, H. Shi, J. I. Yeh, J. I. Zink and A. E. Nel (2008). "Comparison of the Mechanism of Toxicity of Zinc Oxide and Cerium Oxide Nanoparticles Based on Dissolution and Oxidative Stress Properties." ACS Nano **2**(10): 2121-2135.

Xu, L. and J. Wang (2011). "A heterogeneous Fenton-like system with nanoparticulate zero-valent iron for removal of 4-chloro-3-methyl phenol." J Hazard Mater **186**(1): 256-264.

Xuan, Y. J., Y. Endo and K. Fujimoto (2002). "Oxidative degradation of bisphenol a by crude enzyme prepared from potato." J Agric Food Chem **50**(22): 6575-6578.

Xue, X., K. Hanna, C. Despas, F. Wu and N. Deng (2009). "Effect of chelating agent on the oxidation rate of PCP in the magnetite/H2O2 system at neutral pH." Journal of Molecular Catalysis A: Chemical **311**(1): 29-35.

Yamamoto, T., A. Yasuhara, H. Shiraishi and O. Nakasugi (2001). "Bisphenol A in hazardous waste landfill leachates." Chemosphere **42**(4): 415-418.

Yang, C.-w. (2015). "Degradation of bisphenol A using electrochemical assistant Fe(II)-activated peroxydisulfate process." Water Science and Engineering **8**(2): 139-144.

Yang, W. J., J. H. Lee, S. C. Hong, J. Lee, J. Lee and D.-W. Han (2013). "Difference betwen toxicities of iron oxide magnetic nanoparticles with various surface functional groups against human normal fibroblast and fibrosarcoma cells." Materials Chemistry and Physics **6**: 4689-4706.

Yu, M., S. Huang, K. J. Yu and A. M. Clyne (2012). "Dextran and Polymer Polyethylene Glycol (PEG) Coating Reduce Both 5 and 30 nm Iron Oxide Nanoparticle Cytotoxicity in 2D and 3D Cell Culture." International Journal of Molecular Sciences **13**: 5554-5570.

Yu, M. K., Y. Y. Jeong, J. Park, S. Park, J. W. Kim, J. J. Min, K. Kim and S. Jon (2008). "Drug-loaded superparamagnetic iron oxide nanoparticles for combined cancer imaging and therapy in vivo." Angew Chem Int Ed Engl **47**(29): 5362-5365.

Zhang, C., B. Wängler, B. Morgenstern, H. Zentgraf, M. Eisenhut, H. Untenecker, R. Krüger, R. Huss, C. Seliger, W. Semmler and F. Kiessling (2007). "Silica- and Alkoxysilane-Coated Ultrasmall Superparamagnetic Iron Oxide Particles: A Promising Tool To Label Cells for Magnetic Resonance Imaging." Langmuir **23**(3): 1427-1434.

Zhang, E., M. F. Kircher, M. Koch, L. Eliasson, S. N. Goldberg and E. Renström (2014). "Dynamic Magnetic Fields Remote-Control Apoptosis via Nanoparticle Rotation." ACS Nano **8**(4): 3192-3201.

Zhang, G., Y. Gao, Y. Zhang and Y. Guo (2010). "Fe2O3-Pillared Rectorite as an Efficient and Stable Fenton-Like Heterogeneous Catalyst for Photodegradation of Organic Contaminants." Environmental Science & Technology **44**(16): 6384-6389.

Zhang, S., X. Zhao, H. Niu, Y. Shi, Y. Cai and G. Jiang (2009). "Superparamagnetic Fe3O4 nanoparticles as catalysts for the catalytic oxidation of phenolic and aniline compounds." Journal of Hazardous Materials **167**(1): 560-566.

Zhang, X., Y. Ding, H. Tang, X. Han, L. Zhu and N. Wang (2014). "Degradation of bisphenol A by hydrogen peroxide activated with CuFeO2 microparticles as a heterogeneous Fenton-like catalyst: Efficiency, stability and mechanism." Chemical Engineering Journal **236**: 251-262.

Zhang, Y., N. Kohler and M. Zhang (2002). "Surface modification of superparamagnetic magnetite nanoparticles and their intracellular uptake." Biomaterials **23**: 1553-1561.

Zhao, J., Y. Li, C. Zhang, Q. Zeng and Q. Zhou (2008). "Sorption and degradation of bisphenol A by aerobic activated sludge." Journal of Hazardous Materials **155**(1): 305-311.

Zhong, Y., X. Liang, Y. Zhong, J. Zhu, S. Zhu, P. Yuan, H. He and J. Zhang (2012). "Heterogeneous UV/Fenton degradation of TBBPA catalyzed by titanomagnetite: catalyst characterization, performance and degradation products." Water Res **46**(15): 4633-4644.

Zou, J., J. Ma, L. Chen, X. Li, Y. Guan, P. Xie and C. Pan (2013). "Rapid Acceleration of Ferrous Iron/Peroxymonosulfate Oxidation of Organic Pollutants by Promoting Fe(III)/Fe(II) Cycle with Hydroxylamine." Environmental Science & Technology **47**(20): 11685-11691.

Trang Thi Thu Mai Vita

Personal Information:

Place of birth: Hanoi, Vietnam

Education:

Hanoi University of Science and Technology, Hanoi, Vietnam, May 2009

B.S in Chemical Engineering with focus on Physio-Chemical Engineering

University of Science and Technology of Hanoi, Hanoi, Vietnam, September

2012

M.S in Biotechnology and Pharmacology (in partnership with Montpellier II, Lyon

I, Aix-Marseille)

Research positions:

PhD student in Chemical Engineering

University of Kentucky, August 2014-Present

Advisor: Dr. J. Zach Hilt, Gill Eminent Professor of Chemical Engineering

Researcher at Lab of Biomedicals Nanomaterials, Institute of Materials Science

Vietnam Academy of Science and Technology, August 2009 – Present

Advisor: Dr. Xuan Phuc Nguyen, Professor of Physics;

Dr. Phuong Thu Ha, Associate Professor in Chemistry

Publications:

1. Trang Mai, J. Zach Hilt. Functionalization of iron oxide nanoparticles with small molecules and the impact on reactive oxygen species generation for potential cancer therapy. Colloids and Surface A. Colloids and Surface A. 5: 9, 2019.

2. <u>Trang Mai</u>, J. Zach Hilt. Magnetic nanoparticles: reactive oxygen species generation and potential therapeutic applications. Journal of Nanoparticle Research. 19: 253, 2017.

3. J. Devkota, J. Wingo, <u>T.T.T. Mai</u>, X.P. Nguyen, N.T. Huong, P. Mukherjee, H. Srikanth and M.H. Phan; A highly sensitive magnetic biosensor for detection and quantification of anticancer drugs tagged to superparamagnetic nanoparticles; Journal of Applied Physics 115: p17B503, 2014.

4. J. Devkota, <u>T.T.T. Mai</u>, et al. Synthesis, inductive heating, and magnetoimpedance-based detection of multifunctional Fe3O4 nanoconjugates; Sensors and Actuators B: Chemical 190, p715, 2014.

5. Ha Phuong Thu, Phan Thi Hong Tuyet, <u>Mai Thi Thu Trang</u> et al., Preparation and Biological Properties of Platinum (II) complex loaded copolymer PLA-TPGS; Journal of Nanomaterials 768628, 2013.

6. Ha Phuong Thu, Duong Tuan Quang, <u>Mai Thi Thu Trang</u> et al. In Vitro Apoptosis Enhancement of Hep-G2 Cells by PLA-TPGS and PLA-PEG Block Copolymer Encapsulated Curcumin Nanoparticles; Chemistry Letters 42: 255, 2013.

7. Nguyen Le Huy, Nguyen Thi My Thuy, Nguyen Hai Binh, Nguyen Ngoc Thinh, <u>Mai Thu Trang</u> et al. Covalent immobilization of cholesterol oxidase and poly (styrene-co-acrylic acid) magnetic microspheres on polyaniline films for amperometric cholesterol biosensing; Analytical Methods 5: 1392, 2013.

8. <u>Thi Thu Trang Mai</u> et al. A novel nanofiber Cur-loaded polylactic acid constructed by electrospinning; Advances in Natural Sciences: Nanosciences and Nanotechnology 3(2): 025014, 2012.

9. Thi Thu Trang Mai et al. Chitosan and O carboxymethyl chitosan modified Fe3O4 for hyperthermic treatment; Advances in Natural Sciences: Nanosciences and Nanotechnology 3(1): 015006, 2012.

10. Xuan Phuc Nguyen, Dai Lam Tran, Phuong Thu Ha, Hong Nam Pham, Thu Trang Mai et al. Iron oxide-based conjugates for cancer theragnostics; Advances in Natural Sciences: Nanosciences and Nanotechnology 3(3): 033001, 2012.

11. Tai Thien Luong, Thu Phuong Ha, Lam Dai Tran, Manh Hung Do, Trang Thu Mai et al. Design of carboxylated Fe3O4/ poly(styrene-co-acrylic acid) ferrofluids with highly efficient magnetic heating effect; Colloids and Surfaces A: Physicochemical and Engineering Aspects, 384: 23, 2011.

12. Le Mai Huong, Ha Phuong Thu, Nguyen Thi Bich Thuy, Tran Thi Hong Ha, Ha Thi Minh Thi, Mai Thu Trang, et al. Preparation and Antitumor-promoting activity of Curcumin Encapsulated by 1,3-β- Glucan Isolated from Vietnam Medicinal Mushroom Hericium erinaceum; Chemistry Letters, 40(8): 846, 2011.

13. Lam Dai Tran, Hoang Vinh Tran, Trang Thu Mai, et al. Biomedical and Environmental Applications of Chitosan-based Nanomaterials; Journal of Chitin chitosan 16 (1): 7, 2011.

14. Dai Lam Tran, Gia Dien Pham, Xuan Phuc Nguyen, Dinh Hoang Vu, Ngoc Thinh Nguyen, Vinh Hoang Tran, Thi Thu Trang Mai, et al. Some biomedical applications of chitosan-based hybrid nanomaterials; Advances in Natural Sciences: Nanosciences and Nanotechnology 2: 045004, 2011.

15. L.D. Tran, N.M.T. Hoang, T.T. Mai, et al. Nanosized magnetofluorescent Fe3O4 - curcumin conjugate for multimodal monitoring and drug targeting; Colloids and Surfaces A: Physicochemical and Engineering Aspects 371: 104, 2010.

Presentations (oral and posters, presenter in first):

1. S. G. Schuler, T. Mai, T. Dziubla, J.Z. Hilt. Enhanced contaminant degradation via Fenton reaction induced by magnetic nanoparticles in the presence of AMF, 2018 AIChE Conference, Pittsburgh, PA, October 28, 2018 (poster).

2. T. Mai, B. Evers, J.Z. Hilt. Functionalization of iron oxide nanoparticles and the impact on reactive oxygen species generation for potential cancer treatment, 2017 AIChE Conference, Minneapolis, MN, October 31, 2017 (oral).

3. B. Evers, T. Mai, T.D. Dziubla, J.Z. Hilt. The effect of PEG-based polymer coatings of iron oxide nanoparticles on reactive oxygen species generation, 2017 REU, Lexington, KY, August 3, 2017 (poster).

4. T. Mai, J.Z. Hilt. Functionalization of iron oxide nanoparticles with small molecules and the impact on reactive oxygen species generation, 2017 Markey Cancer Center Research Day, Lexington, KY, May 11, 2017 (poster).

5. A. Crupper, T. Mai, T.D. Dziubla, J.Z. Hilt. The effect of poly (beta amino ester) and dopamine coatings on the reactive oxygen species generation of iron oxide nanoparticles, 2017 Southern Student Regional Conference Knoxville, TN, March 31, 2017 (oral).

6. T. Mai, A. Crupper, K. Dray, J.Z. Hilt. Functionalization of iron oxide nanoparticles for enhancement of reactive oxygen species generation, 2016 Ashland Symposium, Lexington, KY, November 2016 (poster).